CROSS SECTIONS FOR COLLISION-INDUCED ROTATIONAL TRANSITIONS OF NH_3

PROEFSCHRIFT

TER VERKRIJGING VAN DE GRAAD VAN DOCTOR
IN DE WISKUNDE EN NATUURWETENSCHAPPEN
AAN DE KATHOLIEKE UNIVERSITEIT TE NIJMEGEN,
OP GEZAG VAN DE RECTOR MAGNIFICUS
PROF DR P G A B WIJDEVELD
VOLGENS BESLUIT VAN HET COLLEGE VAN DEKANEN
IN HET OPENBAAR TE VERDEDIGEN
OP WOENSDAG 23 JUNI 1982
DES NAMIDDAGS OM 2 00 UUR PRECIES

door

Dirk Bernardus Marie Klaassen

geboren te Geleen

krips repro meppel

PROMOTOR : PROF. DR. A. DYMANUS

CO-REFERENT : DR. J. J. TER MEULEN

Met dank aan

de leden en oud-leden van de afdeling Atoom- en Molecuulfysica voor de prettige samenwerking;

de heren J.Holtkamp, E.van Leeuwen, C.Sikkens en F.van Rijn voor hun bijstand op elektronisch en technisch gebied en L.Hendriks bovendien voor het vervaardigen van enkele tekeningen;

drs. N.van Hulst en drs. J.van Vaals, die tijdens hun afstudeerperiode aan het onderzoek hebben meegewerkt;

de dienstverlenende afdelingen van de faculteit der Wiskunde en Natuurwetenschappen in de personen van de heren P.Walraven en J.van Langen, H.Verschoor, W.Verdijk en M.Kuppens, en H.Spruyt en G.Dekkers;

mw. M.van Leeuwen voor het typen van het manuscript.

CONTENTS

CHAPTER 1

INTRODUCTION

1. ASTROPHYSICAL BACKGROUND OF THE EXPERIMENT

Microwave transitions across various inversion doublets of ammonia (NH_3) have been detected in a large number of galactic objects[1,2]. These transitions are seen in absorption or in emission against the isotropic 3 K background radiation, depending on the nature of the doublet and the interstellar source. The observed relative intensities do generally not correspond to thermal equilibrium conditions. Moreover, most of the observed transitions originate from highly excited rotational states. Shortly after the discovery of interstellar NH_3 by Townes and co-workers[1] it was suggested by them[3] that collisional excitation and de-excitation may provide an explanation of the observed features. This suggestion is generally accepted at present.

The observed emissions from interstellar NH_3 do not possess the characteristic properties of maser-type emissions (high intensity, strong polarization, etc.). Consequently the intensities are proportional to the population differences between the doublet levels. Moreover, NH_3 has many inversion transitions lying in a small frequency interval that can be detected with the same telescope and receiver. For these reasons ammonia is regarded as an ideal probe of the physical conditions in interstellar clouds[4].

Several population transfer models have been considered to explain the nonthermal intensities of the observed transitions of interstellar ammonia[3,5,6]. The outcome of all these model calculations depends critically on the rates for population transfer between the inversion-rotation levels, induced by collisions mainly with molecular hydrogen. Thus it is of great astrophysical interest to have accurate values for these rates, or the related collisional cross sections. Schwartz[7] has proposed to evaluate the population transfer rates from hydrogen-broadened linewidth measurements and extrapolate the obtained rates to interstellar temperatures.

Quantitative information about the rates for collision-induced population transfer, or equivalent collisional state-to-state cross sections, can be obtained from experiments and from theoretical calculations. Until now ab initio potential calculations combined with the computation of collisional cross sections have been performed only for the system ammonia-helium[8]. The interstellar abundance of molecular hydrogen is regarded to be an order of magnitude larger than that of helium in the relevant clouds[5]. Unfortunately the NH_3-H_2 system seems too complex for the (currently present) computational techniques. The experiments performed so far (see Sect. 2) failed to produce reliable quantitative information on the relevant rates. Nevertheless, as of now, laboratory work on collisional cross sections for the ammonia-hydrogen system remains the main source of information.

2. EXPERIMENTAL METHODS

Experimental methods used and the results obtained for NH_3 are reviewed by Dymanus[9]. All the measurements performed in the past fall into one of the following categories: line broadening and relaxation, steady-state double-resonance, and molecular beam scattering. Line-broadening and (transient) relaxation studies provide mainly information about the rates for collision-induced transitions across the inversion doublets of ammonia. Steady-state double-resonance experiments[10] yield information about both inversion and rotational collision rates, but the latter ones are difficult to extract from only a single measured quantity, the relative intensity change $\Delta I/I$. The difficulties stem mainly from the fact that the experiments are done in bulk and radiative and collision zones are not separated. These difficulties can be avoided in a beam experiment, where the primary ammonia beam passes through a scattering chamber or crosses a secondary beam.

To measure state-to-state cross sections in a beam experiment initial and final states of the primary beam molecule have to be well-defined in the scattering process. With the electric beam resonance (EBR) technique, applied for the first time by Toennies[11] to measure state-to-state cross sections, electrostatic multipoles are used to focus the initial rotational substate into the scattering region and the final state onto the detector. Until now this method has only been applied to molecules with a large dipole moment (about 3×10^{-29} Cm).

A molecular beam maser[12] makes use of a microwave cavity as state-selective detector. Equipped with a scattering chamber or secondary beam, a beam maser can be used for scattering experiments. This method was developed independently at M.I.T. by Kukolich and co-workers[13] and at Nijmegen by Reijnders[14]. Kukolich et al. used a scattering chamber and an ingenious one- and two-cavity (Ramsey) scheme to separate the inelastic effects. The apparatus of Reijnders was a conventional single-cavity beam maser but with a secondary beam. Both experiments yielded only information about the cross sections for collision-induced transitions across the inversion doublets of ammonia. Details of the experiment and results obtained at Nijmegen are reported in the thesis of Reijnders[14] and in a paper[15], hereafter referred to as I, which is based on that thesis. In the present investigation the set-up of Reijnders is converted into a double-resonance beam maser (DR-BM), which permits measurements of collision-induced rotational transitions in NH_3. These measurements and their interpretation form the main body of this thesis. Paper I is reproduced as Chapter 2 for the sake of completeness and also because it contains information and references essential for understanding

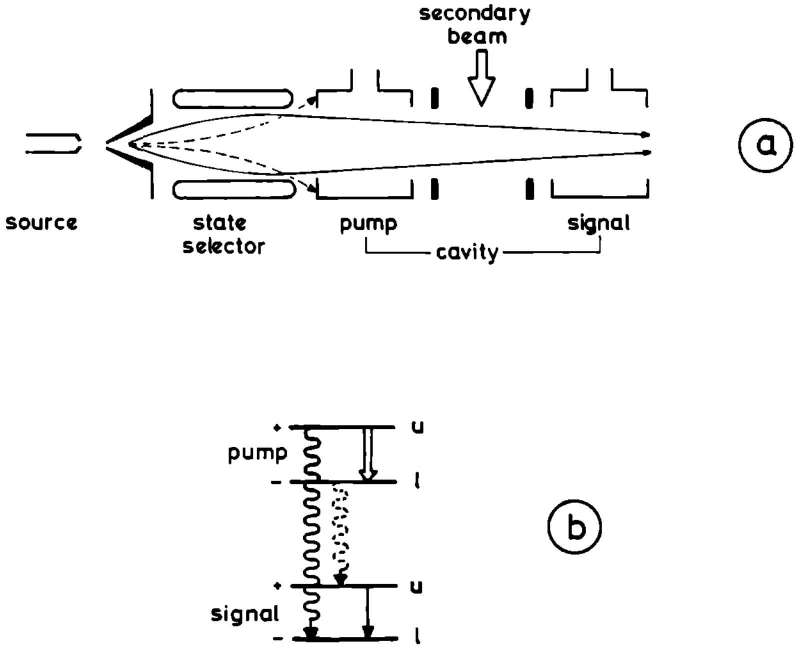

Figure 1: Schematic diagram (a) and simplified working principle (b) of the DR-BM experiment (see text). Plus and minus sign indicate the parity of the levels. Wavy arrows indicate collision-induced parity changing transitions.

the present contribution.

Development of powerful, stable and tunable lasers opens new, promising perspectives to determine state-to-state cross sections. Shimizu and co-workers[16,17] used N_2O-lasers combined with Stark tuning to pump and probe different rotational levels of ammonia in a double-resonance beam experiment. But as no secondary beam or scattering chamber is used, the relation between the measurements and the reported cross section[17] is far from clear. Other techniques involve optical lasers for sensitive state-selective detection via laser-induced fluorescence[18], sometimes combined with labelling of the initial quantum state by laser excitation[19]. These methods are not feasible for ammonia because tunable lasers are not available in the wavelength region of the electronic transitions of NH_3 (170-217 nm).

3. THE DOUBLE-RESONANCE BEAM MASER SCATTERING EXPERIMENT

A schematic diagram of the DR-BM set-up is given in Fig. 1a. A supersonic NH_3 beam produced by a nozzle-skimmer assembly is detected by the signal cavity tuned to the frequency of an inversion transition. The observed signal from this cavity is proportional to the difference between the populations of the upper and lower level of the specific inversion doublet. An electrostatic octopole is used as a state selector to focus the molecules in the upper levels (solid trajectories in Fig. 1a) and remove the molecules in the lower levels (dashed trajectories) of all inversion doublets from the beam. In this way the population difference of the beam molecules entering the cavity and hence the observed maser signal can be increased by several orders of magnitude. In order to perform scattering experiments with the beam maser a secondary beam is inserted between the state selector and the microwave cavity. Between the state selector and the secondary beam a second (pump) cavity is placed, tuned to an other (pump) inversion transition than the signal cavity. To explain the principle of the DR-BM experiment it is assumed that in normal operation of the beam maser the lower states of all inversion doublets, including the pump doublet, are completely depopulated. Moreover the assumption is made that by feeding power to the pump cavity (pumping), the total population of the upper level (u) can be transferred to the lower level (l) of the pump doublet. If only parity changing collision-induced transitions are allowed (wavy arrows in Fig. 1b), without pumping collisions will transfer molecules from the pump doublet to the lower signal level (solid wavy arrow). With pumping, however, molecules will be transferred from the pump doublet to the upper signal level (dashed wavy arrow). In the latter situation the population difference between upper and lower signal level and hence the signal intensity will be larger than in the situation without pumping.

The change in attenuated signal intensity caused by the pumping can be interpreted in terms of apparatus cross sections, i.e. differential cross sections for rotational transitions integrated over the acceptance angle of the microwave detector. By measuring the relative intensity changes as function of the secondary beam flow accurate values for the apparatus cross sections can be determined. Theoretical values for these cross sections are obtained by integration of the differential cross sections, after multiplication with a function called the apparatus function, that takes into account the angular resolution. Measurements, theoretical calculation of differential cross sections and the computation of the apparatus function are described in the next chapters.

4. OUTLINE OF THE PRESENT INVESTIGATION

Chapter 3 (paper II) contains a description of the experimental set-up and of the apparatus function and a derivation of the relation between relative intensity differences and rotational cross sections. For the polar scattering gases NH_3, CH_3F and CF_3H measurements are reported for collision-induced rotational transitions between a number of inversion doublets of ammonia. Transition probabilities are calculated in the low-order permanent-multipole interaction scheme using Anderson's theory combined with a proper treatment of the transition probabilities at small impact parameters. These transition probabilities are combined with the apparatus function via a deflection function. The resulting theoretical values for the apparatus cross sections are in good agreement with the experimental results. With integral cross sections, calculated with the same scattering theory, also a satisfying agreement with the experimental results of the steady-state double-resonance experiments of Oka[10] is obtained.

Experimental results for the scattering of ammonia with the nonpolar molecules CO_2, N_2 and H_2 are reported in Chapter 4 (paper III). The experimental results obtained for CO_2 and N_2 are compared with theoretical values, calculated with the same theory as used for the polar scattering gases. With molecular hydrogen as secondary beam gas, transition probabilities are evaluated using "bent" trajectories instead of the straight-path approximation. The short-range anisotropic repulsive potential for the system NH_3-H_2, which is found to be important for the explanation of the experimentally observed rotational cross sections, is not known to date. Two model functions for the anisotropic potential are introduced with parameters adapted to the experimental results. Integral rotational cross sections are calculated with these empirical potentials, which besides dipole-quadrupole and quadrupole-quadrupole interaction also contain induction and dispersion terms with a long-range R^{-7} dependence (R is the intermolecular distance). These integral cross sections give also a reasonable agreement with the results of Oka[10] and line broadening (Chapter 2) of NH_3 by H_2.

The present investigation shows that with the DR-BM set-up rotational cross sections in forward direction can be measured. For ammonia the first measurements of cross sections for a large number of collision-induced rotational transitions and scattering gases are reported. All the experimental results obtained with polar scattering gases are reproduced by theory, which demonstrates that the experiment is well-described by the present interpretation. The obtained NH_3-H_2 potential can be used for calculations of cross sections at (lower) astrophysically relevant velocities and also for other transitions. For the system ammonia-hydrogen the first state-to-state rotational cross sections are presented.

REFERENCES

1 A.C.Cheung, D.M.Rank, C.H.Townes, D.D.Thornton and W.J.Welch, Phys.Rev.Lett. 21, 1701 (1968)

2 M.Morris, B.Zuckerman, P.Palmer and B.E.Turner, Astrophys.J. 186, 501 (1973); P.R.Schwartz, A.C.Cheung, J.M.Bologna, M.F.Chui, J.A.Waak and D.Matsakis, Astrophys.J. 218, 671 (1977); G.Winnewisser, E.Churchwell and C.M.Walmsley, Astron.Astrophys. 72, 215 (1979)

3 A.C.Cheung, D.M.Rank, C.H.Townes, S.H.Knowles and W.T.Sullivan III, Astrophys.J. 157, L13 (1969)

4 G.Winnewisser, Colloquium on High Resolution Molecular Spectroscopy, Invited Paper, Tours, France (1979)

5 J.S.Sweitzer, Astrophys.J. 225, 116 (1978)

6 M.Morris, P.Palmer and B.Zuckerman, Astrophys.J. 237, 1 (1980); T.Pauls and T.L.Wilson, Astron.Astrophys. 91, L11 (1980)

7 P.R.Schwartz, Astrophys.J.Lett. 229, 45 (1979)

8 S.Green, J.Chem.Phys. 64, 3463 (1976); J.Chem.Phys. 70, 816 (1979); J.Chem. Phys. 73, 2740 (1980); S.L.Davis and J.E.Boggs, J.Chem.Phys. 69, 2355 (1978)

9 A.Dymanus, "Rotational collision cross sections: State of the art", Monograph, Fysisch Laboratorium, Katholieke Universiteit, Nijmegen, The Netherlands (1980)

10 T.Oka, "Collision-induced transitions between rotational levels", Advances in Atomic and Molecular Physics,Vol.9, Academic Press (1973)

11 J.P.Toennies, Disc.Faraday Soc. 33, 96 (1962); Z.Phys. 182, 257 (1965)

12 A.Dymanus, "Beam Maser Spectroscopy", International Review of Science, Physical Chemistry, Series 2, Vol.3, Ed.D.A.Ramsay, Buttersworths (1976); J.P.Gordon, H.J.Zeiger and C.H.Townes, Phys.Rev. 95, 282 (1954)

13 S.G.Kukolich, J.H.S.Wang and D.E.Oates, Chem.Phys.Lett. 20, 519 (1973);

K.R.Chien, P.B.Foreman, K.H.Castleton and S.G.Kukolich, Chem.Phys. 7, 161 (1975); J.R.Williams and S.G.Kukolich, J.Chem.Phys. 66, 251 (1977)

14 J.M.H.Reijnders, Thesis, Katholieke Universiteit, Nijmegen, The Netherlands (1978)

15 D.B.M.Klaassen, J.M.H.Reijnders, J.J.ter Meulen and A.Dymanus, J.Chem.Phys. 76, 3019 (1982)

16 F.Matsuhima, N.Morita, S.Kano and T.Shimizu, J.Chem.Phys. 70, 4225 (1979)

17 T.Shimizu, F.Matsuhima and Y.Honguh, page 212, Laser Spectroscopy V, Ed. A.R.W.McKellar, T.Oka and B.P.Stoicheff, Springer, New York (1981)

18 P.J.Dagdigian, B.E.Wilcomb and M.E.Alexander, J.Chem.Phys. 71, 1670 (1979); P.J.Dagdigian and B.E.Wilcomb, J.Chem.Phys. 72, 6462 (1980)

19 K.Bergmann, R.Engelhardt, U.Hefter and J.Witt, J.Chem.Phys. 71, 2726 (1979); K.Bergmann, U.Hefter and J.Witt, J.Chem.Phys. 72, 4777 (1980)

CHAPTER 2

BEAM MASER INVESTIGATION OF INELASTIC SCATTERING OF NH_3

I. CROSS SECTIONS FOR INVERSION TRANSITIONS INDUCED BY POLAR GASES

Beam maser investigation of inelastic scattering of NH_3 I. Cross sections for inversion transitions induced by polar gases

D B. M. Klaassen, J. M. H. Reijnders, J. J. ter Meulen, and A. Dymanus

Fysisch Laboratorium, Katholieke Universiteit Toernooiveld, 6525 ED Nijmegen, The Netherlands
(Received 23 July 1981, accepted 7 October 1981)

Cross sections for transitions across the inversion doublets $(J, K) = (1, 1), (2, 2), (3, 3)$, and $(6, 6)$, of NH_3 in collisions with NH_3, CF_3H, and CH_3F have been measured in a molecular beam maser The results are in good agreement with values calculated both in Anderson's theory and in first-order Born approximation A comparison is made with results of line broadening and transient experiments

I. INTRODUCTION

Extensive observations, following the discovery by Townes and collaborators,[1] have well established that relative intensities of inversion emissions of interstellar ammonia (NH_3) generally deviate from values expected for thermal equilibrium Several mechanisms have been proposed to explain these deviations [2,3] Nowadays it is generally accepted that collisional excitation by H_2, followed by radiative and collisional de-excitation is the most likely one The results of model calculations on this mechanism depend critically on the values of the collisional cross sections between inversion and rotation levels, which are unknown at the astrophysically relevant very low (10 K) temperatures Some information about collisional cross sections of NH_3 at higher temperatures (200–300 K) is available from line broadening at low and high (saturation) power densities, from transient nutation and double resonance experiments and from inelastic molecular beam scattering.

Extensive measurements on self and foreign-gas broadening of inversion transitions of ammonia have been performed by Bleaney and Penrose,[4–6] by Howard and Smith,[7] and more recently by Legan *et al* [8] From the line broadening constant Γ_{ij} obtained from such measurements, the cross section σ_{ij} for collisions between an absorbing molecule (i) and a perturbing molecule (j) is obtained using the relation

$$\sigma_{ij} = 2\pi \times 10^6 \frac{\Gamma_{ij}}{n_i \bar{v}_{ij}} \; [\mathrm{m}^2] , \tag{1}$$

with Γ_{ij} in MHz/Torr, $\bar{v}_{ij}$ (average relative velocity) in ms^{-1}, and n_i (molecular density at 1 Torr) in m^{-3}. In Table I are collected some representative values of the cross sections for a number of low (J, K) states and secondary molecules relevant for the present series of experiments. The experimental results on line broadening are usually confronted with some version of Anderson's theory of pressure broadening.[9] Murphy and Boggs[10] have shown that their version of the theory[11] with the two-level resonance concept provides a good over-all agreement with the experimental data both on self and foreign-gas broadening.

Linewidth measurements on pure rotational transitions are not known to date Measurements on self broadening of inversion-doubled vibrational–rotation bands have been performed by various groups [12–16] The resulting cross sections are essentially identical to the microwave cross sections and follow the same J and K dependence Margolis and Sarangi[14] have found, that if the temperature dependence of the cross sections is written as

$$\sigma_{ij}(T) = \sigma_{ij}(T_0)(T_0/T)^{(\alpha-1/2)} , \tag{2}$$

($T_0 = 300$ K) then for self broadening α varies from 0.45 to 2.0 (depending on the J and K of the lower level) and for hydrogen broadening from 0.20 to 0.87 with an average of 0.5 for T between 200 and 300 K. Schwartz[17] has proposed to use the relation (2) to extrapolate the cross section of Margolis and Sarangi to interstellar temperatures.

Broadening by hydrogen was found to be independent of J and K and the infrared value is (within the experimental errors) the same as the microwave value.[5,6,8] Recently, Oka has measured broadening by para ($J = 0$) and normal ($J \neq 0$) hydrogen of the (3, 3) and (4, 4) transitions in the microwave region and of the $\nu_1^2Q(3, 3)$ and $\nu_1^2Q(2, 2)$ infrared transitions.[16] Assuming that the cross sections are independent of J and K, and the type of transition, he obtained for para hydrogen a value of 0.21 and 0.22 nm^2 at $T = 294$ and 207 K, respectively, and for normal hydrogen 0.31 and 0.37 nm^2, respectively. The larger cross sections for normal hydrogen are ascribed to anisotropic forces.

It is well established that T_2, the relaxation time for the radiation induced macroscopic polarization of the gas, and T_1, the relaxation time for the return to equilibrium of the difference in population of the two levels involved in the transition, are not necessarily equal. Recent theories[18,19] of these relaxation processes predict for the inversion transition of ammonia $0 \leq T_2/T_1 \leq 2$ depending on the relative magnitude of the inversion rate k_{12}, the adiabatic rate k_a (reorientation and dephasing), and the rate k' to other doublets ($\Delta J \neq 0$ transitions) Since in first-order approximation parity conserving collisions are forbidden k_a will be small Due to the much larger energy defect for $\Delta J \neq 0$ transitions compared with inversion transitions $k_{12} \gg k'$. Consequently, T_2/T_1 should approach the value of two for the inversion transitions

Amano and Schwendeman performed extensive measurements and refined analysis of power-broadened line shapes in mixtures of $^{15}NH_3$–$^{15}NH_3$[20] and $^{15}NH_3$–H_2.[21]

TABLE I. Collision cross sections (in 10^{-20} m^2) obtained from microwave (M) and infrared (IR) line broadening (LB) and transient (TR) experiments at 300 K; $\sigma^{(1)}$ and $\sigma^{(2)}$ is the cross section derived from relaxation time T_1 and T_2, respectively; σ_{inv} is the cross section for inversion transitions J, $M=J\rightarrow J$, $M'=J$ as derived from $\sigma^{(1)}$ and $\sigma^{(2)}$ obtained in transient experiments.[23]

	NH_3						H_2			Ar	N_2	CO_2	CHF_2
	LB–M	LB–IR	LB–$\sigma^{(1)}$	TR–$\sigma^{(1)}$	TR–$\sigma^{(2)}$	TR–σ_{inv}	LB–M	LB–IR	LB–$\sigma^{(1)}$	LB–M	LB–M	LB–M	LB–M
(1, 1)	486(11)[a]		496(55)[a]	720(50)[c]	505(11)[,d] 440(22)[b]	215(52)	39[h]	36[h]	39(4)[a]		123[p]	180[p]	
(2, 2)	502(5)[e] 500[f]	518(10)[h] 470[j] 453[i]		790(40)[c]	560(11)[c]	230(42)[c]		42(2)[h] 30[l] 39(2)[q]			98[p]	170[p] 180(9)[e]	
(2, 1)	360[f] 330(7)[a]	365(21)[h] 340[j]	393(44)[a]	395(35)[c]	350(11)[c,d] 240(4)[m]	45(37)[c]	36(1)[n]	37(3)[h] 38(3)[q]	37(4)[a]				
(3, 3)	540(5)[e] 550(11)[a] 600[f]	536(20)[h] 490[j] 480[i]	775(86)[a]	1000(70)[c]	565(11)[c,d] 562(17)[b] 520(70)[m]	435(71)[c]	34(1)[n,o,l] 31(2)[e,p] 38[l] 27(1)[k]	40(1)[h] 39(1)[q] 31[l]	42(4)[a]	44(1)[k] 45[p]	93[p] 95(3)[k] 93(5)[e] 99(11)[o]	172(8)[e] 175(13)[o] 184(7)[k] 154[p]	845(42)[e] 570(17)[k]
(3, 2)	396(10)[e] 393(14)[a] 430[f]	400(55)[h] 390[j] 417[i]	473(52)[a]	680(36)[c]	430(11)[c,d] 375(1)[m] 430(30)[b]	250(38)[c]	37(1)[n]	38(1)[h,q] 30[l]	39(4)[a]		95[p]	144[p]	
(3, 1)	315[f] 290(8)[e]	310(22)[h,i] 280[j]						32(2)[h] 33(2)[q]					
(6, 6)	540(6)[e] 630[f]	590[h] 510[j] 490[i]			510(15)[m]		31(1)[a] 30(2)[e]	34[h,q] 30[l]		45[p]	85[p,k]	174(8)[e]	910(46)[e]

[a]Reference 20.
[b]Reference 27.
[c]Reference 23.
[d]Reference 24.
[e]Reference 8.
[f]Reference 4.
[h]Reference 14.
[i]Reference 15.
[j]Reference 12.
[k]Reference 7.
[l]Reference 6.
[m]Reference 26.
[n]Reference 21.
[o]Reference 46.
[p]Reference 47.
[q]Reference 13.

Their results for T_2 and a quantity called $(T_1/T_2)_0$ which should be very close (within 10%) to the real value of T_1/T_2, converted to the cross sections $\sigma^{(2)}$ and $\sigma^{(1)}$ according to

$$\sigma_{ij}^{(2)} = (nv_{ij} T_2)^{-1} , \qquad \sigma_{ij}^{(1)} = (T_1/T_2)_0^{-1} \sigma_{ij}^{(2)} , \tag{3}$$

are reproduced in Table I. The $\sigma^{(2)}$ values of Amano and Schwendeman for self- and hydrogen-broadening are in good agreement with the cross sections available from low power linewidth measurements.[4,6,8] The values of $\sigma^{(1)}$ are up to 60% higher than the $\sigma^{(2)}$ values and show a rather complicated J and K dependence.

Transient spectroscopy methods have been applied to study NH_3–NH_3 relaxation by various groups.[22-27] Some of the results for T_2 and T_1, converted to $\sigma^{(2)}$ and $\sigma^{(1)}$ are reproduced in Table I The measurements by Flygare's group[23,27] were all performed on the $M=J$ component. Hoke et al [25] performed extensive measurements on T_2 and T_1 for M components of the (2, 2) and (3, 3) states. The measurements showed that T_2 is independent of M, but T_1 is strongly dependent. The dependence could quite well be explained by Anderson's theory[9] modified for T_1, T_2 calculation, assuming only dipole–dipole interaction. The saturation experiments of Amano and Schwendeman[20] probed simultaneously all $|M|$ transitions in a (J, K) doublet and their analysis resulted in an M averaged quantity $(T_1/T_2)_0$.

Both Anderson's[9,25] and more recent theories of rotational relaxation[18,19] predict that

$$\sigma^{(1)} - \sigma^{(2)} = \sigma_{\text{inv}} , \tag{4}$$

with σ_{inv} the cross section for inversion transitions. The principal assumption underlying (4) is neglect of dephasing effects. The values of σ_{inv} for $M=M'=J$ obtained by Flygare's group are reproduced in Table I.

Hoke et al [24] have also determined T_2 and T_1 at two temperatures, 294 and 196 K (dry ice), for the (2, 2), (3, 2), (3, 3), and (4, 3) transitions. They found that for a given transition T_2/T_1 and the ratio of the values of T_2 at the two temperatures was about 1 5. Also these results could be explained with the modified Anderson's theory with only dipole–dipole interaction

Extensive collision–transfer studies on a large number of inversion doublets of NH_3 have been performed by Oka and his collaborators using steady-state microwave–microwave double-resonance (MM–DR) [28,29] The results of these studies show, that for NH_3–NH_3 and NH_3-polar gases (1) the preferred selection rules are of the dipole–dipole type ($\Delta J=0$, ± 1, $\Delta K=0$, parity $+ \leftrightarrow -$), (2) probability of the $\Delta J=0$ transitions ($\equiv \beta$) is much larger than of the $\Delta J=\pm 1$ ($\equiv \alpha$) transitions for $J=K$ but these become of the same order of magnitude for $J>K$, (3) probability of the $\Delta J=\pm 1$ parity changing ($\equiv \alpha$) and parity conserving ($\pm \to \pm$, $\equiv \gamma$) collisions is of the same order of magnitude; for NH_3–H_2 (4) most of the observed collision induced transitions also obey dipole-selection rules, (5) probability of $\Delta J=2$ collisions is about 0.2 relative to those with $\Delta J=1$, (6) $\Delta k=\pm 3$ collisions occur quite strongly for some doublets. It is very difficult to extract reliable information about individual transition rates from these measurements even when using information from line broadening. Anderson's theory applied to DR yielded a definitely poor agreement between the observed and calculated relative intensity changes $\Delta I/I$

Infrared–infrared and infrared–microwave double-resonance experiments have been performed on NH_3 by a number of groups.[30,31] In all these measurements the (8, 7), $v=0$ level was pumped with an N_2O laser and the effects of this pumping were observed at other $v=0$ inversion transitions. Kreiner et al.[31] conclude from extensive (also triple-resonance) measurements on 28 inversion doublets that only the effects on the (9, 7) and (7, 7) are collision induced, these on all other doublets are caused by heating effects.

Transient-nutation IM–DR experiments have been performed on NH_3 by Levy et al.,[32] Dobbs et al.,[33] and by Amano[20] using N_2O lasers pumping the (8, 7) doublet. The results for T_1 of the pumped level obtained in these measurements show rather large (factor ~ 4) differences.

Toennies[34] was the first to apply the electric beam resonance (EBR) technique to measure state-to-state collisional cross sections between rotational levels. The technique was applied to TlF and recently to CsF[35] scattered by various atoms and molecules. Unfortunately, the EBR technique is not easily applicable to NH_3 because of considerable loss in detection sensitivity for molecules which do not contain alkalis (or halides).

Development of stable and tunable optical lasers opened a new era in state-to-state collisional studies. Detection via laser-induced fluorescence[36] in combination with electrostatic state selection[37] or laser excitation labeling[38] is a very powerful method to study both total and differential cross sections. The technique cannot (yet) be applied to NH_3 because its lowest electronic transitions ($\tilde{A} - \tilde{X}$) are in the UV region (217–170 nm).

Kukolich and his co-workers have used a beam-maser spectrometer to measure T_2- and T_1-like cross sections (σ_{II} and σ_I, respectively, in the notation of Kukolich et al).[39] In these experiments transitions of NH_3 in a selected quantum state to other states, induced by collisions with secondary molecules, are measured by observing the change in the maser emission from the selected state. A single-cavity arrangement was used to obtain σ_I, and a two-cavity arrangement with the Ramsey separated field method[40] to obtain σ_{II}. Measurements have been performed on the (3, 2) and (7, 6) inversion transitions of NH_3 scattered by polar and nonpolar molecules.[39,41-43] The experimental results were analyzed using the Feynman–Vernon–Hellwarth vector representation[44] and related via the coefficients of the relaxation matrix to those of the scattering S matrix.[41,45] The relations for the cross sections are

$$\sigma_I = \sigma_s + 2\sigma_{\text{inv}} , \qquad \sigma_{II} = \sigma_s + \sigma_{\text{inv}} . \tag{5}$$

Herein σ_s is the cross section for combined elastic and inelastic scattering over an angle larger than Θ_R, the

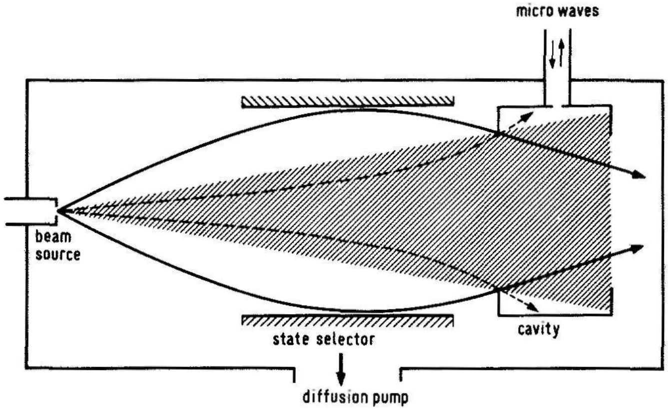

FIG. 1. Schematic diagram of a beam maser spectrometer. The grey area gives the beam reaching the detector in the absence of state selection. The solid and dashed curves represent the limiting trajectories of a molecule in the upper and the lower state, respectively, reaching the detector in the presence of state selection.

angular resolution; σ_{inv} is the cross section for inelastic scattering across the inversion doublet over angles smaller than Θ_R. For large values of Θ_R the value of σ_{inv} should approach the value of $\sigma^{(1)}$ obtained in power broadening experiments if adiabatic collisions are neglected.

In the investigation reported in this paper a set-up similar to the one cavity arrangement of Kukolich is used to obtain σ_{inv} for NH_3-polar gases collisions. Instead of a scattering chamber a secondary beam was used to simplify the analysis of the results. Corrections are made for finite angular resolution via calculated differential cross sections. The results are compared with predictions from both Anderson's theory and the first-order Born approximation. In subsequent papers results will be reported on σ_{inv} for NH_3-nonpolar (including H_2) collisions and on rotational cross sections obtained with a double-resonance beam-maser technique.

II. THE BEAM MASER SCATTERING MACHINE

The principle of operation of a beam maser spectrometer is well known and documented.[48] Only a brief summary is given below for the sake of nonspecialists.

A molecular beam (Fig. 1) passes through a state selector, for polar molecules usually an electrostatic n pole, and a resonant region, at microwave frequencies normally a resonant cavity. The cavity field induces transitions between molecular levels whose energy difference (divided by h) equals the resonance frequency of the cavity. These transitions result in a change in the power reflected (or transmitted) by the cavity, that is proportional to the difference in the population of the levels involved. Normally the population distribution of the molecular levels is thermal and the relative population difference between two neighboring levels can be 10^{-2}–10^{-4}. This results in poor sensitivity in beam absorption experiments at microwave frequencies. The function of a state selector is to transmit to the cavity molecules, for example, in the upper state and reject those in the lower state of the transition. In an ideal situation the beam entering the cavity consists only of molecules in the upper state and all these molecules may contribute to the (emission) transition signal. The gain in sensitivity due to state selection can easily be a few orders of magnitude.

In the present investigation an ammonia beam maser is converted into a scattering machine by inserting a secondary beam, which crosses the primary ammonia beam perpendicularly after the state selector. In the following some features of the machine, schematically depicted in Fig. 2 are described.

The ammonia beam is formed by a nozzle–skimmer assembly. The nozzle itself is just a small hole drilled in a thin brass foil (0.025 mm). With nozzle orifices in the range of 30–80 μ it is possible to obtain a stable beam at stagnation pressures up to 2000 Torr and background pressures of 2.10^{-4} Torr. The skimmers are truncated cones, machined from brass with a full cone angle of 90° and diameters of about 1 mm. The skimmer is fixed in the wall separating the nozzle exhaust chamber and the (first) buffer chamber. The molecular beam is modulated at 120 Hz by a mechanical chopper mounted directly behind the skimmer.

Velocity distribution measurements performed on the NO scattering machine in our laboratory[49] yield already at moderate pressures a most probable velocity in the ammonia beam of 1080 ms^{-1}, in agreement with the assumption of complete isentropic expansion. A univelocity beam at 1080 ms^{-1} in the maser is assumed in theoretical considerations. This assumption is confirmed by a matching dependence of the microwave line intensities on the Stark voltage applied to the state selector (Fig. 3) and the fact that attenuation measurements are in agreement with Beer's law. In this assumption thermalizing collisions among the primary ammonia molecules can be neglected. The measured relative intensities on different inversion levels correspond with a rotational temperature of about 95 K.

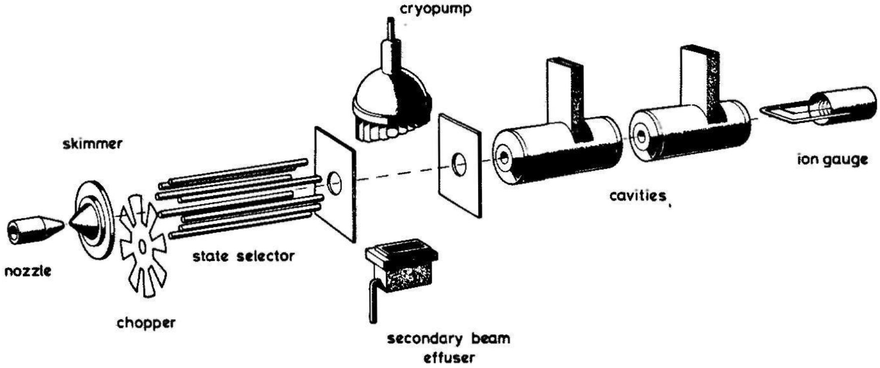

FIG. 2. Artist's view of the beam maser scattering set-up.

In the first buffer chamber the state selector, consisting of two octopoles, is placed 5.5 cm from the source. The electrodes, polished stainless steel rods 2.5 mm in diameter, 26.5 (octopole 1), and 26.9 cm (octopole 2) long, are arranged symmetrically on a cylinder with a diameter of 10 mm. The distance between neighboring rods is 2 mm. The selector is surrounded by a liquid nitrogen trap, yielding a background pressure in the order of 10^{-7} Torr. Breakdown typically occurred at 40 kV. As the static electric field increases in a direction perpendicular to the beam axis, ammonia molecules in upper inversion states are forced towards the selector axis, while those in the lower states are deflected out of the beam (Fig. 1). The resulting microwave line intensity is determined by the efficiency of these two actions. As both the sensitivity and the angular resolution of the microwave detector depend on the operation of the state selector calculations on the trajectories of the molecules through the state selector are carried out. These are described in the next section.

The secondary beam, formed by a multichannel array, crosses the primary beam in the second buffer chamber. The fused glass capillary array (Mosaic Inc.) consists of about 8.10^{6} channels with a mean diameter (2a) of 5.5 μ at a transparency of 50%. The length of the capillaries is 3.2 mm, yielding a length to radius ratio of 1164. The array is 46 mm long in the direction of the primary beam and 8 mm wide. The distance from the primary beam axis is 20 mm and the angle of incidence of the secondary beam is 90°. The distance between the exit opening of the state selector and the middle of the secondary beam is 70 mm. The multi-channel array is used because the primary beam in a maser is fairly broad. The total flow rates through the multi-channel array are monitored with an absolute flow meter (Brooks). For the secondary beam gases NH_3, CH_3F, and CF_3H the applied flow, corresponding with an attenuation of the primary beam over roughly one decade, ranges from 2.5×10^{17} to 3.5×10^{18} mol s^{-1}. The mean free path λ of the molecules at the inlet of the effuser varies between 0.013 and 0.21 mm. The capillaries are therefore driven in the opaque mode. The intensity distribution in this mode is taken from Zugenmaier.[50] The numerical results[51] are found to be in good agreement with measurements done by Beijerinck[52] except for small angles. The calculations show that the angular

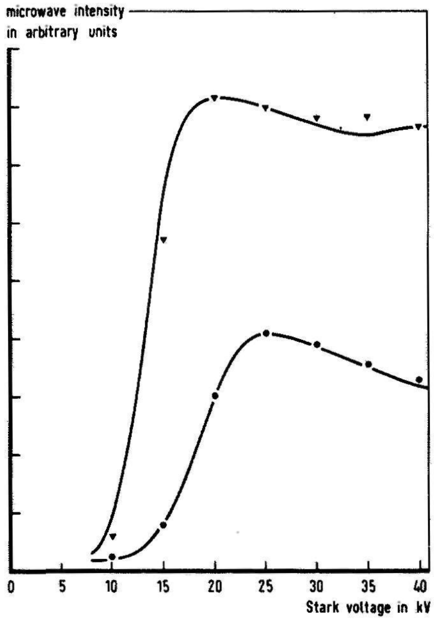

FIG. 3. Measured (solid curves) and calculated (points) microwave line intensity as a function of Stark voltage for the $(J, K) = (1, 1)$ level (solid circles) and (2, 2) level (triangles) with the cavity in frontside position.

distribution at angles larger than 2° is independent of the flow intensities and gases used. As the attenuation measurements have been performed with fairly broad primary beams, these measurements are not sensitive to changes of the angular distribution at smaller angles. For the same reason in our calculations the velocity distribution of the secondary beam is assumed to be Maxwellian at room temperature for all angles.

The secondary beam molecules are pumped by a cryopump attached to the bottom of a Leybold 500 ℓ/s Klipping Verdampferkryostat (VMK 500).[48] The cryopump consists of a number of thin walled copper pipes directed to the effuser in order to form an optically closed structure in two directions. The length of the cryopump pipes increases from the top to the bottom ensuring a stable operation, without pressure bursts due to detachment of "ice" or "frost" of secondary beam molecules. A pumping speed of 10^6 ℓ/s^{-1} and a background pressure of 5×10^{-7} Torr with secondary beam on have been achieved. Influx of radiation heat is prevented by a closely fitting cylindrical shield and gold plating of the cryo-assembly. The shield carries the secondary beam source and contains two diaphragms, 10 cm apart and with a diameter of 8 mm, through which the primary beam enters and leaves the scattering region. In this way, the scattering region is well defined and separated from the radiative zone in the microwave cavity.

In the detector chamber two microwave cavities and an ion gauge (to monitor the total beam) are placed All cavities used in the present experiment were cylindrical reflection type cavities oscillating in the TM_{010} mode. The length of the cavities is 16 cm The beam entrance and exit holes have diameters of 4 mm. Cavities are placed at distances of 48 cm (front side position) and 65.5 cm (backside position) from the exit opening of the state selector. This set-up allows simultaneous measurements with two different angular resolutions of 0.28° and 0.20° in the laboratory system. The angular resolution of the ion gauge is 0.15°. A superheterodyne system requiring only a single klystron is used in the present investigation. This klystron is stabilized using a combined Schomandl, Rohde, and Schwarz frequency synthesizing system SRS.[53] This system is locked to a Rhode and Schwarz XSRM Rubidium frequency standard. By comparing the measured signal to noise ratios for the various inversion transitions with a theoretical expression, the rotational temperature in the primary ammonia beam is determined to be 95(10)K.

III. STATE SELECTION

Calculations on the trajectories of the ammonia molecules through the state selector are required for two reasons: (1) to predict the number of molecules in a specific state passing through the microwave cavity per second in order to evaluate the theoretical expression for the signal to noise ratios and (2) to describe the scattering process Inside the state selector the inversion doublet levels of the ammonia molecules are characterized by the rotational quantum numbers J, K, M_J, according to the strong field case. The transitions detected in a beam maser, however, are those between the hyperfine sublevels $|F, M_F\rangle$. The used coupling scheme of angular momenta is $\mathbf{J}+\mathbf{I}_N=\mathbf{F}_1$ and $\mathbf{F}_1+\mathbf{I}_H=\mathbf{F}$, where $\mathbf{I}_N$ is the spin of the nitrogen nucleus and $\mathbf{I}_H$ is the total nuclear hydrogen spin. So, the relevant hyperfine states must be correlated with the rotational substates determining the molecular trajectories through the state selector. It is assumed that the population of the closely spaced hyperfine levels due to hydrogen spins is randomized by transitions induced by Fourier components of the state selector field as seen by the molecule. Therefore, only the quadrupole $|F_1, M_{F_1}\rangle$ substates are relevant in the correlation. From the field-free quadrupole splitting, weak field Stark effect calculations and the noncrossing rule the following correlation between the quadrupole $|F_1, M_{F_1}\rangle$ and rotational $|J, K, M_J\rangle$ substates can be derived for the upper inversion level (notation F_1, $|M_{F_1}| \text{—} |M_J|$):

$$
\begin{array}{lll}
J,\ J \text{—} J-\tfrac{1}{2}+\tfrac{1}{2}Z_{JK}\,, & J+1,\ J+1 \text{—} J\,, & J-1,\ z \text{—} z-Z_{JK}\,,\\
J,\ z \text{—} z+Z_{JK}\,, & J+1,\ J \text{—} J-\tfrac{1}{2}-\tfrac{1}{2}Z_{JK}\,, & J-1,\ 0 \text{—} \tfrac{1}{2}-\tfrac{1}{2}Z_{JK}\,,\\
J,\ 0 \text{—} \tfrac{1}{2}+\tfrac{1}{2}Z_{JK}\,, & J+1,\ z \text{—} z\,, & \\
 & J+1,\ 0 \text{—} 0,\ 1\,, &
\end{array}
$$

with $z=1, 2, \ldots, J-1$ and $Z_{JK}=[3K^2-J(J+1)]/[|3K^2-J(J+1)|]$.

The results of a computer program solving the differential equations that describe the motion of the ammonia molecules in the state selector show that within the acceptance angle of the cavity the population of the lower inversion state is unaffected. So there is no need for the correlation in the lower inversion levels. In the (assumed) field free region between the state selector and the cavity, all degenerate M_{F_1} substates are mixed up and each $(F_1, M_{F_1} \text{—} M_J)$ correlation gets the same weight

$$\rho(F_1, M_{F_1} \text{—} M_J)=\frac{1}{2F_1+1}\ . \tag{6}$$

The weighted correlation between the quadrupole $|F_1, |M_{F_1}|\rangle$ and rotational $|J, K, |M_J|\rangle$ substate is obtained by taking the summation $\sum_{M_{F_1}}\rho(F_1, |M_{F_1}| \text{—} |M_J|)$. Multiplying with $|\mu_{F_1F_1}|^2$ and summing over F_1 gives finally the relative contribution $W(J, |M_J|)$ of a J, M_J-trajectory to the microwave signal. Herein $\mu_{F_1F_1}$ stands for the electric dipole moment matrix element for a $\Delta F_1=0$ transition.

As the measured linewidth of the monitored $\Delta F_1=\Delta F$

$=0$ component was nearly equal to the expected linewidth of a single line under the present experimental conditions and as the stimulating power was kept far below saturation, the gain in microwave intensity $I(V)$ of the $\Delta F_1 = \Delta F = 0$ component because of the state selector operating at a voltage V, can be written as

$$\frac{I(V)}{I(0)} = \frac{\sum_{F_1}[N_{F_{1u}}(V) - N_{F_{1l}}(V)]h\nu_{JK}|\mu_{F_1F_1}|^2}{|\sum_{F_1}[N_{F_{1u}}(0) - N_{F_{1l}}(0)]h\nu_{JK}|\mu_{F_1F_1}|^2|} \quad . \qquad (7)$$

Herein the summation is over all the unresolved quadrupole hyperfine components of the studied main line, $N_{F_{1u,l}}(V)$ and $N_{F_{1u,l}}(0)$ represent the flow of ammonia molecules in the particular quadrupole hyperfine upper (u) or lower (1) state through the microwave cavity with and without state selection, respectively; ν_{JK} is the transition frequency. As $N_{F_{1l}}(V) \simeq N_{F_{1l}}(0)$ and ν_{JK} is in the microwave region, the following expression is obtained for the normally well satisfied condition $[I(V)/I(0)](kT/h\nu_{JK})^{-1} \gg 1$

$$\frac{I(V)}{I(0)} \simeq \frac{\sum_{|M_J|\neq 0} W(J, |M_J|) N_{|M_J|u}(V)}{\sum_{F_1} |\mu_{F_1F_1}|^2 N_{F_{1l}}(0)} \left(\frac{kT}{h\nu_{JK}}\right) \quad , \qquad (8)$$

where T is the temperature determining the relative population difference of the inversion states at thermal equilibrium; $N_{|M_J|u}(V)$ represents the number of NH_3 molecules in the relevant rotational substates leaving the state selector within the acceptance angle of the cavity.

In Fig. 3 the measured microwave line intensities as function of the Stark voltage for the (1, 1) and (2, 2) inversion lines are compared with the values obtained with Eq. (8) using the computer program for trajectory calculations to evaluate $N_{|M_J|u}(V)$. The calculations were performed with 200 initial trajectories for each rotational $|J, K, |M_J|\rangle$ substate assuming a monochromatic beam and neglecting the fringing fields. The number of trajectories contributing to the calculated microwave line intensities was about 100. The good agreement between the calculations and the measurements demonstrated in Fig. 3 proves that the trajectory calculations are reliable. From the calculated trajectories the radial distribution of the ammonia molecules in the upper inversion state in front of the secondary beam is calculated (Fig. 4). This information is used to describe the scattering process.

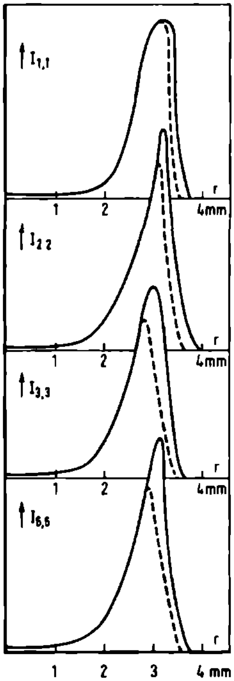

FIG. 4. Radial distribution of ammonia molecules in the upper states of the (1, 1), (2, 2), (3, 3), and (6, 6) inversion doublets in front of the secondary beam, contributing to the microwave signal The solid and dashed curves represent the distribution for the cavity in frontside, and backside position, respectively

IV. THE RELATION BETWEEN MEASURED ATTENUATION AND CROSS SECTIONS

The interpretation of the microwave line and total beam attenuations in terms of total (in)elastic collision cross sections is complicated for three reasons. (1) a broad primary beam and a rather low angular resolution of the microwave detector compared with standard scattering experiments, (2) a wide effusive secondary beam, resulting in a larger scattering region, and (3) interwoven elastic and inelastic effects. The following illustrates the extent of problems associated with (3). A collision induced transition from the upper to the lower level of an inversion doublet within the opening angle of the detectors, will not change the total beam intensity, but diminishes the microwave line intensity (proportional to the difference in the population of the upper and lower level) twice ! The same collision but with an angular deflection outside the opening angle does change the total beam intensity and reduces the microwave line intensity by only one unit. Total cross sections obtained from so called "apparatus cross sections" via angular resolution corrections are rather unreliable.[38,41,43] In the present investigation the scattering data in the maser are related to theoretical differential cross sections by an apparatus function $G(v_{rel}, \Theta_{cm})$, which, for each relative velocity v_{rel}, represents the averaged probability that a molecule which is scattered over an angle Θ_{cm} in the center-of-mass system will, enter the detector.

It is assumed that the inversion transitions are dominant over the rotational transitions and that the elastic differential cross section does not depend on the specific inversion level upper or lower. The microreversibility property[54] for scattering implies that the inelastic differential cross sections from the upper to the lower level and vice versa are nearly the same. To simplify the construction of the apparatus function the assumption is made that the lower state molecules have

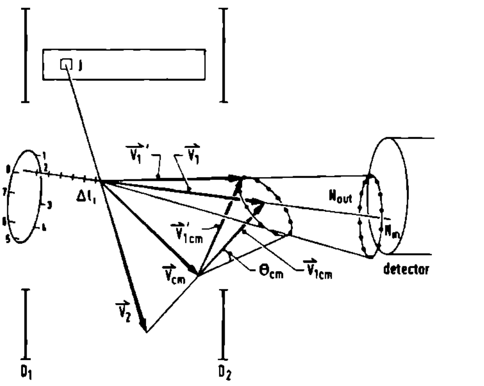

FIG. 5 Transformation of the laboratory to the center-of-mass frame. The ratio N_{in}/N_{out} gives the numerical value of $[\int_{id}(d\varphi_{cm}/2\pi)]_{\vartheta_{cm} ijv_2}$ (see the text). D_1 and D_2 is the entrance and exit diaphragm, respectively, of the scattering region.

the same trajectories through the scattering region as the upper state molecules. Trajectories of molecules in the lower state are in fact quite different from those in the upper state. Because of the large population differences the uncertainty introduced by this approximation is well below the experimental errors. Fig. 4 shows that the primary beam is fairly broad in front of the secondary beam source. Therefore, in the construction of the apparatus function the primary beam is represented by eight line beams, passing through the secondary beam at a radial distance corresponding to the maximum in the radial distribution. The beams form edges of a regular octagonal pyramid with the base at the exit of the state selector and the top near the detector. For each line beam a different apparatus function is constructed. These eight apparatus functions are afterwards averaged, resulting in one function for the total primary beam. Each line beam is divided into equal sections along the length of the scattering region. The effuser surface is also divided into equal areas each represented by one channel in its center (Fig. 5). The flow pattern of this channel is given by the flow per channel in the opaque mode.[50]

The density of secondary beam molecules, coming with velocity $\mathbf{v}_{2ij}$ within Δv_2 from a specific effuser channel j at a specific section i on a line beam is given by

$$n_{v_2}(r_{ij}) = I(\hat{v}_{2ij}) P(v_2) \frac{\Delta v_2}{r_{ij}^2 v_2} \quad , \tag{9}$$

where $I(\hat{v}_{2ij})$ is the secondary beam intensity in the direction $\hat{v}_{2ij}$, $P(v_2)$ is the Maxwellian velocity distribution, and r_{ij} is the distance between channel j and point i on the line beam. The probability per traveled section Δl_i for a primary beam molecule with velocity $\mathbf{v}_1$ to collide with a secondary beam molecule with velocity $\mathbf{v}_{2ij}$ and to be deflected into $d\Omega$ in the direction $(\vartheta_{cm}, \varphi_{cm})$ in the center-of-mass system is

$$I(\hat{v}_{2ij}) P(v_2) v_{rel} \left[\frac{d\sigma}{d\Omega}(\vartheta_{cm}, \varphi_{cm})\right]_{v_{rel} ij} d\Omega \, \frac{\Delta v_2 \Delta l_i}{r_{ij}^2 v_2 v_1} \quad , \tag{10}$$

where $\mathbf{v}_{rel} = \mathbf{v}_2 - \mathbf{v}_1$ and $[d\sigma/d\Omega(\Theta_{cm}, \varphi_{cm})]v_{rel}ij$ is the relevant differential cross section. If we neglect double collisions (attenuation measurements in agreement with Beer's law), summation over all chosen subareas on the effuser and intervals Δv_2, yields for the change ΔN_{u_i} of primary molecules in the upper inversion level per section Δl_i[55].

$$\Delta N_{u_i} = \sum_{j,v_2} I(\hat{v}_{2ij}) P(v_2) v_{rel} \frac{\Delta v_2 \Delta l_i}{r_{ij}^2 v_2 v_1} \Bigg(-N_{u_i} \sigma^{tot}(v_{rel}) + 2\pi \int d\vartheta_{cm} \sin\vartheta_{cm} \Bigg\{ N_{u_i} \left[\frac{d\sigma^{el}}{d\Omega}(\vartheta_{cm})\right]_{v_{rel}} + N_{l_i} \left[\frac{d\sigma^{inel}}{d\Omega}(\vartheta_{cm})\right]_{v_{rel}} \Bigg\} \left(\int_{id} \frac{d\varphi_{cm}}{2\pi}\right)_{\vartheta_{cm} ijv_2} \Bigg) \tag{11}$$

Herein σ^{tot} is the sum of the integral elastic (el) and inelastic (inel) cross section. The subscript id (inside detector) under the integration sign indicates that the integral is confined to those angles, which correspond to trajectories through the detector after the collision. The assumption is made that the differential cross sections do not depend on φ. A similar expression is obtained for ΔN_{l_i} by replacing all indices u by l and vice versa. The resulting differential equations $d/dl\,(N_u \pm N_l)$ can be solved for each line beam,

$$(N_u \pm N_l) = (N_u \pm N_l)_0 \exp\Bigg[-\sum_{ijv_2} I(\hat{v}_{2ij}) P(v_2) v_{rel} \frac{\Delta v_2 \Delta l_i}{r_{ij}^2 v_2 v_1} \times \Bigg\{ \sigma^{tot}(v_{rel}) - 2\pi \int d\vartheta_{cm} \sin\vartheta_{cm} \left[\frac{d\sigma^{el}}{d\Omega}(\vartheta_{cm}) v_{rel} \pm \frac{d\sigma^{inel}}{d\Omega}(\vartheta_{cm}) v_{rel}\right] \left(\int_{id} \frac{d\varphi_{cm}}{2\pi}\right)_{\vartheta_{cm} ijv_2} \Bigg\}\Bigg]. \tag{12}$$

For each choice of i, j, v_2 and a fixed angle ϑ_{cm} the Newton diagram relating the laboratory and center of mass velocities is completely determined. The integral $[\int_{id}(d\varphi_{cm}/2\pi)]\ \vartheta_{cm} ijv_2$ can be calculated by stepping on a cone with top angle ϑ_{cm} around $\mathbf{v}_1 - \mathbf{v}_{cm}$ and checking if the resulting $\mathbf{v}_1'$ (after the collision) will give a trajectory through the detector (Fig. 5). Each choice of i, j, and v_2 in the sum of Eq. (12) gives a certain value of v_{rel}. To avoid calculation of differential cross section for every v_{rel}, the calculations are done only for discrete values $v_{rel,m}$. Now the linear interpolation

$$\frac{d\sigma}{d\Omega}(\vartheta_{cm}, v_{rel}) = \frac{v_{rel,m+1} - v_{rel}}{\Delta v_{rel}} \frac{d\sigma}{d\Omega}(\vartheta_{cm}, v_{rel,m}) + \frac{v_{rel} - v_{rel,m}}{\Delta v_{rel}} \frac{d\sigma}{d\Omega}(\vartheta_{cm}, v_{rel,m+1}) \ , \tag{13}$$

with $\Delta v_{rel} = v_{rel,m+1} - v_{rel,m}$ and $v_{rel,m} \leq v_{rel} \leq v_{rel,m+1}$ is used to rearrange the sum over i, j, and v_2 in a sum over only the relative velocity. For a line beam the resulting function $G(v_{rel,m}, \vartheta_{cm})$, in the following called apparatus function, is

$$G(v_{\mathrm{rel},m},\vartheta_{\mathrm{cm}})=\sum_{ijv_2}\left[1-\frac{|v_{\mathrm{rel}}-v_{\mathrm{rel},m}|}{\Delta v_{\mathrm{rel}}}\right]I(\vartheta_{2ij})P(v_2)\times v_{\mathrm{rel}}\frac{\Delta v_2\Delta l_i}{r_{ij}^2 v_1 v_2}\left(\int_{id}\frac{d\varphi_{\mathrm{cm}}}{2\pi}\right)_{\vartheta_{\mathrm{cm}} ij v_2}, \tag{14}$$

where negative terms are dropped. In terms of this apparatus function Eq. (12) for the difference between (sum of) the numbers of molecules in the upper and lower state, that are entering the detector per second on a line beam, is given by

$$(N_u\pm N_l)=(N_u\pm N_l)_0\exp\Biggl(-\sum_{v_{\mathrm{rel},m}}G(v_{\mathrm{rel},m},0)\Biggl\{\sigma^{\mathrm{tot}}(v_{\mathrm{rel},m})-2\pi\int d\vartheta_{\mathrm{cm}}\sin\vartheta_{\mathrm{cm}}\frac{G(v_{\mathrm{rel},m},\vartheta_{\mathrm{cm}})}{G(v_{\mathrm{rel},m},0)}\times\left[\frac{d\sigma^{\mathrm{el}}}{d\Omega}(\vartheta_{\mathrm{cm}},v_{\mathrm{rel},m})\pm\frac{d\sigma^{\mathrm{inel}}}{d\Omega}(\vartheta_{\mathrm{cm}},v_{\mathrm{rel},m})\right]\Biggr\}\Biggr). \tag{15}$$

Herein $G(v_{\mathrm{rel},m},0)$ results from the fact that in forward direction ($\vartheta_{\mathrm{cm}}=0$) the integral $\int_{id}(d\varphi_{\mathrm{cm}}/2\pi)$ is equal to unity.

For each rotation state $|J,K\rangle$ and each beam p of the eight line beams, representing the primary beam, the apparatus function $G^p_{JK}(v_{\mathrm{rel}},\vartheta_{\mathrm{cm}})$ is different. The attenuated microwave intensity I_{JK} is proportional to

$$I_{JK}\div\sum_{p=1}^{8}(N_u-N_l)^p_{JK}, \tag{16}$$

where the summation involves the eight line beams. For $(N_u-N_l)^p_{JK}$ Eq. (15) has to be substituted with the apparatus function $G^p_{JK}(v_{\mathrm{rel}},\Theta_{\mathrm{cm}})$ for the specific line beam p. This procedure is called post-averaging. The unattenuated intensities of the line beams are equal because of the cylindrical symmetry of the primary beam. The corresponding expression for the attenuated total beam intensity I_{TB} is

$$I_{\mathrm{TB}}\div\sum_{JK}\sum_{p=1}^{8}(N_u+N_l)^p_{JK}, \tag{17}$$

where the first summation is over the population distribution of inversion–rotational states in the primary beam, determined by the rotational temperature in the beam and the state selector efficiencies. Numerical calculations wherein an apparatus function averaged over the different line beams

$$G_{JK}(v_{\mathrm{rel}},\vartheta_{\mathrm{cm}})=\frac{1}{8}\sum_{p=1}^{8}G^p_{JK}(v_{\mathrm{rel}},\vartheta_{\mathrm{cm}}), \tag{18}$$

was used for *each* line beam instead of the corresponding apparatus function $G^p_{JK}(v_{\mathrm{rel}},\vartheta_{\mathrm{cm}})$, yielded within 2% the same attenuations as in the case of post-averaging. Using this preaveraged apparatus function the summation over p in Eqs (16) and (17) gives a factor 8 and the integrations of differential cross sections have to be done only once instead of eight times In order to reduce computation time preaveraged apparatus functions (Fig 6) are used in the calculations. As stated in Sec. II, the angular *and* velocity distribution of the secondary beam are independent of the flow. So the apparatus function depends linearly on the flow and it is sufficient to perform the calculations for only one flow value.

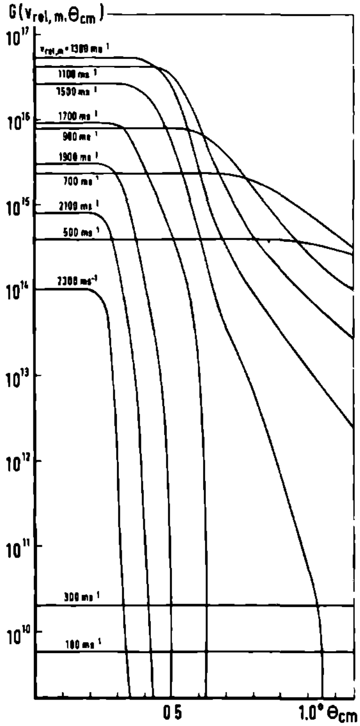

FIG. 6. Apparatus function (in m^{-2}) for the (1,1) cavity in front-side position and a secondary beam of ammonia molecules.

From Eqs. (15)–(17) the expressions for the attenuated microwave and total beam intensities are

$$I_{JK}=I^0_{JK}\exp\Biggl\{-\sum_{v_{\mathrm{rel},m}}(n_2l)_{JK,v_{\mathrm{rel},m}}\left[\sigma^{\mathrm{tot}}_{JK}(v_{\mathrm{rel},m})-\sigma^{\mathrm{el}}_{JK,\mathrm{app}}(v_{\mathrm{rel},m})+\sigma^{\mathrm{inel}}_{JK,\mathrm{app}}(v_{\mathrm{rel},m})\right]\Biggr\}, \tag{19}$$

and

$$I_{\mathrm{TB}}=I^0_{\mathrm{TB}}\exp\Biggl\{-\sum_{v_{\mathrm{rel},m}}\langle(n_2l)_{JK,v_{\mathrm{rel},m}}\rangle\left[\langle\sigma^{\mathrm{tot}}_{JK}(v_{\mathrm{rel},m})\rangle-\langle\sigma^{\mathrm{el}}_{JK,\mathrm{app}}(v_{\mathrm{rel},m})\rangle-\langle\sigma^{\mathrm{inel}}_{JK,\mathrm{app}}(v_{\mathrm{rel},m})\rangle\right]\Biggr\}, \tag{20}$$

where

$(n_2l)_{JK,v_{\mathrm{rel},m}}=G_{JK}(v_{\mathrm{rel},m},0)\sim$ secondary beam flow,

and

$$\sigma^{(\mathrm{in})\mathrm{el}}_{JK,\mathrm{app}}(v_{\mathrm{rel}})=2\pi\int d\vartheta_{\mathrm{cm}}\sin\vartheta_{\mathrm{cm}}\frac{G_{JK}(v_{\mathrm{rel},m},\vartheta_{\mathrm{cm}})}{G_{JK}(v_{\mathrm{rel},m},0)}\frac{d\sigma^{(\mathrm{in})\mathrm{el}}_{JK}}{d\Omega}. \tag{21}$$

The brackets $\langle\ \rangle$ stand for a pre-averaging over the rotational states J and K It has to be emphasized that for the cavity in front, respectively backside position and total beam detector different apparatus functions have to be used. The extraction of cross sections, σ_{JK} for the microwave signal and σ_{TB} for the total beam signal, directly from the attenuation measurements is performed using the relations

$$I_{JK} = I^0_{JK} \exp[-(n_2 l)_{JK,\mathrm{eff}}\, \sigma_{JK}] \tag{22}$$

and

$$I_{\mathrm{TB}} = I^0_{\mathrm{TB}} \exp[-(n_2 l)_{\mathrm{TB,eff}}\, \sigma_{\mathrm{TB}}] , \tag{23}$$

where the index eff(ective) stands for a summation over v_{rel} and σ_{JK} and σ_{TB} are regarded as taken at the mean relative velocity:

$$\sigma_{JK} = \sigma^{\mathrm{tot}}_{JK} - \sigma^{\mathrm{el}}_{JK,\mathrm{app}} + \sigma^{\mathrm{inel}}_{JK,\mathrm{app}} , \tag{24}$$

$$\sigma_{\mathrm{TB}} = \langle\sigma^{\mathrm{tot}}_{JK}\rangle - \langle\sigma^{\mathrm{el}}_{JK,\mathrm{app}}\rangle - \langle\sigma^{\mathrm{inel}}_{JK,\mathrm{app}}\rangle . \tag{25}$$

V. THEORY

Most of the experimental investigations of collision induced population transfer in ammonia were, until now, line broadening experiments. Results were usually compared with calculations following Anderson's theory.[9–11,56] For that reason the same theory is also used in this paper, although it has two disadvantages: (1) the result is a transition probability as a function of the impact parameter, instead of a differential cross section and (2) an elastic differential cross section cannot be obtained. To account for these drawbacks inelastic *and* elastic differential cross sections are derived in the first Born approximation for dipole–dipole scattering

In Anderson's theory[65] the total transition probability at impact parameter b and relative velocity v_{rel} for a collision involving two (1, 2) symmetric top molecules, regarding only low order multipole moments, is[57]

$$P_T^{l_1 l_2}(b) = 2C_l^2 \sum_{J_1' K_1' J_2' K_2'} (2J_1'+1)(2J_2'+1) \times \begin{pmatrix} J_1 & l_1 & J_1' \\ -K_1 & 0 & K_1' \end{pmatrix}^2 \begin{pmatrix} J_2 & l_2 & J_2' \\ -K_2 & 0 & K_2' \end{pmatrix}^2 f_l(\omega\tau) , \tag{26}$$

where C_l is a dimensionless constant given by

$$C_l = \frac{Q_{l_1} Q_{l_2} 2^l (l-1)!}{4\pi\epsilon_0 \hbar v_{\mathrm{rel}} b^l \sqrt{(2l_1+1)!\,(2l_2+1)!}} \tag{27}$$

and $f_l(\omega\tau)$ is the so-called resonance function, as tabulated by Tsao and Curnutte[56]:

$$f_l(\omega\tau) = \frac{1}{2} \sum_{m=-1}^{+1} \left[\frac{2}{2^l (l-1)!} \times \sqrt{\frac{(2l)!}{(l+m)!\,(l-m)!}}\, (\omega\tau)^l K_m(\omega\tau) \right]^2 . \tag{28}$$

In these formulas J_i and K_i are the quantum numbers of the symmetric tops involved, primes indicate the situation after the collision; Q_{l_i} is a molecular multipole, K_m is a modified Bessel function, $\hbar\omega$ is the gain in kinetic energy, and $\tau = b/v_{\mathrm{rel}}$. In the case of rigid nonoverlapping charge distributions (long-range interactions) only the maximum value of $l = l_1 + l_2$ occurs. The polar symmetric top molecules, used as secondary beam gases, have nonzero multipole-moment matrix elements for $\Delta J_2 = 0$. This type of transitions will be dominant in the secondary beam molecule as follows from the resonance function $f_l(\omega\tau)$. The beam maser is only sensitive for changes in a particular internal state of the ammonia molecule (suffix 1). The target molecules (suffix 2) are assumed to form a Boltzmann distribution over the rotation (inversion) states. In that case Eq. (26) can be approximated by

$$P_T^{l_1 l_2}(b) = 2C_l^2 \sum_{J_1'} (2J_1'+1) \begin{pmatrix} J_1 & l_1 & J_1' \\ -K_1 & 0 & K_1 \end{pmatrix}^2 \times \left\langle (2J_2'+1) \begin{pmatrix} J_2 & l_2 & J_2' \\ -K_2 & 0 & K_2 \end{pmatrix}^2 \right\rangle f_l(\omega\tau) , \tag{29}$$

where the brackets $\langle\ \rangle$ denote Boltzmann averages. For molecules with a symmetry axis the Boltzmann averages are given by

$$\langle F(J,K)\rangle = \frac{\sum_{J=0}^{\infty} \sum_{K=-J}^{J} F(J,K)(2J+1) \exp\{-[BJ(J+1) + (C-B)K^2]h/kT\}}{\sum_{J=0}^{\infty} \sum_{K=-J}^{J} (2J+1) \exp\{-[BJ(J+1) + (C-B)K^2]h/kT\}} . \tag{30}$$

From Eq. (26) it follows that in the permanent multipole interaction scheme the dipole and quadrupole moments of ammonia will lead to the selection rules

$$|\Delta J_1| = |J_1 - J_1'| \le l_1,$$

$$J_1 + J_1' \ge l_1,$$

$$\Delta K_1 = 0 .$$

In addition to these quantum number selection rules, there is the parity selection rule

$$+ \longleftrightarrow - \quad \text{for odd } l_1 , \qquad \begin{matrix} + \longleftrightarrow + \\ - \longleftrightarrow - \end{matrix} \quad \text{for even } l_1 .$$

Transitions with $\Delta K = \pm 3$ can be caused by the permanent octopole and the distortion dipole moment of ammonia. The leading terms to cause these transitions, however, will be provided by induction and dispersion forces. So the $\Delta K = \pm 3$ collision induced transitions are only feasible in fairly hard collisions.

The transition probability is related to the inelastic cross sections measured in the maser by Eq. (21):

$$\sigma^{\mathrm{inel}}_{JK,\mathrm{app}}(v_{\mathrm{rel}}) = 2\pi \int_0^{\infty} P_{JK}^{l_1 l_2}(b) \frac{G_{JK}[v_{\mathrm{rel}}, \vartheta_{\mathrm{cm}}(b, v_{\mathrm{rel}})]}{G_{JK}(v_{\mathrm{rel}}, 0)}\, b\,db , \tag{31}$$

where $P_{JK}^{l_1 l_2}(b)$ represents the term with $(J_1', K_1') = (J_1, K_1) \equiv (J, K)$ in the summation in Eq. (29), depending also on the relative velocity, and $G_{JK}[v_{rel}, \vartheta_{cm}(b, v_{rel})]$ is the apparatus function introduced in Sec. IV. To evaluate Eq. (31) a relation between the deflection angle ϑ_{cm} and the impact parameter b is needed. Averaged over all possible orientations the classical deflection function for two nonrotating dipoles μ_1 and μ_2 in the impulse approximation can be written as[58]

$$\vartheta_{cm}(b, v_{rel}) = \frac{\pi^2}{8} \frac{\mu_1 \mu_2}{4\pi\epsilon_0 (\frac{1}{2}\mu v_{rel}^2)} b^{-3} , \tag{32}$$

where μ is the reduced mass. Since no better deflection function is available for collisions involving symmetric top molecules this $\vartheta_{cm}(b, v_{rel})$ is used for the calculation of $\sigma_{JK,app}^{inel}(v_{rel})$ according to Eq. (31). Because it cannot be greater than unity, $P_{JK}^{l_1 l_2}(b)$ is set equal to unity for impact parameters smaller than b_1, where b_1 is solved by iterative solution of $P_{JK}^{l_1 l_2}(b_1) = 1$. These approximations have been successfully applied to pressure broadening of ammonia,[9,10] and should even better describe the results obtained in the beam maser, because in the interpretation using Anderson's theory only inelastic effects in small angle (large impact parameter) scattering are taken into account.

In order to obtain directly the angular distribution of the (in)elastic scattering it is necessary to include the relative translational motion in the quantum mechanical calculations. This is done using the Born approximation, which gives for the differential cross section for the collision induced transition $n \to n'$

$$\frac{d\sigma}{d\Omega_{n'n}}(\vartheta, \varphi) = \frac{k_n'}{k_n} |f_{n'n}(\vartheta)|^2 , \tag{33}$$

where k_n and k_n' are the wave vectors of the relative motion of the two molecules before and after the collision, respectively, and $f_{n'n}(\vartheta)$ is the scattering amplitude. In evaluating this scattering amplitude the following restrictions have to be made: (1) the scattering takes place for large impact parameters or large angular momentum (l) values resulting in small deflection angles and (2) the transfer of collisional angular momentum and translational energy is small. Three intervals of angular momentum values are considered:

(1) $l > l^*$, where l^* is determined by the following relation for the T matrix elements

$$\sum_{n' l' m_1' 0} |T^{(Born)}_{n'nl'l^*m_1'0}|^2 = 1 . \tag{34}$$

(2) $l^{**} < l \le l^*$, the angular momentum l^{**} is determined by the condition

$$|T_{n'nl'l^{**}m_1'0}|^2_{rot\ chan} \simeq |T_{n'nl'l^{**}m_1'0}|^2_{inv\ chan} \tag{35}$$

(3) $l < l^{**}$.

In the interval $l > l^*$ (soft collisions) the T matrix elements are calculated using the first Born approximation. For $l < l^*$ (hard collisions) the Born approximation breaks down. In the region $l^{**} < l < l^*$ all inversion channels are equally probable and the random phase approximation is used, with

$$T_{n'nl'lm_1'0} = \frac{\exp(i\varphi_{n'nl'lm_1'0})}{\sqrt{N_{0_i}}} - \delta_{n'n}\delta_{l'l}\delta_{m_1'0} , \tag{36}$$

wherein $\varphi_{n'nl'lm_1'0}$ is a function which varies rapidly with l and the energy, and N_{0_i} is the number of open inversion channels. Both inversion and rotation channels are open in the interval $l > l^{**}$, but the probability of a rotation excitation is at least one order of magnitude below the inversion transition probability. Therefore only inversion channels are effectively open, and contribute to the summation in Eq. (34). In the region $l < l^{**}$ inversion and rotational transitions become equally important. Because the number of open channels becomes very large the T matrix can be approximated by

$$T_{n'nl'lm_1'0} \simeq -\delta_{n'n}\delta_{l'l}\delta_{m_1'0} . \tag{37}$$

This implies that for large scattering angles the elastic differential cross section exceeds its inelastic counterpart. With these approximations straightforward calculations[57,58] yield the following result for the differential cross section in first order Born approximation for the case of dipole–dipole interaction.

$$\frac{d\sigma}{d\Omega_{n'n}}(\vartheta) = \left[\frac{l^{**}}{k_n} \frac{J_1(l^{**}\vartheta)}{\vartheta} \delta_{n'n}\right]^2 + \frac{1}{5} \sum_{m_1'=-2}^{+2} \frac{1}{k_n^2} \int_{l^{**}}^{l^*} J^2_{m_1'}(l\vartheta)\, l^2\, dl + (2J_1'+1) \begin{pmatrix} J_1 & 1 & J_1' \\ -K_1 & 0 & K_1 \end{pmatrix}^2$$
$$\times \left\langle (2J_2'+1) \begin{pmatrix} J_2 & 1 & J_2' \\ -K_2 & 0 & K_2 \end{pmatrix}^2 \right\rangle 6 \left[\frac{(l_0^2/k_n) x_0^2}{x_0^2 + l_0^2 \vartheta^2}\right]^2 \sum_{m_1'=-2}^{+2} \frac{[l^*\vartheta K_{m_1'}(x^*) J_{m_1'-1}(l^*\vartheta) + x^* K_{m_1'-1}(x^*) J_{m_1'}(l^*\vartheta)]^2}{(2-m_1')!\,(2+m_1')!} . \tag{38}$$

where J_i denotes a Bessel function and $x = l\Delta x/k_n$; l_0 and so x_0 are defined in terms of the interaction strength of the involved dipole moments μ_i and the relative velocity v_{rel}

$$l_0 = k_n \sqrt{\frac{2}{3} \frac{\mu_1 \mu_2}{4\pi\epsilon_0} \frac{1}{\hbar v_{rel}}} ; \tag{39}$$

the brackets denote again Boltzmann averages over the secondary beam molecules [Eq. (30)].

As the value of the collision angular momentum l^{**} is about an order of magnitude smaller than l^*, the second term in Eq. (38), representing an extra contribution to the inelastic differential cross section due to inversion transitions, is primarily determined by l^*. The first term in Eq. (38) stands for the contribution to the differential cross section of the elastic diffraction scat-

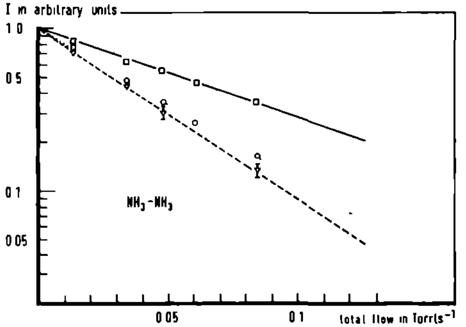

FIG. 7. Attenuation of the total beam intensity (squares and solid line) and of the inversion line intensities of the $(J, K) = (1, 1)$ level (circles and dotted line) and the (6, 6) level (triangles and dashed line), as a function of the NH_3 flow through the effuser (cavity in backside position). Vertical bars represent three standard deviations

tering. This scattering is strongly peaked in the forward direction, because the de Broglie wavelength $\lambda = h/\mu v_{rel}$ of the system is small compared to the characteristic elastic collision diameter $d^* = 1^*/k_n$. The last term in Eq. (38) is the contribution of inelastic scattering at large impact parameters. Since the dipole–dipole interaction is of extremely long range and only inelastic collisions are allowed for a pure dipole–dipole intermolecular potential, the peaking of the inelastic differential cross section in forward direction is even stronger than in the case of elastic collisions.

VI. EXPERIMENTAL RESULTS AND INTERPRETATION

For accurate measurements of the attenuation of the microwave and total beam intensity a digital measuring procedure with the aid of a minicomputer (PDP/11E10) has been developed. In order to minimize the influence

TABLE II. Direction coefficients in Torr^{-1} l^{-1} s of the "best" straight lines as discussed in the text. Errors are based on three standard deviations.

		Secondary beam molecule		
	(J, K)	CH_3F	CF_3H	NH_3
Frontside position	(1,1)	34.6(7)	55.5(11)	20.5(4)
	(2,2)	28.4(13)	52.7(11)	21.2(6)
	(3,3)	29.3(7)	56.2(15)	22.5(3)
	(6,6)	33.0(12)	64.3(46)	23.4(20)
Backside position	(1,1)	34.7(8)	56.8(11)	21.5(4)
	(2,2)	29.5(7)	55.0(11)	22.6(9)
	(3,3)	31.7(8)	60.0(14)	23.3(6)
	(6,6)	33.4(13)	63.9(18)	24.0(25)
Ion gauge		19.4(4)	29.3(9)	12.5(3)

TABLE III. Acceptance angles in the center-of-mass system (in degrees).

	Secondary beam molecule		
	CH_3F	CF_3H	NH_3
Frontside position	0.42	0.35	0.56
Backside position	0.29	0.24	0.39
Ion gauge	0.23	0.19	0.31

of inevitable drift effects such as thermal instabilities of the resonant cavities, primary and secondary beam fluctuations, this procedure consists of a repetition of a certain number of steps in reflection symmetric sequence. Each step is defined by the setting of a number of experimental conditions, such as: secondary beam on/off; beam stop in front of the ion-gauge in/out. The base-line intensity of the microwave signal is measured by shifting the frequency of the source klystron by 48 to 300 kHz. This is done by coupling a low frequency signal (16–100 kHz) to the 10 MHz reference signal used for the klystron stabilization. The signals of the microwave power detector and the ion-gauge are fed into phase sensitive detectors, whose output is sampled by A/D converters with a gate of 10 s. After each step the digital results are transferred to the disk unit of the computer. Delay times between the steps are chosen long enough to account for RC effects caused by the phase sensitive detectors (RC times are 1 s) and for stabilization of the secondary beam flow.

Attenuation measurements up to one decade were performed on metastable inversion levels of both the spin modifications, the (1, 1) and (2, 2) para ($I_H = \frac{1}{2}$) and the (3, 3) and (6, 6) ortho ($I_H = \frac{3}{2}$) levels. The main line resulting from transitions $\Delta F_1 = \Delta F = 0$ is taken as a representative for each inversion level $|J, K\rangle$, i.e., it is assumed that the collision-induced inversion transition probabilities do not depend on the hyperfine levels involved. This assumption is justified by the fact that the quadrupole hyperfine splitting of the inversion levels[59] is small compared to the Stark effect in the electric field of the perturbing molecule. Secondary beam gases used were CH_3F, CF_3H and NH_3. Figure 7 shows a typical plot of the microwave line and total beam intensities for NH_3–NH_3 scattering.

The measured microwave and total beam signal attenuations, plotted on a logarithmic scale versus the secondary beam flow, are fitted by a straight line according to Eqs. (22) and (23). The results obtained in terms of direction coefficients of the "best" straight lines are summarized in Table II. The apparatus cross sections σ_{JK} and σ_{TB} depend on the angular resolution and involve both elastic *and* inelastic effects. From Table II it is clear that the variations in microwave line attenuation for the different inversion doublets (J, K) are significant. The results obtained for the two positions of the microwave cavity differ at most 6%. The weak dependence of the microwave cross section on the angular resolution (Table III) can be understood from Eq. (24). This equation shows that the microwave cross sec-

TABLE IV. Permanent multipole moments of the secondary beam molecules.

Secondary beam molecule	Dipole moment in D	Quadrupole moment in 10^{-26} esu
NH_3	1.476(2)[b]	−2.92(8)[c]
CH_3F	1.8584(5)[d]	−1.4[a]
CF_3H	1.6512(5)[d]	3 6[a]

[a]Reference 60.
[b]Reference 61
[c]Reference 62.
[d]Reference 63.

tion is sensitive to the acceptance angle via the difference between elastic and inelastic effects, which compensate each other. The direction coefficients for the microwave line attenuations are roughly twice those obtained for the total beam attenuation This difference originates from the last two terms in Eq. (25). The fact that the logarithm of the attenuation is proportional to the secondary beam flow confirms that the apparatus function depends linearly on the secondary beam flow. Furthermore, it indicates that the secondary beam molecules are properly trapped by the cryopump and double collisions do not occur.

In the following the results are confronted with the predictions of Anderson's theory and Born approximation. Anderson's theory does not supply elastic cross sections. To extract information from the measurements about the inelastic cross section alone, the following assumptions have to be made: (1) the collision cross sections depend only weakly on the rotational quantum numbers and (2) the microwave cavity and the ion gauge have the same angular resolution Although in practice the acceptance angles of the microwave cavities and ion gauge are different (Table III) the latter assumption is quite reasonable because of the weak dependence of the microwave attenuation on the angular resolution (Table II). With these assumptions the expression for the ratio of attenuated microwave line and total beam signal is [Eqs. (19), (20), and (31)]

$$\frac{I_{JK}}{I_{TB}}=\frac{I^0_{JK}}{I^0_{TB}}\exp\left\{-4\pi\sum_{v_{\rm rel,m}}\int db\,bG_{JK}[v_{\rm rel,m},\vartheta(b,v_{\rm rel})]\times P_{JK}(b,v_{\rm rel,m})\right\}. \quad (40)$$

Herein $P_{JK}(b, v_{\rm rel,m})$ is the inversion transition probability summed over the dipole–dipole and dipole–quadrupole term of the multipole expansion (Table IV). The deflection function $\vartheta_{\rm cm}(b, v_{\rm rel})$ is given by Eq. (32) where the dipole moment of the primary ammonia and the secondary beam molecule is replaced by the matrix element for the studied inversion and rotational levels, respectively. The latter matrix element is also averaged over a Boltzmann distribution at room temperature [see Eq (30)]. In analogy with Eqs. (22) and (23) an inelastic apparatus cross section is defined by the relation

$$\frac{I_{JK}}{I_{TB}}=\frac{I^0_{JK}}{I^0_{TB}}\exp[-2(n_2 l)_{JK,\rm eff}\,\sigma^{\rm inel}_{JK,\rm app}]\,. \quad (41)$$

In Table V the theoretical predictions for I_{JK}/I_{TB} resulting from Eq. (40) are compared with the experimental results for the cavity in the backside position, where the difference in angular resolution between the cavity and the ion gauge is smaller (see Table III) Except for the (1, 1) transition in collisions with CH_3F (to be discussed in the next section) the comparison shows an excellent agreement between theoretical and experimental values.

For the comparison with the Born approximation the experimental attenuations are interpreted in terms of (in)elastic cross sections for the studied inversion level of ammonia assuming that the collision induced inversion transitions are dominant over rotational transitions. Differential (in)elastic cross sections for small angle dipole–dipole scattering [Eq. (38)] are substituted into the expressions for the signal attenuations [Eqs. (19) and (20)]. Values of the relevant multipole moments used in the calculations are given in Table IV, while the Boltzmann averages of the multipole moment matrix elements are taken according to Eq. (30). The resulting

TABLE V. Comparison between experiment and Anderson's theory All cross sections are in 10^{-20} m^2 Errors are based on three standard deviations

Secondary beam molecule and flow in Torr l s^{-1}	Inversion line (J, K)	I_{JK}/I_{TB} Measured	I_{JK}/I_{TB} Calculated Eq. (40)	$\sigma^{\rm inel}_{JK,\rm app}$ measured Eq. (41)	$\sigma^{\rm inel}_{JK}$ $2\pi\int_0^\infty P_{JK}(b)\,b\,db$
NH_3	(1,1)	0.728(12)	0 719	111(6)	446
0.0335	(2,2)	0 701(22)	0 718	134(12)	516
	(3,3)	0 685(15)	0.651	140(8)	548
	(6,6)	0 670(56)	0 634	141(29)	586
CF_3H	(1,1)	0 704(13)	0.758	192(10)	566
0.01225	(2,2)	0 720(13)	0.755	191(10)	655
	(3,3)	0 678(14)	0.698	213(11)	696
	(6,6)	0 645(16)	0 677	241(14)	745
CH_3F	(1,1)	0.715(13)	0 823	156(8)	352
0.020	(2,2)	0 804(16)	0 822	108(10)	408
	(3,3)	0.769(14)	0.777	122(8)	433
	(6,6)	0 745(21)	0.765	138(13)	465

TABLE VI. Comparison between theory and experiment in the framework of the Born approximation for the cavity in backside position. All cross sections in 10^{-20} m^2. Errors are based on three standard deviations

Secondary beam molecule and flow in Torr l s^{-1}	Inversion level $(J\ K)$	$\bar{v}_{rel}$ (m s^{-1})	I_{JK}/I^0_{JK} Measured	I_{JK}/I^0_{JK} Calculated Eq. (19)	I_{TB}/I^0_{TB} Measured	I_{TB}/I^0_{TB} Calculated Eq. (20)	σ_{JK} Eq. (22)	σ_{TB} Eq. (23)	Theoretical integral cross sections (Born approximation) σ^{tot}_{JK}	σ^{inel}_{JK}	σ^{el}_{JK}
NH_3 0.0335	(1, 1)	1288	0.487(7)	0.533	0.658(5)	0.625	505(9)	300(6)	418	299	119
	(2, 2)		0.469(14)	0.486			573(22)		515	366	149
	(3, 3)		0.458(9)	0.444			578(14)		563	399	164
	(6, 6)		0.448(37)	0.391			565(59)		622	439	183
CF_3H 0.01225	(1, 1)	1134	0.499(7)	0.506	0.698(8)	0.624	763(15)	395(13)	712	493	219
	(2, 2)		0.510(7)	0.493			787(15)		782	541	241
	(3, 3)		0.480(8)	0.457			805(19)		808	559	249
	(6, 6)		0.457(10)	0.443			860(24)		836	579	257
CH_3F 0.020	(1, 1)	1189	0.499(8)	0.662	0.678(5)	0.698	647(15)	362(7)	368	260	108
	(2, 2)		0.554(8)	0.619			586(14)		458	322	136
	(3, 3)		0.530(8)	0.571			591(15)		499	350	149
	(6, 6)		0.513(13)	0.539			622(24)		550	385	165

theoretical attenuations are compared with the experimental values in Table VI. As in the comparison with Anderson's theory only the (1, 1) transition in the NH_3–CH_3F system shows a significant deviation. For the other transitions and scattering gases the theoretical and experimental values are in good agreement. The comparison is given only for the cavity in backside position. Theory and experimental results for the cavity in frontside position agree equally well. All comparative calculations are only necessary at one setting of the flow, because the apparatus function is proportional to the flow and the measured signal attenuations depend exponentially on the secondary beam flow.

VII. DISCUSSION

In view of the assumptions made, the agreement between the experimental results and Anderson's theory is remarkably good (Table V). This agreement is partly due to the fact that for the interpretation only inelastic collisions in forward direction are taken into account [Eqs. (40) and (41)]. These collisions with large impact parameters and small transition probabilities are well described by Anderson's theory combined with the classical deflection function. Calculations performed with this theory applied to rotational transitions yield cross sections which are at least an order of magnitude smaller than the cross sections for inversion transitions. Only for the system NH_3–CH_3F the cross sections for rotational transitions between the $(J, K) = (1, 1)$ and (2, 1) levels, seem to be larger. This is confirmed by preliminary results of experiments on collision induced rotational transitions, to be reported in a following communication. Calculations and preliminary results confirm the validity of the assumption of an isolated inversion doublet made to derive the formula for the attenuated intensities in the maser [Eqs. (19) and (20)] The discrepancy between experimental results and predictions of Anderson's theory found for CH_3F on the (1, 1) level (Table V) is most probably caused by resonant rotational transitions, which are not taken into account in the interpretation.

In comparing the experimental results with the Born approximation, the full dependence of the cross sections on the rotational quantum numbers J, K is regarded and the angular resolution is properly taken into account. For NH_3–NH_3 and NH_3–CF_3H the agreement of the theory with the experimental results is quite satisfactory (Table VI). Apparently NH_3–NH_3 and NH_3–CF_3H scattering is well-described by a dipole–dipole intermolecular potential. For NH_3–CH_3F the explanation for the discrepancy between theory and experimental results on the $(J, K) = (1, 1)$ level is the same as with Anderson's theory. For the other levels there are small systematic deviations towards too small theoretical cross sections. This may be due to the fact that at room temperature only states with low values of K are populated in the prolate symmetric top CH_3F, yielding a small effective dipole moment. So for CH_3F higher-order multipole interactions should be included in future calculations. This explanation is confirmed by the fact that with Anderson's theory, with dipole–dipole and dipole–quadrupole interaction, no deviations are found.

The rotational dependence of the microwave line attenuations measured at different inversion levels is in agreement with the theoretical predictions. For the total beam attenuation the agreement of theory with experimental results is almost as satisfactory as for the microwave line attenuation (Table VI) Inspection of Eqs. (24) and (25) shows that the total beam attenuation is more sensitive to the angular resolution. Moreover, the total beam attenuation must be averaged in the theoretical calculations over the population distribution in the primary beam. In the actual calculations only the metastable levels $J = K = 1$, 2, 3 and 6 are involved in this (post-)averaging procedure.

In Tables V and VI the calculated integral (in)elastic and total cross sections are given as well. Comparison of the results for σ^{inel}_{JK} obtained with Born's, respectively Anderson's theory, shows that the latter predicts too large inelastic cross sections. The dipole–quadrupole interaction, which is only taken into account in Anderson's theory, contributes at most 10% to the cross section. However, at small impact parameters the transition probabilities calculated in a straight path approximation become too large, leading to unreliable integral cross sections. Independently of the angular resolution

TABLE VII. Integral cross sections (in 10^{-20} m^2) calculated in Born approximation and converted to the relative velocities in a gas cell at 300 K.

	(J, K)	σ_{JK}^{el}	σ_{JK}^{inel}
NH_3	(1,1)	177	446
	(2,2)	222	545
	(3,3)	244	595
	(6,6)	273	654
CF_3H	(3,3)	413	928
	(6,6)	427	961

(frontside, respectively backside), the apparatus cross sections σ_{JK} for scattering with NH_3 and CF_3H are close to the sums (σ_{JK}^{tot}) of the calculated integral elastic and inelastic cross sections. According to Eq. (24) this implies that $\sigma_{JK,app}^{inel}$ and $\sigma_{JK,app}^{el}$ are approximately equal over the range of applied acceptance angles. The calculated integral cross sections σ_{JK}^{inel} and σ_{JK}^{el} differ, however, by an amount of about 200×10^{-20} m^2 which is approximately equal to half the value of σ_{JK}^{inel}. This leads to the conclusion that for dipole–dipole scattering at least half of the inelastic collisions result in deflection angles larger than 0.2° (in the laboratory system). This conclusion is confirmed by the fact that $\sigma_{JK,app}^{inel}$ (Table V) is much smaller (about 50%) than σ_{JK}^{inel} (Table VI). Hence incomplete inelastic cross sections are measured in the maser, making it difficult to compare the experimental results directly with the outcome of other experiments.

The results for σ_{JK} and σ_{TB} should be compared with σ_I and σ_{BAM} of Wang *et al.*[41] and Williams *et al.*[43] Comparison with the results of Wang *et al.* is complicated by the uncertainty in their angular resolution (about 0.5° in the laboratory system) and the use of an effusive primary beam, which results in a large spread of relative velocities and a lower mean relative velocity. Therefore it is not surprising that the results they obtained on the $(J, K) = (3, 2)$ and (7, 6) inversion transitions differ 30% (their uncertainty) with the results given in Table VI. Nevertheless the dependence on the scattering gases and rotational quantum numbers (larger cross sections for higher inversion levels) is the same. Williams *et al.* used a primary nozzle beam and their results for the $(J, K) = (3, 2)$ level are quite close to the results of this investigation for NH_3–NH_3. Their observation, that σ_I (or σ_{JK}) is insensitive to the angular resolution (Θ_R) over a range from 0.2° to 1.5° in the laboratory system, is confirmed for a small part of the range (0.20°–0.28°) by the experimental results and theoretical calculations reported in this paper. This insensitivity implies that the difference between $\sigma_{JK,app}^{inel}$ and $\sigma_{JK,app}^{el}$ should be constant within the experimental error over the applied range of Θ_R. It was shown above that for (NH_3–NH_3) scattering with $\Theta_R = 0.2°$ $\sigma_{JK,app}^{inel} - \sigma_{JK,app}^{el}$ was roughly 200×10^{-20} m^2 smaller than $\sigma_{JK}^{inel} - \sigma_{JK}^{el}$ for all investigated inversion levels, there is no reason to expect a different behavior for the (3, 2) state. From this result combined with the implication of the observation of Williams *et al.* follows that even at $\Theta_R = 1.5°$ $\sigma_{JK,app}^{inel} - \sigma_{JK,app}^{el}$ is significantly smaller than $\sigma_{JK}^{inel} - \sigma_{JK}^{el}$. This would lead to the conclusion that quite a large part of the collisions result in deflection angles even larger than 1.5° for NH_3–NH_3, which is in contradiction with the assumptions made by Williams *et al.* to explain the coincidence of σ_I (or σ_{JK}) and the line broadening data.

As the integral cross sections calculated in Born approximation can be regarded as experimentally confirmed, they can be confronted with the results of line broadening and transient experiments. In Table VII the values for σ_{JK}^{el} and σ_{JK}^{inel} from Table VI are given, converted to the relative velocity in a gas cell ($\sigma \sim v^{-1}$). The values of $2\sigma_{JK}^{inel}$ should be equal to the results of transient T_1 experiments (fourth column of Table I). The M dependence of the latter complicates the comparison. Nevertheless the calculated $2\sigma_{JK}^{inel}$ values are about 20% too large, but the (J, K) dependence is correct. The results of line broadening and transient T_2 experiments (columns one and two, respectively five of Table I) should be compared with the sum of σ_{JK}^{inel} and the cross section for "adiabatic" collisions.[18,19,64] Comparison of Table I with Table VII shows that σ_{JK}^{inel} is within 10% of the results of line broadening and transient experiments, while the sum of σ_{JK}^{inel} and σ_{JK}^{el} differs roughly 30% from these results. This leads to the conclusion that the "adiabatic" cross section is not identical with the quite large elastic cross section involved in the maser experiments.

The experiment reported in this paper shows the feasibility of measuring inelastic cross sections in forward direction in a beam maser. Although comparison with theoretical predictions is quite complicated, both Anderson's and Born's theory fit with the experimental results. The outcome of the latter theory agrees with the results of line broadening and transient experiments as well, which are, however, somewhat ambiguously related to the collision cross sections as measured in the maser.

[1]A. C. Cheung, D. M. Rank, C. H. Townes, D. P. Thornton, and W. J. Welch, Phys. Rev. Lett. **21**, 1701 (1968).

[2]T. Oka, F. O. Shimizu, T. Shimizu, and J. K. G. Watson, Astrophys. J. **165**, 15 (1971). T. Oka, Mémoires Societé Royale des Sciences de Liège, 6e Série, tome III (1972), p. 37.

[3]A. C. Cheung, D. M. Rank, C. H. Townes, S. H. Knowles, and W. T. Sullivan, Astrophys. J. **157**, 13 (1969).

[4]B. Bleaney and R. P. Penrose, Proc. R. Soc. London **189**, 358 (1947).

[5]B. Bleaney and R. P. Penrose, Proc. Phys. Soc. London **60**, 83 (1948).

[6]B. Bleaney and R. P. Penrose, Proc. Phys. Soc. London **60**, 540 (1948).

[7]R. R. Howard and W. V. Smith, Phys. Rev. **79**, 128 (1950); **79**, 132 (1950).

[8]R. L. Legan, J. A. Roberts, E. A. Rinehart, and C. C. Lin, J. Chem. Phys. **43**, 4337 (1965).

[9]P. W. Anderson, Phys. Rev. **76**, 647 (1949).

[10]J. S. Murphy and J. E. Boggs, J. Chem. Phys. **50**, 3320 (1969).

[11]J. S. Murphy and J. E. Boggs, J. Chem. Phys. **47**, 691 (1967).

[12](a) W. S. Benedict, E. K. Plyler, and E. D. Tidwell, J.

Res. Natl. Bur Stand. 61, 123 (1958); (b) J. Chem Phys 29, 829 (1958)
[13]J. S Margolis, J. Quant Spectrosc. Radiat. Transfer 15, 637 (1975)
[14]J. S Margolis and S. Sarangi, J. Quant Spectrosc. Radiat. Transfer 16, 405 (1976)
[15]P. Varanasi, J. Quant Spectrosc. Radiat Transfer 12, 1283 (1972).
[16]T Oka, Invited paper, IAU Symposium No 87 on Interstellar Molecules, Mount Tremblant, Ontario, Canada 1979
[17]P R. Schwartz, Astrophys J. 229, 45 (1979).
[18]W. Liu and R A Marcus, J Chem Phys. 63, 272 (1975); 63, 290 (1975)
[19]R. H. Schwendeman and T Amano, J. Chem Phys 70, 962 (1979)
[20]T. Amano and R H Schwnedeman, J. Chem. Phys. 65, 5133 (1976)
[21]T. Amano, T Amano, and R H. Schwendeman, J. Chem. Phys 73, 1238 (1980).
[22]A H Brittain, P. J Manor, and R H. Schwendeman, J. Chem Phys 58, 5735 (1973)
[23]W. E Hoke, J Ekkers, and W H Flygare, J. Chem. Phys 63, 4075 (1975)
[24]W E Hoke, D. R Bauer, J Ekkers, and W H Flygare, J. Chem Phys 64, 5276 (1976)
[25]W E Hoke, D. R Bauer, and W H. Flygare, J. Chem. Phys 67, 3454 (1977)
[26]T Amano and T Shimizu, J Phys. Soc. Jpn 35, 237 (1973).
[27]J. C. McGurk, H. Mader, R T. Hofmann, T. G Schmalz, and W. H. Flygare, J. Chem Phys 61, 3759 (1974)
[28]T Oka, J. Chem Phys. 47, 4852 (1967), 48, 4919 (1968), 49, 3135 (1968), Adv. At Mol Phys. 9, 127 (1973).
[29]P. W Daly and T. Oka, J Chem Phys 53, 3272 (1970), A R. Fabris and T. Oka, 56, 3168 (1972), R. M. Lees and T. Oka, 49, 4234 (1968).
[30]T Shimizu and T Oka, J Chem. Phys 53, 2536 (1970), Phys Rev. A 2, 1177 (1970), S Kano, T Amano, and T Shimizu, Chem. Phys Lett 25, 119 (1974), W A Kreiner, M Romheld, and H D Rudolph, Z Naturforsch Teil A 28, 1707 (1973), J Lamaire, J. Thibault, F Herlemont, and J Hourlez, Mol Phys 27, 611 (1974)
[31]W A Kreiner, A Eyer, and H Jones, J. Mol Spectrosc. 52, 420 (1974)
[32]J M. Levy, J H S Wang, S. G Kukolich, and J I Steinfeld, Phys Rev Lett 28, 395 (1972), Chem. Phys Lett 21, 598 (1973)
[33]E M Dobbs, R. H. Michels, and J I. Steinfeld, J. Chem. Phys. 63, 1904 (1975).
[34]J P. Toennies, Discuss. Faraday Soc. 33, 96 (1962), Z. Phys. 182, 257 (1965)
[35]U. Borkenhagen, H. Malthan, and J P Toennies, Chem Phys Lett 41, 222 (1976), J. Chem. Phys. 71, 1722 (1979)
[36]J. L. Kinsey, J Chem Phys 66, 2560 (1977), W. D Phillips, J. A Serri, D J. Ely, D E. Pritchard, K. R Way, and J. L. Kinsey, Phys Rev Lett 41, 937 (1978)
[37]P. J. Dagdigian, B E Wilcomb, and M. H. Alexander, J Chem. Phys. 71, 1670 (1979), P. J Dagdigian and B E Wilcomb, *ibid* 72, 6462 (1980).
[38]K. Bergmann, R. Engelhardt, U. Hefter, P. Hering, and J. Witt, Phys Rev. Lett. 40, 1446 (1978), J Phys E 12, 507 (1979), K Bergmann, R. Engelhardt, U. Hefter, and J Witt, J. Chem. Phys. 71, 2726 (1979). K. Bergmann, U. Hefter, and J. Witt, *ibid*. 72, 4777 (1980).
[39]S G Kukolich, J. H S Wang, and D. E Oates, Chem Phys. Lett 20, 519 (1973)
[40]N. F. Ramsey, *Molecular Beams* (Clarendon, Oxford, 1956).
[41]J H. S Wang, D. E. Oates, A Ben-Reuven, and S. G Kukolich, J Chem Phys 59, 5268 (1973)
[42]K R Chien, P B Foreman, K H Castleton, and S G Kukolich, Chem Phys 7, 161 (1975)
[43]J R Williams and S G Kukolich, J Chem Phys 66, 251 (1977)
[44]R P Feynman, F L Vernon, and R W Hellwarth, J Appl Phys 28, 49 (1957)
[45]A Ben-Reuven and S G Kukolich, Chem Phys Lett 23, 376 (1973)
[46]H Feeny, W Madigosky, and B. Winters, J Chem Phys 27, 898 (1957)
[47]K Matsura, Res Electrotch Lab. Tokyo, 24, 579 (1960)
[48]A Dymanus, *International Review of Science*, *Physical Chemistry*, edited by D A Ramsay (Butterworths, London, 1976), Vol 3, J P Gordon, H J Zeiger, and C H Townes, Phys Rev 95, 282 (1954)
[49]S. Stolte, thesis, Katholieke Universiteit, Nijmegen, The Netherlands, 1972.
[50]P Zugenmaier, Z Angew Phys 20, 184 (1966)
[51]D Klaassen, Q R 53 (1976), Q R stand for "Quarterly Report of the Atomic and Molecular Research Group, ' Fysisch Laboratorium, Katholieke Universiteit, Nijmegen, The Netherlands.
[52]H C W. Beijerinck and N F. Verster, J Appl Phys 46, 2083 (1975)
[53]J. A. Th. Verhoeven, thesis, Katholieke Universiteit, Nijmegen, The Netherlands, 1978.
[54]A Messiah, *Quantum Mechanics* (North-Holland, Amsterdam, 1965), Vol II
[55]D Klaassen, Q R 55 (1977) (see Ref. 51).
[56]C J Tsao and B Curnutte, J Quant Spectrosc Radiat Transfer 2, 41 (1962)
[57]J. M. H. Reijnders, thesis, Katholieke Universiteit, Nijmegen, The Netherlands, 1978.
[58]E A Gislason and D R Herschbach, J Chem Phys 64, 2133 (1976)
[59]J T Hougen, J Chem Phys 57, 4207 (1972)
[60]P B Foreman, K R Chien, and S G Kukolich, J Chem Phys 62, 4710 (1975)
[61]E A Cohen and R L Poynter, J Mol Spectrosc 53, 131 (1974)
[62]J A Th Verhoeven and J M H Reijnders, Q. R 27 (1970) (see Ref. 51).
[63]W L Meerts, Q R 40 (1973) (see Ref 51).
[64]G Birnbaum, *Advances in Chemical Physics*, *Intermolecular Forces*, edited by J O Hirschfelder (Interscience, New York, 1967), Vol 12
[65]In this paper modifications of Anderson's theory and Born approximation are used Nevertheless they are referred to as Anderson's theory and Born approximation

BEAM MASER INVESTIGATION OF INELASTIC SCATTERING OF NH_3

II. CROSS SECTIONS FOR ROTATIONAL TRANSITIONS INDUCED BY POLAR GASES

D.B.M. Klaassen, J.J. ter Meulen and A. Dymanus

Fysisch Laboratorium, Katholieke Universiteit

Toernooiveld, 6525 ED Nijmegen, The Netherlands

ABSTRACT

A molecular beam maser is used in a double-resonance scheme to measure cross sections for rotational transitions between levels of different inversion doublets of NH_3 induced by collisions with NH_3, CH_3F and CF_3H. Theoretical values, calculated with a modification of Anderson's theory, are in good agreement with present experimental results and steady-state double-resonance experiments of Oka (J.Chem.Phys. 48, 4919 (1968)).

1. INTRODUCTION

In a previous paper[1], hereafter referred to as I, we reported measurements on cross sections for inversion transitions of ammonia (NH_3) induced by collisions with polar gases in a beam-maser scattering set-up. The experimental results were interpreted using Born approximation and Anderson's theory. Also a brief summary was given of other experiments (and theories) yielding collision-induced population transfer rates between inversion and rotation levels relevant for the astrophysical NH_3 problem. Special attention was paid to the steady-state double-resonance experiments of Oka[2], practically the only experiments capable of yielding collisional rates between rotational levels of NH_3. It was pointed out that it is very difficult to extract information about the state-to-state collision cross sections from those experiments, because they are sensitive to the ratio of rotational transition rates to the sum of a number of transition rates, including (twice) that for inversion transitions (Eq. (23)). This is caused by the fact that those experiments are done in steady-state and radiative and collision zones are not separated. Recently Shimizu et al.[3] reported a laser double-resonance experiment on the $(J,K)=(3,2)\rightarrow(2,2)$ transition induced by NH_3 collisions.

In this paper a double-resonance (DR) experiment is described, employing the beam-maser (BM) scattering set-up reported in I. A schematic diagram of the DR-BM experiment is shown in Fig. 1a. The ammonia beam passes through a state selector, which focusses the molecules in the upper states and removes the molecules in the lower states of all inversion doublets from the beam. In an additional cavity, inserted between the state selector and the secondary beam (Fig. 1a), the molecules of a specific inversion doublet (J_p,K_p) can be transferred (pumped) to the lower level. To explain the principle of operation of the DR-BM experiment it is assumed that all molecules can be

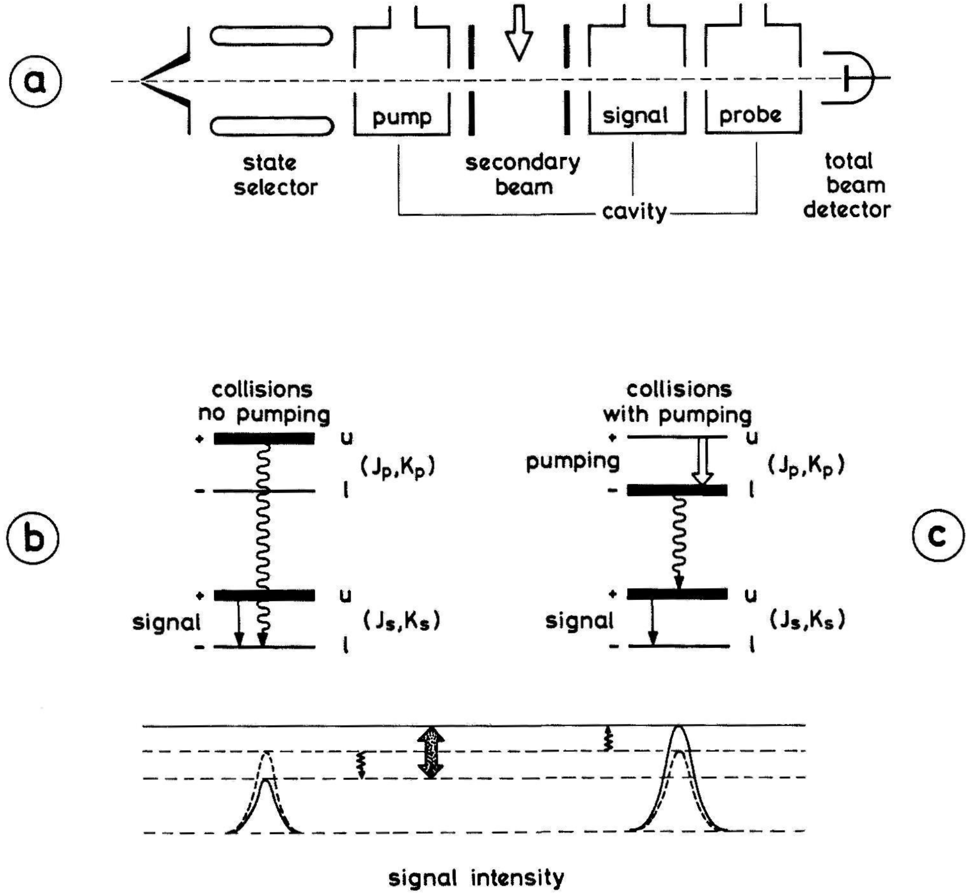

Figure 1: Schematic diagram (a) and simplified working principle (b,c) of the DR-BM experiment (see text). Plus and minus sign indicate the parity of the levels. The dashed intensity corresponds to the situation where collision-induced rotational transitions are neglected. The shaded arrow indicates the change in attenuated signal intensity due to pumping.

pumped from the upper to the lower level (J_p,K_p). Furthermore only collision-induced transitions from the pump (J_p,K_p) to the signal (J_s,K_s) doublet levels are regarded. Taking into account for the moment only collision-induced transitions involving the dipole moment of ammonia, collisions with the secondary beam can transfer molecules from the upper level (J_p,K_p) to the lower level of another doublet $(J_s,K_s)=(J_p \pm 1,K_p)$ or from the lower level (J_p,K_p) to the upper level (J_s,K_s). The microwave line intensity, detected with the signal cavity, tuned to the inversion transition (J_s,K_s), is proportional to the difference between the numbers of molecules in upper and lower states (J_s,K_s) (Ref. I). Collision-induced transitions between the doublet levels (J_p,K_p) and (J_s,K_s) therefore decrease the signal (J_s,K_s) when only the upper level (J_p,K_p) is populated (Fig. 1b). However, when the inversion transition (J_p,K_p) is pumped, the lower level (J_p,K_p) is populated and these collision-induced transitions are increasing the signal (J_s,K_s) (Fig. 1c). The difference between the attenuated signal in the presence and absence of microwave pumping is proportional to the small-angle cross section for transitions between the doublet levels (J_p,K_p) and (J_s,K_s). In practice not all molecules can be pumped from the upper state to the lower state of inversion doublet (J_p,K_p). Therefore the pumping efficiency is measured with the probe cavity, tuned to the same inversion transition (J_p,K_p). Furthermore also collision-induced transitions involving the quadrupole moment of ammonia and transitions between the (J_p,K_p) or (J_s,K_s) doublet and all other doublet levels are regarded in the interpretation of the measurements (Sect. 3).

Results are reported for a number of rotational transitions and the polar scattering gases NH_3, CH_3F and CF_3H. The measurements are interpreted in terms of the difference between the differential collision cross sections for parity changing and conserving rotational transitions. A modification of

Anderson's theory is presented, which gives a more realistic behaviour of the transition probability at small impact parameters. Predictions from this theory are compared with the experimental results. Integral cross sections for parity changing and conserving transitions are calculated. A theoretical prediction, using these cross sections, for the outcome of DR steady-state experiments[4] is also given.

2. THE EXPERIMENTAL SET-UP

The molecular beam apparatus is basically the same as that described in I. In the following only the relevant modifications are described. The main modification is the replacement of the second state selector by a microwave pump cavity (Fig. 1a). This cavity is used to change the population distribution over the levels of a specific inversion doublet (J_p, K_p) of the ammonia molecules entering the scattering region. Molecules in the selected upper state are pumped to the nearly empty lower state by the microwave power, which is switched periodically on and off by a shutter placed in the waveguide. The klystron system, used to generate the power, is similar to the superheterodyne detection system. The pump, signal and probe cavities (length 0.16 m, diameter about 9 mm, TM_{010} mode) are identical to the microwave cavities used in I. However, the end caps are removed from the pump cavity to avoid attenuation of the primary beam. The efficiency of pumping is monitored with a probe cavity tuned to the same inversion transition (J_p, K_p). The probe cavity is shielded against possible leaks of radiation from the pump cavity by a metal mesh with a transparency of about 90%, placed across the entrance hole. By feeding power to the pump cavity the signal from the probe cavity could be reduced by a factor of about 10 indicating an almost equal population of upper and lower state of the (J_p, K_p) inversion doublet.

In all measurements reported in this paper commercial platinum-iridium diaphragms (Siemens), with a diameter of 30 μm, are used as nozzles producing the primary NH_3 beam. With a stagnation pressure of 1.6×10^5 Pa the most probable velocity of the beam was 950 m/s [5]. The secondary beam is produced by a circular metal multi-channel array (Brunswick Corporation) with a diameter of 14 mm. With this source the scattering region is better defined than in I. The array consists of about 335000 channels with a length of 0.433 mm and a mean diameter of 8.9 μm, yielding a length to radius ratio of 50. The secondary beam source is mounted 22 mm from the primary beam axis. The flow through this effuser is regulated by a calibrated mass flow controller (Tylan Corporation). The control head is calibrated for 0-10 sccm NH_3 (1 sccm = 4.55×10^{17} molecules per second) and conversion factors are used for CH_3F and CF_3H. The linearity is 0.5% and the reproducibility 0.2%, both of full scale. In front of the scattering region, 295 mm from the exit opening of the state selector, a diaphragm with a diameter of 3.4 mm is placed to ensure that all molecules entering the scattering zone will reach the signal cavity in absence of the secondary beam.

In order to measure apparatus cross sections which are close to the integral cross sections the acceptance angle of the signal cavity is enlarged as much as possible. To this end the cavity is mounted at a distance of 0.473 m from the exit opening of the state selector. Moreover the end caps have beam transition holes with a diameter of 6 mm. The acceptance angle of the signal cavity is increased to 1.58° in the laboratory system (0.28° in I). With this set-up the radiative zones of pump and signal cavity are well separated from the collision region.

3. THE RELATION BETWEEN ATTENUATION DIFFERENCES AND ROTATIONAL CROSS SECTIONS

The effect of collision-induced rotational transitions from one inversion doublet (J_p,K_p) to another (J_s,K_s) is studied by measuring the difference in attenuated intensity from the signal cavity (tuned to inversion transition (J_s,K_s)) with and without power fed into the pump cavity (tuned to inversion transition (J_p,K_p)). Previous investigations (I) showed that the main line in the inversion spectrum ($\Delta F_1=\Delta F=0$) can be taken as a representative for each inversion doublet, to which all rotational substates $|J,K,M_J\rangle$ equally contribute. Consequently the scattering process can be described in terms of these substates and degeneracy averaged cross sections. For an evaluation of the measured effects a relation has to be set up between them and the rotational cross sections. In I such a relation was constructed using calculations of the molecular trajectories through the state selector. These calculations were considered as quite reliable in view of the good agreement between the calculated and measured dependence of the microwave line intensity on the state selector voltage. For the present investigation the acceptance angle of the signal cavity was increased with a factor of five compared to I. In this geometry the contribution of molecules with trajectories close to the rods of the state selector, which cannot be taken into account in the trajectory calculations, has become too large. This was evidenced by the failure of trajectory calculations to reproduce the experimental line intensities as function of the state selector voltage. Thus there is no reliable prediction for the radial and angular distribution of molecules leaving the state selector. As a way out the primary beam is treated as a line beam with only one (the most probable) velocity.

In a many-level scheme the number N_{JKMu} of molecules entering the microwave cavity per second in the upper level (u) of state $|J,K,M_J\rangle$ can be written

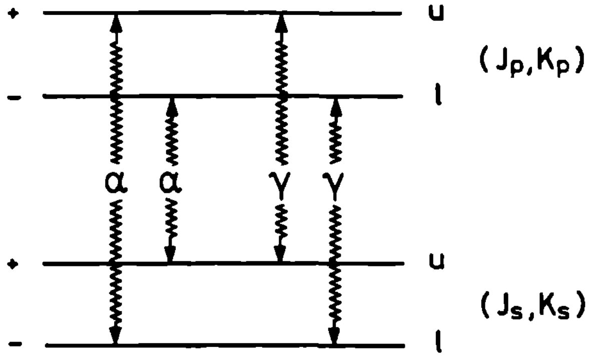

Figure 2: Level scheme for parity changing (α) and conserving (γ) transitions. Plus and minus sign indicate the parity of the levels (K_p and K_s odd).

as (see Appendix A)

$$N_{JKMu} = \Big[N^0_{JKMu} + \sum_{\substack{J'K'M' \\ i=u,l}} \left\{ \int_0^z n \frac{v_r}{v_1} \sigma^{eff}_{J'K'i \to JKu} \, dz' + O(n^2) \right\} N^0_{J'K'M'i} \Big] e^{-\int_0^z n \frac{v_r}{v_1} \sigma^{tot}_{JK} dz'} \quad ; \tag{1}$$

a similar expression holds for N_{JKMl}, the number of molecules in the lower level. Herein v_1 is the primary beam velocity, v_r is the relative velocity, n is the density of secondary beam molecules, z is the length of the scattering region, σ^{tot}_{JK} is the integral total cross section for state $|J,K\rangle$ averaged over M_J and

$$\sigma^{eff}_{J'K'i \to JKu} \equiv \int_{id} \frac{d}{d\Omega} \sigma_{J'K'i \to JKu} \, d\Omega \tag{2}$$

is the differential cross section for the transition $|J',K',i\rangle \to |J,K,u\rangle$, averaged over M'_J and M_J and integrated over those angles in the centre of mass system that correspond to trajectories through the detector after the collision; furthermore N^0_{JKMu} is the number of molecules entering the scattering region per second in the upper inversion level of state $|J,K,M_J\rangle$ and $O(n^2)$ stands for terms proportional to $n^2 \times (\sigma^{tot}_{J'K'} - \sigma^{tot}_{JK})$. Following Oka[2] (Fig. 2) we write for the cross sections for parity changing (α) and conserving (γ) transitions (for $|K_p - K_s|$ even)

$$\sigma_{J_pK_pu \to J_sK_s l} = \sigma_{J_pK_p l \to J_sK_su} \equiv \sigma^{\alpha}_{p\to s}$$

$$\sigma_{J_pK_pu \to J_sK_su} = \sigma_{J_pK_p l \to J_sK_s l} \equiv \sigma^{\gamma}_{p\to s} \tag{3}$$

where p and s stand for J_pK_p and J_sK_s, respectively. If $|K_p-K_s|$ is odd, α and γ have to be interchanged in Eq. (3).

With Eqs. (1) and (3) the change Δ in the population difference $(N_u-N_l)_{J_sK_sM_s}$ between the situation with and without pumping the inversion transition (J_p,K_p), can be written (for $|K_p-K_s|$ even) as (see App. A)

$$\Delta(N_u-N_l)_{J_sK_sM_s} = \sum_{M_p}\left[\left\{\int_0^z n\,\frac{v_r}{v_1}\,(\sigma^{\gamma,\mathrm{eff}}_{p\to s} - \sigma^{\alpha,\mathrm{eff}}_{p\to s})\,dz'\right\} \times \Delta(N_u-N_l)^0_{J_pK_pM_p}\right] e^{-\int_0^z n\,\frac{v_r}{v_1}\,\sigma_s^{\mathrm{tot}}\,dz'} \tag{4}$$

In the present interpretation the term $O(n^2)$ is disregarded. Assuming that all degenerate sublevels contribute equally to the microwave signal I_s, the following expression is obtained for the relative intensity change due to pumping, $\Delta I_s/I_s^0$,

$$\frac{\Delta I_s}{I_s^0} = \frac{\sum\limits_{M_p}\Delta(N_u-N_l)^0_{J_pK_pM_p}}{\sum\limits_{M_s}(N_u-N_l)^0_{J_sK_sM_s}} \sum_{M_s}\left\{\int_0^z n\,\frac{v_r}{v_1}\,(\sigma^{\gamma,\mathrm{eff}}_{p\to s} - \sigma^{\alpha,\mathrm{eff}}_{p\to s})\,dz'\right\} \times e^{-\int_0^z n\,\frac{v_r}{v_1}\,\sigma_s^{\mathrm{tot}}\,dz'} \tag{5}$$

This relative intensity change depends on the pumping efficiency through

$\Delta(N_u - N_l)^0_{J_pK_pM_p}$. In order to obtain a quantity ζ^0 that is independent of this efficiency, a multiplier F_p is introduced that can be determined experimentally

$$F_p = \frac{1}{1 - I_p^{0*}/I_p^0} \tag{6}$$

where I_p^0 stands for the signal from the probe cavity; the asterisk indicates the situation with power fed to the pump cavity. This multiplier equals unity when upper and lower levels of the pumped inversion doublet (J_p, K_p) are equally populated. With Eqs. (5) and (6) ζ^0 can be defined as (see Appendix A)

$$\zeta^0 \equiv F_p \frac{\Delta I_s}{I_s^0} = R_s^p \sum_{M_s} \left\{ \int_0^z n \frac{v_r}{v_1} \left(\sigma_{p\to s}^{\alpha,\mathrm{eff}} - \sigma_{p\to s}^{\gamma,\mathrm{eff}}\right) dz' \right\} \times e^{-\int_0^z n \frac{v_r}{v_1} \sigma_s^{\mathrm{tot}} dz'} \tag{7}$$

where R_s^p, the ratio of population differences, is given by

$$R_s^p = \frac{\sum_{M_p} (N_u - N_l)^0_{J_pK_pM_p}}{\sum_{M_s} (N_u - N_l)^0_{J_sK_sM_s}} \tag{8}$$

The exponential factor in Eq. (7) can be written as I_s/I_s^0 (App. A). Herewith ζ^0 is transformed into a new quantity ζ defined by

$$\zeta \equiv F_p \frac{\Delta I_s}{I_s} = R_s^p \sum_{M_s} \left\{ \int_0^z n \frac{v_r}{v_1} (\sigma^{\alpha,\mathrm{eff}}_{p\to s} - \sigma^{\gamma,\mathrm{eff}}_{p\to s}) \, dz' \right\} \tag{9}$$

The main advantage of ζ over ζ^0 is its linearity in the secondary beam density n, which facilitates the determination of $(\sigma^{\alpha,\mathrm{eff}}_{p\to s} - \sigma^{\gamma,\mathrm{eff}}_{p\to s})$.

The computation of the rotational cross sections is rather complicated. In order to simplify these calculations a normalized apparatus function $H_{p\to s}(\theta_{cm})$, averaged over the relative velocity, is introduced (see Appendix B). It can be expressed in the apparatus function $G_{p\to s}(v_{r,m},\theta_{cm})$ used in I

$$H_{p\to s}(\theta_{cm}) = \frac{\sum\limits_{v_{r,m}} G_{p\to s}(v_{r,m},\theta_{cm})}{\sum\limits_{v_{r,m}} G_{p\to p}(v_{r,m},\theta_{cm})} \tag{10}$$

The cross sections are now calculated only at the mean relative velocity $\langle v_r \rangle$, given by

$$\langle v_r \rangle = \frac{\sum\limits_{v_{r,m}} v_{r,m}\, G_{p\to p}(v_{r,m},0)}{\sum\limits_{v_{r,m}} G_{p\to p}(v_{r,m},0)} \tag{11}$$

With Eqs. (10) and (11) the expression for ζ is transformed into (see Appendix B)

$$\zeta = R_s^p \, (nl)_{\mathrm{eff}} \left(\sigma^{\alpha,\mathrm{app}}_{p\to s} - \sigma^{\gamma,\mathrm{app}}_{p\to s} \right) \tag{12}$$

where $(n\ell)_{eff} = \sum_{v_{r,m}} G_{p\to p}(v_{r,m},0) \sim$ secondary beam flow (13)

and

$$\sigma^{app}_{p\to s} = 2\pi \int d\theta_{cm} \sin\theta_{cm} H_{p\to s}(\theta_{cm}) \left\{ \sum_{M_s} \frac{d}{d\Omega}\sigma(\theta_{cm},\langle v_r\rangle)_{p\to s} \right\} \tag{14}$$

The subscript $p\to s$ of the apparatus functions indicates that the change in kinetic energy of the molecules, or energy defect, has to be taken into account in the calculation of the relative velocity after the collision[6]. This change δE can be written as

$$\delta E = E_s + E_{2'} - E_p - E_2 \tag{15}$$

where 2 stands for J_2K_2 and the prime indicates that $E_{2'}$ is the internal energy of the secondary beam molecule after the collision. Because it is not feasible to consider the dependence of δE on the initial and final states of the secondary beam molecule, two types of apparatus functions are used: (A) with $\delta E = E_s - E_p$, and (B) with $\delta E = 0$. The latter type corresponds to exactly resonant transitions of both molecules, whereas the first type implies completely non-resonant collisions.

4. THEORY

As shown in I the collision cross sections, measured in the maser, can be expressed in terms of transition probabilities. For rotational transitions the relevant relation can be written as

$$\sigma^{app}_{p\to s} = 2\pi \int_0^\infty H_{p\to s}\;(\theta_{cm}(b))\,(2\;J_s+1)\;P_{p\to s}(b)\;\;bdb \tag{16}$$

where $P_{p\to s}(b)$ is the degeneracy averaged transition probability evaluated at $<v_r>$. The transition probability is calculated in the permanent multipole interaction scheme, following Anderson's theory[7,8,9]. To obtain the total transition probability the individual transition probabilities have to be multiplied with the appropriate Boltzmann factor of the initial state (J_2,K_2) of the secondary beam molecule and summed over the final states (J_2',K_2') of that molecule

$$P_{p\to s}(b) = \sum_{\substack{J_2K_2\\ J_2'K_2'}} (2\;J_2'+1)\;\;(2\;J_2+1)\;g_{J_2K_2}\;\;e^{-E_2/kT}\;P^{2\to 2'}_{p\to s}\;\;(b) \tag{17}$$

where $g_{J_2K_2}$ is the statistical weight factor and the superscripts 2 and 2' stand for (J_2,K_2) and (J_2',K_2'), respectively. The expression for $P^{2\to 2'}_{p\to s}(b)$ is

$$P^{2\to 2'}_{p\to s}(b) = \sum_{l_1 l_2} 2\;C_l^{\;2} \begin{pmatrix} J_p & l_1 & J_s \\ -K_p & 0 & K_s \end{pmatrix}^2 \begin{pmatrix} J_2 & l_2 & J_2' \\ -K_2 & 0 & K_2' \end{pmatrix}^2 \;f_l\;\;(\omega\tau) \tag{18}$$

where $\hbar\omega = |\,\delta\;E\,|$. All symbols are defined in I. Because a rotational transition of the primary beam molecule gives a quite large energy defect, which may be partly compensated by a rotational transition of the secondary beam molecule, the full dependence of ω on initial and final states of both molecules is taken into account.

Due to the large acceptance angle in the maser quite small impact parameters are probed. But in that region the transition probability, according to Eq. (18), can become larger than unity. Although several solutions to the problem have been suggested[7], none of them seems to be adequate for the problem of calculating the probability for a rotational transition, if the probability for an inversion transition is predicted to be larger than unity. Therefore a procedure suggested by Rabitz and Gordon[10] for the Born approximation, is combined with Anderson's theory:

- each individual transition probability $P^{2\to2'}_{p\to1'}(b)$ is truncated to unity if the theoretical prediction is larger;
- if the total transition probability, $P^2_p(b)$, for one set of initial states of primary and secondary beam molecules

$$P^2_p(b) = \sum_{J_1'K_1'J_2'K_2'} (2\,J_1'+1)(2\,J_2'+1)\;P^{2\to2'}_{p\to1'}(b) \tag{19}$$

is larger than unity, each contributing term $P^{2\to2'}_{p\to1'}(b)$ is divided by $P^2_p(b)$. Without this modification Anderson's theory yielded about 45% larger integral cross sections than the Born theory if applied to the (J,K)=(1,1) and (2,2) inversion transitions and NH_3-NH_3 scattering (Ref. I). With the modification both theories yielded within 3% the same values.

To evaluate $\sigma^{app}_{p\to s}$ (Eq. (14)) a relation between the impact parameter b and deflection angle θ_{cm} is needed. For the interpretation of the previous experiments (I) the classical deflection function for two nonrotating dipoles μ_1 and μ_2 was used

$$\theta_{cm}(b) = \frac{\pi^2}{8} \frac{\mu_1 \mu_2}{4\,\pi\varepsilon_0 (\frac{1}{2}\,\mu\, v_r^{\,2})}\; b^{-3} \tag{20}$$

where μ is the reduced mass. The dipole moments μ_1 and μ_2 were replaced by the matrix elements. This was justified by the fact that the probed impact parameters were relatively large, resulting in long collision times $\tau = b/v_r$ compared to the rotation time of the individual molecules. As the present experiments are sensitive to smaller impact parameters, this substitution cannot be made. In fact the relative rotation of the molecules during the collision should be regarded in the deflection function. This approach was followed by Gislason and Herschbach[11] for diatomic molecules. They found that if the colliding molecules make resonant transitions ($\hbar\omega = |\delta E| = 0$) the deflection function is practically identical with that for nonrotating molecules. An approximation (estimated accuracy of about 20%) was used in order to get an analytical expression for the deflection function in the case of non-resonant collisions. This expression yields decreasing deflection angles for increasing ω. In the approximation of Gislason and Herschbach[11] this $\omega = |\delta E|/\hbar$ equals the difference in angular velocities of the two molecules. For two symmetric top molecules the problem is more difficult. Each rotating dipole has a nonrotating component proportional to K and directed along the angular momentum vector $\vec{J}$ and also a rotating component perpendicular to $\vec{J}$. For two symmetric top molecules, each in a quantum state with K=J, one can expect a deflection angle as function of the impact parameter as given in Eq. (20). It is, however, not likely that a reasonably accurate analytical expression can be obtained, describing the deflection angle for two symmetric top molecules in arbitrary quantum states. Therefore instead of $\pi^2/8$ in Eq. (20) an adjustable parameter κ_g is introduced for each scattering gas and fitted to the experimental results. The same parameter is used for all investigated transitions. Moreover it should be mentioned that the influence of the quadrupole moments on the deflection is neglected.

For the data acquisition the digital measuring procedure of I was adapted to the new experimental condition: pump power on/off. The base-line intensities are now measured by making use of the possibilities for remote control of the frequency synthesizing system SRS[12]. In order to correct for possible influence of the pump cavity on the signal cavity the centre-line and base-line intensities of both attenuated and unattenuated microwave signals were measured <u>with</u> and <u>without</u> pumping power. For the same reasons base-line intensities are determined separately for I_p^{0*} and I_p^0 when measuring the ratio I_p^{0*}/I_p^0 (Eq.(6)). This measurement was performed before and after each experimental run in order to determine the factor F_p (cf. Eqs. (6), (7) and (9)). As the calculations on the trajectories of the molecules through the state selector are not reliable (Sect. 3), no theoretical values for the ratios of population differences R_s^p (Eq. (8)) are available. Consequently these ratios have to be determined from the experiment. To this end the stagnation pressure of the primary beam and the voltage of the state selector were always set to the same values (1.6×10^5 Pa and 30 kV, respectively) in all measurements.

Rotational cross sections were determined for a number of inversion doublets and transitions (Table 1). The scattering gases were NH_3, CH_3F and CF_3H. The following relations were used to extract information out of the measurements:

$$\frac{\Delta I_s}{I_s^0} = \left(\frac{I_s}{I_s^0}\right)^* - \left(\frac{I_s}{I_s^0}\right) \tag{21}$$

and

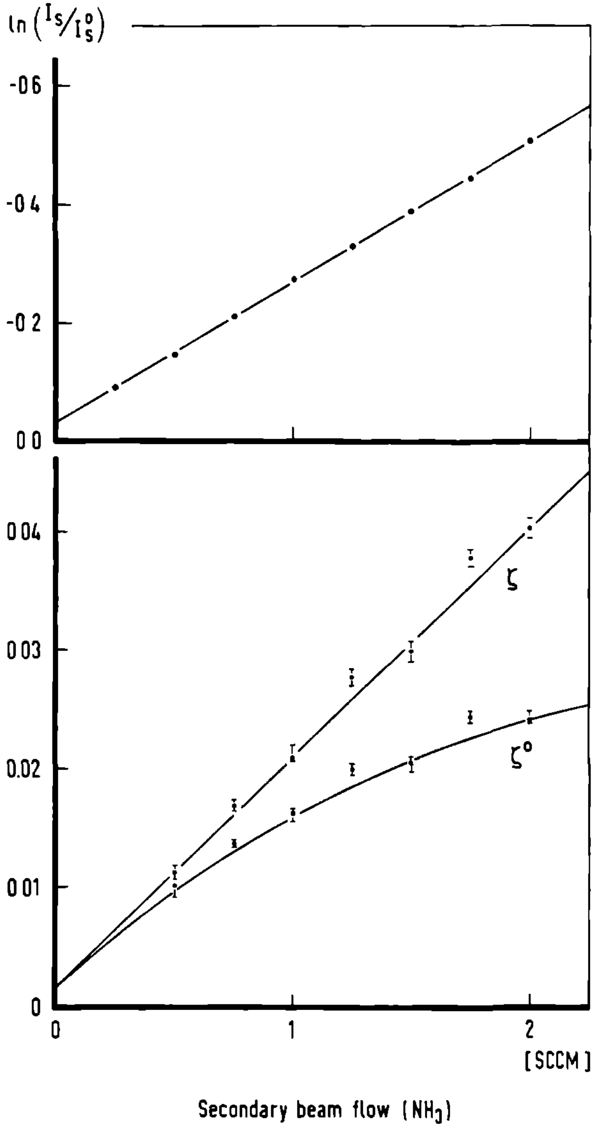

Figure 3: ζ and ζ^0 as function of the secondary beam flow (NH_3) for the transition p=(2,2) → s=(3,2). In the upper part the attenuation of the (3,2) microwave line intensity is shown.

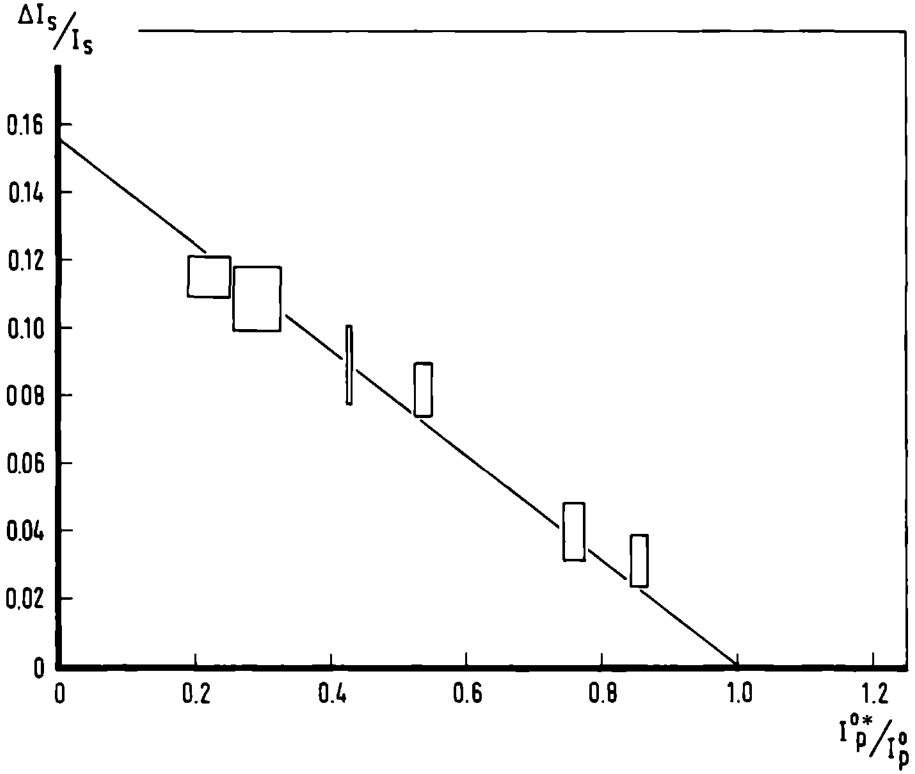

Figure 4: $\Delta I_s/I_s$ as function of I_p^{o*}/I_p^o for the transition $p=(1,1) \rightarrow s=(2,1)$ and a secondary beam flow of 0.65 sccm CH_3F.

$$\frac{\Delta I_s}{I_s} = \frac{I_s^0}{I_s} \left[\left(\frac{I_s}{I_s^0} \right)^* - \left(\frac{I_s}{I_s^0} \right) \right] \tag{22}$$

where the asterisk indicates the situation with pump power. In Fig. 3 ζ^0 and ζ are shown as function of the secondary beam flow for the p=(2,2) → s=(3,2) transition and NH_3-NH_3 scattering. From this figure it is clear that ζ is linear in the secondary beam flow. This justifies the assumptions made in the derivation of Eq. (9). To investigate the influence of the pumping efficiency $\Delta I_s/I_s$ was measured for different pump powers for the transition p=(1,1) → s=(2,1) and a secondary beam flow of 0.65 sccm CH_3F. In Fig. 4 the result is shown as function of I_p^{0*}/I_p^0. All points are lying clearly on the theoretically expected straight line (cf. Eqs. (6) and (9)), which crosses the horizontal axis at the point $I_p^{0*}/I_p^0=1$. This confirms that ζ and ζ^0 are independent of the pumping efficiency.

In the expression for ζ^0 (Eq. (7)) the ratio of population differences R_s^p depends on the state selector voltage V. The difference between the effective cross sections $\sigma_{p\to s}^{\alpha,eff} - \sigma_{p\to s}^{\gamma,eff}$ in Eq. (7) is determined by the acceptance angle of the signal cavity, as seen by the molecules in the centre of mass (Eq. (2)). This acceptance angle depends therefore on the trajectories of the molecules through the scattering region and consequently on the operation of the state selector. In order to investigate a possible influence of this operation upon the experimental cross sections, ζ^0 was measured as a function of V for the transition p=(1,1) → s=(2,1) and a secondary beam flow of 0.65 sccm CH_3F (Fig. 5). Also the microwave line intensities on the (1,1) and (2,1) inversion transitions were measured as function of V in order to correct for the V-dependence of R_s^p. From Fig. 5 it is seen that the intensity on the (2,1) transition changes with a factor 10 between V=18 kV and 30 kV. However, ζ^0

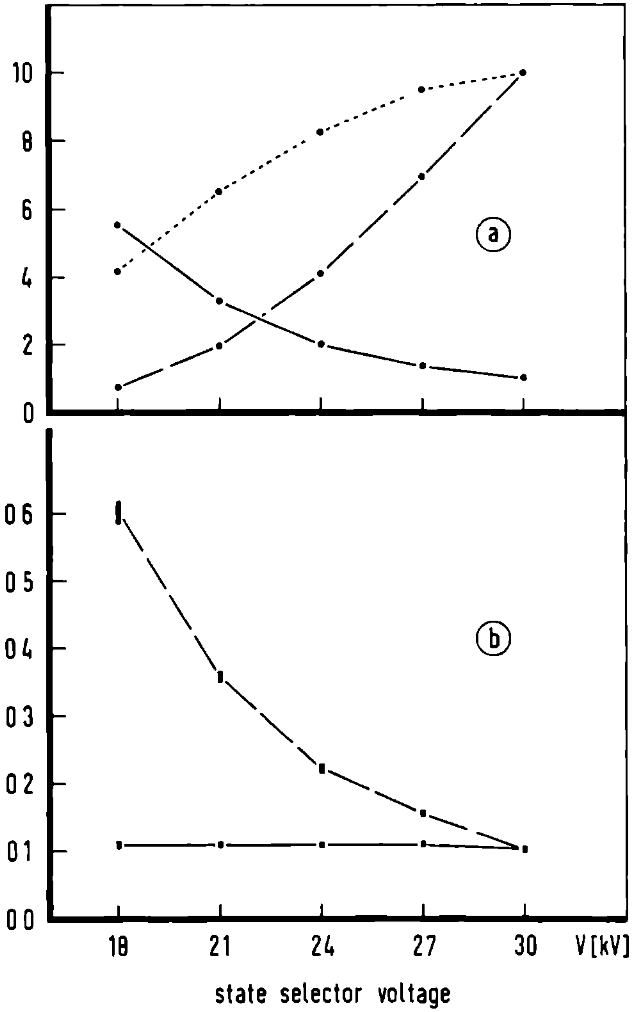

Figure 5: (a) Microwave line intensities (in arbitrary units) for the (1,1) (dotted) and (2,1) (dashed) inversion transitions and $R_{21}^{11}(V)/R_{21}^{11}(30kV)$ (solid line) as function of the state selector voltage V;
(b) ζ^0 (dashed) and $(R_{21}^{11}(30kV)/R_{21}^{11}(V))\times\zeta^0$ (solid line) as function of V.

corrected for the V-dependence of R_s^p by multiplying with $R_{21}^{11}(30\text{kV})/R_{21}^{11}(V)$, is nearly independent of V. This proves that $\sigma_{p\to s}^{\alpha,\text{eff}} - \sigma_{p\to s}^{\gamma,\text{eff}}$ is almost independent of the state selector voltage for the applied range, which in turn justifies the treatment of the primary beam as a line beam in the apparatus functions.

For each set of pump and signal inversion doublet levels measurements were performed as function of the secondary beam flow. A straight line was fitted through the ζ values, plotted against the secondary beam flow, yielding not only the slope but also an intercept of the vertical axis. A non-zero intercept could be caused by background scattering; within three standard deviations all intercepts were equal to zero. The errors found in slopes and intercepts originate mainly from the experimental error in ζ. Using the method as described in Sect. 4, for all transitions the probabilities were evaluated for the interaction between dipole and quadrupole moments of both primary and secondary beam molecules (Table 4 of I). With the computed probabilities and apparatus functions (see Appendix B) theoretical apparatus cross sections were calculated from Eq. (16). For each scattering gas the adjustable parameter κ_g was introduced in Eq. (20). From the calculation of the apparatus functions also $(nl)_{\text{eff}}$ as function of the secondary beam flow was obtained (Eq. (13)). With the aid of Eq. (12), finally, theoretical values for the slope of ζ as function of the secondary beam flow were obtained, with the ratios of population differences $R_s^p=(R_p^s)^{-1}$ as adjustable parameters. The fit of the theoretical slopes to the experimental values yielded values for κ_g and R_s^p (Table 2). With the values for R_s^p and $(nl)_{\text{eff}}$ again the experimental cross sections $\sigma_{p\to s}^{\alpha,\text{app}} - \sigma_{p\to s}^{\gamma,\text{app}}$ were obtained from the experimental slopes. For the calculation of the uncertainties in the experimental cross sections the errors in the experimental slopes and in R_s^p were regarded as not correlated. A summary of these results is given in Table 1 for both types of apparatus functions (see Sect. 3). The uncertainties in the theoretical apparatus cross sections originate from the errors in κ_g and were calculated by the fit program.

	$\sigma^{\alpha,app}_{p\to s} - \sigma^{\gamma,app}_{p\to s}$				
		type A		type B	
	$p\to s$	theory	experiment	theory	experiment
	(1,1)→(2,1)	17.8(15)	15.1(13)	15.9(17)	14.6(12)
NH_3	(2,1)→(1,1)	13.1(12)	16.9(26)	11.7(13)	17.5(27)
1192 m/s	(2,2)→(3,2)	13.9(12)	14.6(13)	16.1(16)	16.7(13)
$0.332\times10^{17}m^{-2}$	(3,2)→(2,2)	14.0(10)	16.8(23)	15.2(14)	14.7(19)
	(2,1)→(3,1)	24.0(22)	21.1(35)	27.6(29)	23.6(35)
	(3,1)→(2,1)	24.5(20)		26.2(27)	
	(1,1)→(3,1)	-1.13(15)	-2.08(50)	-1.63(31)	-2.25(51)
	(1,1)→(2,1)	120.1(56)	130.2(94)	116.9(94)	125.9(84)
CH_3F	(2,1)→(1,1)	99.1(69)	95.7(80)	94.4(67)	98.9(78)
1078 m/s	(2,2)→(3,2)	13.2(11)	11.0(12)	14.8(16)	12.5(12)
$0.434\times10^{17}m^{-2}$	(3,2)→(2,2)	14.0(13)	14.9(24)	14.3(17)	13.1(20)
	(2,1)→(3,1)	18.3(16)	19.4(29)	19.9(16)	21.7(29)
	(3,1)→(2,1)	25.5(35)		24.2(32)	
	(1,1)→(3,1)	-0.10(4)		-0.04(2)	
	(1,1)→(2,1)	21.5(46)	21.1(18)	20.8(37)	20.4(16)
CF_3H	(2,1)→(1,1)	15.7(34)	22.5(42)	15.1(29)	23.3(43)
1014 m/s	(2,2)→(3,2)	0.63(18)	0.59(48)	0.62(15)	0.68(54)
$0.590\times10^{17}m^{-2}$	(3,2)→(2,2)	0.62(18)		0.60(16)	
	(2,1)→(3,1)	1.23(38)	2.3(44)	1.15(32)	2.5(49)
	(3,1)→(2,1)	1.13(39)		1.06(31)	
	(1,1)→(3,1)	-0.004(1)		-0.001(1)	

TABLE 1 : Summary of theoretical and experimental apparatus cross sections (in 10^{-20} m^2). In the first column also $\langle v_r \rangle$ and $(nl)_{eff}$ for a flow of 1 sccm are given.

	type A	type B
κ_{NH_3}	0.78(12)	1.10(11)
κ_{CH_3F}	0.66(13)	0.86(10)
κ_{CF_3H}	2.15(30)	2.29(27)
R^{11}_{21}	3.96(26)	4.09(25)
R^{22}_{32}	4.07(35)	3.57(28)
R^{21}_{31}	17.2(24)	15.5(19)

TABLE 2 : Values of κ_g and the population ratios R^p_s, obtained in the fits.

All computations for the apparatus functions and theoretical predictions of cross sections were performed with a numerical error smaller than 1%, which is well below the experimental error.

In addition to the measurements, yielding the values given in Table 1, also combinations of those doublets with $\Delta K \neq 0$ were tried. But no effects were observed larger than three experimental standard deviations. Also for some combinations with $\Delta K=0$ no value for the rotational cross section could be obtained. In some cases (e.g. CF_3H) cross sections are simply too small; in other cases (cf. $(3,1) \rightarrow (2,1)$) the ratio of population differences is too small. But for all transitions the ratio between parity conserving and changing apparatus cross sections is roughly the same (Table 3). All transitions in Table 1 are of the $\Delta J=\pm 1$, $\Delta K=0$ type, except for the $(1,1) \rightarrow (3,1)$ transition of NH_3-NH_3 scattering. Although the experimental error is quite large for the last transition, it clearly indicates that for a rotational transition with $\Delta J=\pm 2$, $\Delta K=0$ the parity conserving collision-induced transitions are dominant over those changing the parity. This is just the opposite situation as with the $\Delta J=\pm 1$, $\Delta K=0$ rotational transitions, where the parity changing collision-induced transitions are dominant.

6. DISCUSSION

The agreement between theory and experiment is satisfactory in view of the assumptions and simplifications made for the interpretation. In the present investigation the experimental cross sections can be obtained from the experimental data via the ratios of population differences R_s^p. These ratios are determined by fitting a theoretical model to the experimental results. This model includes not only the calculation of transition probabilities, deflection functions and apparatus functions, but also their relation to the measured effects (Eq. (12)). The number of experimental data used in the fits is twice the number of fit parameters. Consequently the fits test, besides the models used, also the deduced experimental cross sections and their consistency for different transitions and scattering gases. The fact that both fits, with different types of apparatus functions, yield almost the same values for the ratios of population differences and nearly the same experimental cross sections, is regarded as a strong support for the present interpretation. Both types of apparatus functions treat the primary beam as a line beam and differences between them are apparently compensated by the deflection function. Differences between these (line-beam) apparatus functions and (real-beam) apparatus functions that take into account the radial and angular distribution of the primary beam, are expected to be small, because the acceptance angle and consequently the latter functions are nearly independent of the state selector voltage (Sect. 5). Therefore nearly the same experimental cross sections would be obtained also with the real-beam apparatus functions. The values for χ^2, found in the fits with apparatus functions of type A and B, are 48.4 and 38.6, respectively. These quite large values indicate that the used models could be improved. The energy defect δE (Eq. (15)) is not treated properly either in the apparatus function or in the deflection function.

From Table 2 it is seen that the fit with the "nonresonant" apparatus function (type A) yields smaller values for κ_g than the fit with the "resonant" apparatus function (type B). It appears that when the collision dynamics in the apparatus function are treated as if the molecules are making "resonant" transitions, the factor κ_g in the deflection function is closer to the "non-rotating" value of $\pi^2/8$ (Eq. (20) and further). The scattering gas CF_3H yields a value for κ_g well above this "nonrotating" factor. It is however determined mainly by transitions between the (1,1) and (2,1) inversion levels of ammonia. For the other two scattering gases κ_g is determined also by transitions between the (2,2) and (3,2) and between the (2,1) and (3,1) inversion levels. The difference in κ_g for CH_3F and CF_3H can be understood from the rotational constants of these molecules. The molecule CF_3H is an oblate symmetric top with relatively high population of levels (J,K) with large K values (at a temperature of 300 K). This means that the molecule is preferentially rotating around an axis almost parallel to the symmetry axis and behaves as an almost "nonrotating" dipole. The molecule CH_3F, however, is a prolate symmetric top with well-populated levels (J,K) for low K values, resulting in a "rotating" dipole (Sect. 4) and a smaller factor κ_g. As with diatomic molecules, for symmetric tops rotation of the dipole moment decreases the deflection angle. The ammonia molecule as scattering partner is a special case, because almost the complete cross section comes from "resonant" collisions. The agreement between theory and experiment could be improved by introducing a separate factor κ_g in the deflection function for each rotational transition, which would make the deflection function dependent on (J,K). But both the limited amount of experimental data and the fact, that the energy defect cannot be treated exactly in the computation of the apparatus function, render such refined treatment highly questionable. Even with the present interpretation the uncertainties in theoretical and experimental values are overlapping for practically all measured cross sections.

In Table 3 the parity changing (α) and conserving (γ) contributions to the rotational apparatus cross sections are given for both types of apparatus functions used. The table contains also the integral cross sections (α- and γ-type) for each transition. For all transitions measured, the α-type transition connects upper and lower levels and the γ-type transition connects upper with upper and lower with lower inversion doublet levels (Eq. (3) and Fig. 2). Comparison of $\sigma^{\gamma,app}$ with $\sigma^{\alpha,app}$ in Table 3 shows that the first one is only about 10% of the second one. So only the latter is really probed in the maser. This is due to the fact that the dipole-dipole interaction, which is the main interaction for large impact parameters and small deflection angles, contributes only to $\sigma^{\alpha,app}$ and not to $\sigma^{\gamma,app}$. The parity conserving transitions originate from interactions involving the quadrupole moment of ammonia, which have rather a short-range character. Therefore the integral cross sections for these transitions depend more critically on the normalization procedure (Sect. 4) for the transition probabilities than those for parity changing transitions. In the small impact parameter region there is a coupling due to this procedure between the probabilities for parity changing (α) and conserving (γ) transitions. This may produce too large cross sections of type γ on transitions with small cross sections of type α. Nevertheless for NH_3-NH_3 scattering the ratio between the cross sections for excitation and de-excitation is for all parity changing and conserving transitions within a few percent equal to the ratio following from the principle of detailed balance.

The angles in the centre of mass system for which the apparatus function of type B has the value 0.5 are 2.8^{o}, 2.2^{o} and 1.9^{o} for NH_3, CH_3F and CF_3H, respectively. From Table 3 it is seen that with this angular resolution for NH_3 about 35% of the cross sections for parity changing and about 8% of the cross sections for parity conserving transitions are probed. For CH_3F these

		integral		type A		type B	
	$p\to s$	$\sigma^{\alpha}_{p\to s}$	$\sigma^{\gamma}_{p\to s}$	$\sigma^{\alpha,app}_{p\to s}$	$\sigma^{\gamma,app}_{p\to s}$	$\sigma^{\alpha,app}_{p\to s}$	$\sigma^{\gamma,app}_{p\to s}$
	(1,1)→(2,1)	59.4	21.3	19.6	1.9	17.3	1.3
	(2,1)→(1,1)	43.6	14.7	14.6	1.5	12.8	1.1
	(2,2)→(3,2)	47.4	19.2	15.4	1.5	17.5	1.4
NH_3	(3,2)→(2,2)	39.4	14.7	15.3	1.4	16.5	1.3
	(2,1)→(3,1)	72.3	9.7	24.7	0.6	28.2	0.6
	(3,1)→(2,1)	66.3	8.0	25.1	0.6	26.8	0.6
	(1,1)→(3,1)	0	18.4	0	1.1	0	1.6
	(1,1)→(2,1)	211.6	99.7	132.6	12.5	125.6	8.7
	(2,1)→(1,1)	176.1	73.9	107.5	8.4	100.4	6.0
	(2,2)→(3,2)	55.6	55.5	17.2	4.0	17.4	2.6
CH_3F	(3,2)→(2,2)	52.8	71.8	17.5	3.5	16.6	2.3
	(2,1)→(3,1)	62.8	29.5	20.0	1.7	21.0	1.1
	(3,1)→(2,1)	93.1	29.2	26.9	1.4	25.2	0.9
	(1,1)→(3,1)	0	12.8	0	0.1	0	0.04
	(1,1)→(2,1)	110.5	103.5	22.5	1.0	21.6	0.8
	(2,1)→(1,1)	108.4	78.0	16.3	0.6	15.7	0.6
	(2,2)→(3,2)	23.2	50.4	0.7	0.1	0.7	0.1
CF_3H	(3,2)→(2,2)	22.4	71.4	0.7	0.1	0.7	0.1
	(2,1)→(3,1)	38.9	27.1	1.3	0.05	1.2	0.03
	(3,1)→(2,1)	57.2	27.2	1.2	0.04	1.1	0.03
	(1,1)→(3,1)	0	13.3	0	0.004	0	0.001

TABLE 3 : The theoretical integral cross sections and the parity changing and conserving parts of the apparatus cross section (in 10^{-20} m^2) for both types of apparatus functions.

umbers are 31% and 6%, respectively, except for the transitions between the ,K)=(1,1) and (2,1) levels, where they are twice as large. This is due to gher transition probabilities at large impact parameters. Consequently the ormalization procedure becomes effective at quite a large impact parameter d decreases the probability for smaller impact parameters. With the attering gas CF_3H only parity changing transitions between the (J,K)=(1,1) d (2,1) doublet levels are probed for about 18%. The cross sections for the her transitions are too small to be measured in the maser.

The dependence of the integral cross section for parity changing ansitions on the rotational quantum numbers is also different for the three attering gases. For NH_3 the cross section shows no clear behaviour, whereas r CH_3F and CF_3H the cross sections connecting the (1,1) and (2,1) levels are 4 times as large as those connecting the (2,2) and (3,2) levels. The cross ctions for transitions between the (2,1) and (3,1) levels are again only mewhat larger than the latter. For parity conserving transitions the integral oss section shows a more complicated dependence on the rotational quantum mbers. This might be due to the more short-range character of the interactior at are responsible for these transitions. Comparison of the α-type cross ctions for the three scattering gases shows, that for the (J,K)=(1,1) to (2,1 ansition the ratios $NH_3:CH_3F:CF_3H$ are roughly 1:4:2. Besides the differences permanent multipoles (Table 4 of I) and the influence of the rotational antum numbers via the 3-j symbols in Eq. (18), also the population stribution over the initial states of the secondary beam molecules plays an portant role in the explanation of these facts (Eq. (17)). For ammonia as a attering gas, all collision-induced transitions are almost completely sonant and only one initial state of the secondary molecule is contributing the cross section. This results in nearly constant cross sections as nction of the rotational quantum numbers and an almost constant fraction of the integral cross section that is probed in the maser. For the other two scattering gases there are many initial states of the secondary beam molecule, from which the molecule can make almost resonant transitions, due to the smaller rotational constants. However only the states from which transitions can be induced with energy differences matching the (1,1)-(2,1) transition of NH_3 are well-populated in these molecules. This results in larger cross sections for transitions between these inversion doublets, compared to other transitions.

Because incomplete integral cross sections are measured in the maser, a direct confrontation of the experimental results with the outcome of other experiments is not possible. Nevertheless quite a large fraction of the integral cross sections is probed and can be explained using the modification of Anderson's theory (Eq. (19)). Therefore it is interesting to use this theory for a prediction of the outcome of other experiments. Oka[2] performed many experiments on collision-induced population transfer in NH_3 using a steady-state double-resonance method. The interpretation of the measurements with a simplified form of Anderson's theory yielded a poor agreement between observed and calculated relative intensity changes $\Delta I/I$[4]. Peterson[13] has used the sudden approximation formalism to predict the $\Delta I/I$ values, measured by Oka for the system NH_3-NH_3, but did not find any improvement compared with Oka's attempt. For a relative velocity of 865 m/s, being the mean relative velocity in a cell at 300 K, all cross sections, which are needed in the interpretation, including inversion cross sections, are calculated using the modification of Anderson's theory presented in this paper. It should be noted that, whereas in the maser cross sections summed over the final rotational substates M_J' of the ammonia molecule are measured (Eq. (16)), the relative intensity changes measured in Oka's experiments are expressed in M_J-averaged rate constants (Eq. (9) of Ref. 4)

$$\frac{\Delta I}{I} = \frac{\nu_p}{\nu_s} \frac{k_\alpha\uparrow - k_\gamma\uparrow}{k_\alpha\uparrow + k_\gamma\uparrow + 2k_\beta + k_\xi} \tag{23}$$

where ν_p and ν_s are the frequencies of pump and signal inversion transitions, respectively; the arrows indicate that transitions $s \rightarrow p$ have to be taken; the subscript β stands for inversion transitions of the signal doublet and ξ indicates the sum over all other transitions out of the signal doublet. The rate constants can be expressed in cross sections by $k = \langle v_r \sigma \rangle$. In Fig. 6 a comparison is made between the experimental and theoretical values of $\Delta I/I$. The agreement is good, especially if compared to that obtained by Oka[4], whose calculated values are on the average a factor five too large. The maximum in the deviation between theory and experiment for K=3 is also found by Oka. There is no easy explanation for this maximum in the deviation; the fact that it appears for ortho-NH_3 (K=3; I_H=3/2) may be purely accidental. Shimizu et al.[3] calculated a cross section of 25×10^{-20} m^2 from their laser double-resonance experiment on the $(3,2)\rightarrow(2,2)$ transition. But both experiment and its interpretation are subject to serious doubts.

The present investigation shows that it is possible to measure cross sections for rotational (de-)excitation of ammonia in a beam maser. Only for collision-induced transitions with ΔK=0, effects could be observed. Interpretation, using a modified form of Anderson's theory and permanent multipole interaction, yielded good agreement between theory and experiment. Moreover this modification gives a satisfying agreement with the steady-state double-resonance experiments of Oka[4].

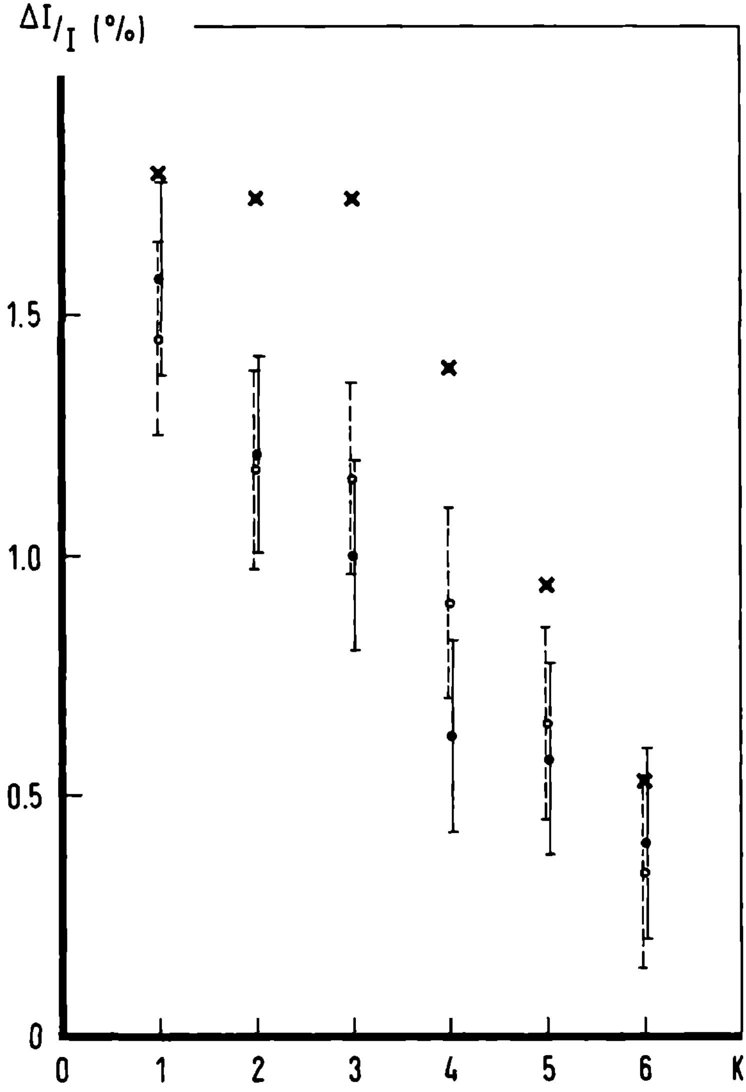

Figure 6: Comparison between double-resonance experiments of Oka on NH_3 and calculations with the theory presented in this paper (unfilled circles for 0.3 m cell; filled circles for 3 m cell; crosses for theoretical results); pumping J=K+1, signal J=K.

ACKNOWLEDGEMENTS

The authors thank Professor J. Reuss for his critical reading of the manuscript and Mr. N. van Hulst for his enthusiastic assistance during the measurements. The technical assistance of Messrs. J. Holtkamp and E. van Leeuwen is greatly appreciated.

The primary beam is regarded as a line beam with only one velocity. Per travelled path length dz through the scattering region the change of the flux N_{JKMu} of molecules in a particular rotational substate is

$$\frac{dN_{JKMu}}{dz} = \sum_{\substack{J'K'M' \\ i=u,l}} n \frac{v_r}{v_1} \sigma^{eff}_{J'K'i \to JKu} N_{J'K'M'i} - n \frac{v_r}{v_1} \sigma^{tot}_{JK} N_{JKMu} \tag{A1}$$

The corresponding relation for N_{JKMl} is obtained by interchanging u and l in Eq. (A1). Herein v_1 is the primary beam velocity, v_r is the relative velocity, n is the density of the secondary beam, σ^{tot}_{JK} is the integral total cross section for state $|J,K\rangle$ averaged over M_J and

$$\sigma^{eff}_{J'K'i \to JKu} \equiv \int_{id} \frac{d\sigma}{d\Omega}_{J'K'i \to JKu} d\Omega \tag{A2}$$

is the differential cross section for the transition $|J',K',i\rangle \to |J,K,u\rangle$, averaged over M_J' and M_J and integrated over those angles in the centre of mass that correspond to angles in the laboratory system within the acceptance angle of the detector.

The dependence of the density and the cross section in Eq. (A1) on the different internal states of the secondary beam molecule is not indicated for brevity's sake. The cross sections for rotational transitions are smaller than those for inversion transitions and also smaller than the elastic cross sections. So only a very small part of the molecules that collide twice will make a rotational transition. With the assumption that only molecules that make a single collision contribute to the first term of Eq. (A1) the following expression

$$N_{JKMi} = N^0_{JKMi} \; e^{-\int_0^z n \frac{v_r}{v_1} \sigma^{tot}_{JK} dz'} \tag{A3}$$

is substituted in this term. Herewith Eq. (A1) can be written in the form

$$\frac{d}{dz}\left[e^{\int_0^z n \frac{v_r}{v_1} \sigma^{tot}_{JK} dz'} N_{JKMu}\right] =$$

$$\sum_{\substack{J'K'M'\\ i=u,l}} n \frac{v_r}{v_1} \sigma^{eff}_{J'K'i \to JKu} N^0_{J'K'M'i} \, e^{-\int_0^z n \frac{v_r}{v_1}\left(\sigma^{tot}_{J'K'} - \sigma^{tot}_{JK}\right) dz'} \tag{A4}$$

where N^0_{JKMi} is the flux of molecules entering the scattering region in a particular substate. If σ^{tot}_{JK} and $\sigma^{tot}_{J'K'}$ are almost equal, Eq. (A4) has the approximate solution

$$N_{JKMu} = \left[N^0_{JKMu} + \sum_{\substack{J'K'M'\\ i=u,l}} \left\{ \int_0^z n \frac{v_r}{v_1} \sigma^{eff}_{J'K'i \to JKu} dz' + O(n^2) \right\} \times N^0_{J'K'M'i} \right] e^{-\int_0^z n \frac{v_r}{v_1} \sigma^{tot}_{JK} dz'} \tag{A5}$$

Herein $O(n^2)$ stands for terms proportional to $n^2 \times (\sigma^{tot}_{J'K'} - \sigma^{tot}_{JK})$.

If the pump and signal inversion doublets are denoted by (J_p,K_p) and (J_s,K_s), respectively, the following expression is obtained for the difference Δ between the situation with and without pumping

$$\Delta N_{J_s K_s M_s u} = \sum_{\substack{M_p \\ i=u,l}} \left\{ \int_0^z n \frac{v_r}{v_1} \sigma^{eff}_{J_p K_p i \to J_s K_s u} dz' \right\} \Delta N^0_{J_p K_p M_p i} \times e^{-\int_0^z n \frac{v_r}{v_1} \sigma^{tot}_{J_s K_s} dz'} \tag{A6}$$

The term $O(n^2)$ in Eq. (A5) can be omitted for small densities of the secondary beam. From the dependence of the experimental results on the secondary beam density it can be checked whether the used densities are not too large. With the definition

$$\Delta(N_u - N_l)_{JKM} \equiv \Delta N_{JKMu} - \Delta N_{JKMl} \tag{A7}$$

substitution of Eq. (A6) yields

$$\begin{aligned} \Delta(N_u - N_l)_{J_s K_s M_s} = \sum_{M_p} \Bigg[& \left\{ \int_0^z n \frac{v_r}{v_1} \left(\sigma^{eff}_{J_p K_p u \to J_s K_s u} - \sigma^{eff}_{J_p K_p u \to J_s K_s l} \right) dz' \right\} \\ & \times \Delta N^0_{J_p K_p M_p u} + \left\{ \int_0^z n \frac{v_r}{v_1} \left(\sigma^{eff}_{J_p K_p l \to J_s K_s u} - \sigma^{eff}_{J_p K_p l \to J_s K_s l} \right) dz' \right\} \\ & \times \Delta N^0_{J_p K_p M_p l} \Bigg] e^{-\int_0^z n \frac{v_r}{v_1} \sigma^{tot}_{J_s K_s} dz'} \end{aligned} \tag{A8}$$

Following Oka[2] we write

$$\sigma_{J_p K_p u \to J_s K_s u} = \sigma_{J_p K_p l \to J_s K_s l} \equiv \sigma^{\gamma}_{p \to s} \tag{A9a}$$

$$\sigma_{J_pK_pu\to J_sK_sl} = \sigma_{J_pK_pl\to J_sK_su} \equiv \sigma^{\alpha}_{p\to s} \tag{A9b}$$

if $|K_p-K_s|$ is even and

$$\sigma_{J_pK_pu\to J_sK_su} = \sigma_{J_pK_pl\to J_sK_sl} \equiv \sigma^{\alpha}_{p\to s} \tag{A9c}$$

$$\sigma_{J_pK_pu\to J_sK_sl} = \sigma_{J_pK_pl\to J_sK_su} \equiv \sigma^{\gamma}_{p\to s} \tag{A9d}$$

if $|K_p-K_s|$ is odd. In this notation α stands for parity changing, γ for parity conserving transitions, p for J_pK_p and s for J_sK_s. Using these definitions Eq. (A8) yields for $|K_p-K_s|$ is even

$$\Delta(N_u-N_l)_{J_sK_sM_s} = \sum_{M_p} \left[\left\{ \int_0^z n \frac{v_r}{v_1} \left(\sigma^{\gamma,\mathrm{eff}}_{p\to s} - \sigma^{\alpha,\mathrm{eff}}_{p\to s}\right) dz' \right\} \times \Delta(N_u-N_l)^0_{J_pK_pM_p} \right] e^{-\int_0^z n \frac{v_r}{v_1} \sigma_s^{\mathrm{tot}}\, dz'} \tag{A10}$$

The intensity I_{JK} of a detected inversion transition is proportional to the population difference of the levels involved, i.e.

$$I_{JK} \propto \sum_M (N_u-N_l)_{JKM} \tag{A11}$$

With Eqs. (A10) and (A11) the following expression is obtained, after summing over M_s, for the relative intensity change $\Delta I_s/I_s^0$

$$\frac{\Delta I_s}{I_s^0} = \frac{\sum\limits_{M_p} \Delta(N_u-N_l)^0_{J_pK_pM_p}}{\sum\limits_{M_s} (N_u-N_l)^0_{J_sK_sM_s}} \sum_{M_s} \left\{ \int_0^z n \frac{v_r}{v_1} \left(\sigma^{\gamma,\mathrm{eff}}_{p\to s} - \sigma^{\alpha,\mathrm{eff}}_{p\to s} \right) dz' \right\}$$

$$\times\, e^{-\int_0^z n \frac{v_r}{v_1} \sigma_s^{\mathrm{tot}} \, dz'} \tag{A12}$$

The efficiency of the microwave pumping on doublet (J_p,K_p) enters Eq. (A12) via $\sum\limits_{M_p} \Delta(N_u-N_l)^0_{J_pK_pM_p}$. This efficiency can be determined experimentally by comparing the signals from the probe cavity <u>with</u> (I_p^{0*}) and <u>without</u> (I_p^0) pumping. Now a multiplier F_p is introduced

$$F_p = \frac{1}{1 - \frac{I_p^{0*}}{I_p^0}} = - \frac{\sum\limits_{M_p} (N_u-N_l)^0_{J_pK_pM_p}}{\sum\limits_{M_p} \Delta(N_u-N_l)^0_{J_pK_pM_p}} \tag{A13}$$

which is unity if in the pump cavity upper and lower levels of the (J_p,K_p) doublet are equally populated. A quantity ζ^0 independent of the pumping efficiency is obtained by multiplying Eq. (A12) by F_p

$$\zeta^0 \equiv F_p \frac{\Delta I_s}{I_s^0} = R_s^p \sum_{M_s} \left\{ \int_0^z n \frac{v_r}{v_1} \left(\sigma^{\alpha,\mathrm{eff}}_{p\to s} - \sigma^{\gamma,\mathrm{eff}}_{p\to s} \right) dz' \right\}$$

$$\times\, e^{-\int_0^z n \frac{v_r}{v_1} \sigma_s^{\mathrm{tot}} \, dz'} \tag{A14}$$

where R_s^p, the ratio of population differences, is given by

$$R_s^p = \frac{\sum\limits_{M_p} (N_u - N_l)^0_{J_p K_p M_p}}{\sum\limits_{M_s} (N_u - N_l)^0_{J_s K_s M_s}} \tag{A15}$$

For small acceptance angles the elastic and inversion effects cancel for the microwave line intensity (see I). In the assumption that with the present angular resolution the same cancellation occurs one can write (Eq. (19) of I)

$$e^{-\int_0^z n \frac{v_r}{v_1} \sigma_s^{tot}} = \frac{I_s}{I_s^0} \tag{A16}$$

The validity of this assumption is confirmed by the linear dependence of the experimental results on the secondary beam density. Substitution of Eq. (A16) into Eq. (A14) yields

$$\zeta \equiv F_p \frac{\Delta I_s}{I_s} = R_s^p \sum_{M_s} \left\{ \int_0^z n \frac{v_r}{v_1} \left(\sigma^{\alpha,eff}_{p\to s} - \sigma^{\gamma,eff}_{p\to s} \right) dz' \right\} \tag{A17}$$

From Eq. (A17) it is seen that ζ is linear in the secondary beam density n, while $\Delta I_s/I_s^0$ (Eq. (A12)) and also ζ^0 are not. This simplifies considerably the determination of cross sections from the observed signal intensity changes.

In terms of the apparatus function G used in I, Eq. (9) can be written as

$$\zeta = R_s^p \sum_{v_{r,m}} 2\pi \int d\theta_{cm} \sin\theta_{cm}\, G_{p\to s}(v_{r,m},\theta_{cm}) \times \sum_{M_s} \left[\frac{d}{d\Omega}\sigma(\theta_{cm},v_{r,m})^{\alpha}_{p\to s} - \frac{d}{d\Omega}\sigma(\theta_{cm},v_{r,m})^{\gamma}_{p\to s} \right] \tag{B1}$$

The subscript $p\to s$ of the apparatus function indicates that the change in kinetic energy of the molecules has to be taken into account in the calculation of the relative velocity after the collision[6]. In order to simplify the computation of the differential cross sections for rotational transitions a uniform mean relative velocity is assumed:

$$\langle v_r \rangle = \frac{\sum_{v_{r,m}} v_{r,m}\, G_{p\to p}(v_{r,m},0)}{\sum_{v_{r,m}} G_{p\to p}(v_{r,m},0)} = \frac{1}{(nl)_{eff}} \sum_{ijv_2} I(\hat{v}_{2ij})\, P(v_2) v_r^2 \frac{\Delta v_2\, \Delta z_i}{r_{ij}^2\, v_1\, v_2} \tag{B2}$$

where the expression for $(nl)_{eff}$ is (see I)

$$(nl)_{eff} = \sum_{v_{r,m}} G_{p\to p}(v_{r,m},0) = \sum_{ijv_2} I(\hat{v}_{2ij})\, P(v_2) v_r \frac{\Delta v_2\, \Delta z_i}{r_{ij}^2\, v_1\, v_2} \tag{B3}$$

Herein i gives the position on the line beam (divided in sections Δz), j gives the channel on the effuser, $I(\hat{v}_{2ij})$ is the secondary beam intensity in the direction $\hat{v}_{2ij}$ ⁶, $P(v_2)$ is the Maxwellian velocity distribution of the secondary beam molecules and r_{ij} is the distance between channel j and point i on the line beam. At the velocity $\langle v_r \rangle$ a (new) normalized apparatus function is defined as

$$H_{p\to s}(\theta_{cm}) = \frac{\sum\limits_{v_{r,m}} G_{p\to s}(v_{r,m},\theta_{cm})}{\sum\limits_{v_{r,m}} G_{p\to p}(v_{r,m},0)} \tag{B4}$$

$$= \frac{1}{(nl)_{eff}} \sum_{ijv_2} I(\hat{v}_{2ij})\, P(v_2)\, v_r \frac{\Delta v_2\, \Delta z_i}{r_{ij}^2\, v_1\, v_2} \left(\int_{id} \frac{d\phi_{cm}}{2\pi} \right)_{\theta_{cm} ij v_2}$$

the subscript id (inside detector) under the integration sign indicates that the integral is confined to those angles that correspond to trajectories through the detector after the collision. Introducing a step size $\Delta\theta_{cm}$, Eq. (B4) can be written as

$$H_{p\to s}(\theta_{cm,k}) = \frac{1}{(nl)_{eff}} \sum_{ijv_2} I(\hat{v}_{2ij})\, P(v_2) v_r \frac{\Delta v_2\, \Delta z_i}{r_{ij}^2\, v_1 v_2} \times \frac{1}{\Delta\theta_{cm}} \int_{id} \frac{d\Omega_{cm}}{2\pi} \frac{T_k(\theta_{cm})}{\sin\theta_{cm}} \tag{B5}$$

$$\begin{aligned} &\text{with } T_k(\theta_{cm})=1 \text{ for } \theta_{cm,k} - \tfrac{1}{2}\Delta\theta_{cm} \leq \theta_{cm} \leq \theta_{cm,k} + \tfrac{1}{2}\Delta\theta_{cm} \\ &\quad T_k(\theta_{cm})=0 \quad \text{otherwise.} \end{aligned} \tag{B6}$$

To simplify the computation of the integral in Eq. (B5) two transformations are performed*:

(1) from the centre of mass system to the laboratory system (lab)

$$d\Omega_{cm} = \left(\frac{v_1'}{u_1'}\right)^2 \frac{1}{\cos\alpha}\, d\Omega_{lab} \tag{B7}$$

(2) from the laboratory system to the plane of the detector opening

$$d\Omega_{lab} = \frac{1}{R^2 \cos\xi}\, dx_d\, dy_d \tag{B8}$$

Herein v_1' is the primary velocity in the laboratory system after the collision, u_1' is the same velocity in the centre of mass system, α is the angle between those two velocities, (x_d, y_d) is taken in the detector opening, R is the distance between the point where the collision takes place and (x_d, y_d), ξ is the angle between $\vec{v}_1'$ and the machine axis.

With these transformations the computation of $H_{p\to s}(\theta_{cm,k})$ is done following the Monte Carlo method, where each "event" is determined by the choice of (i, j, v_2, x_d, y_d).

In terms of the apparatus function $H_{p\to s}(\theta_{cm})$, the expression for ζ (Eq. (B1)) is

---

* M.A.D.Fluendy and K.P.Lawley, "Chemical Applications of Molecular Beam Scattering", page 40, Chapman and Hall, London 1973

$$\zeta = R_s^p(n\ell)_{eff}\ 2\pi \int d\theta_{cm} \sin\theta_{cm}\ H_{p\to s}(\theta_{cm})$$

$$\times \sum_{M_s} \left[\frac{d}{d\Omega}\sigma\ (\theta_{cm}, <v_r>)^{\alpha}_{p\to s} - \frac{d}{d\Omega}\ \sigma(\theta_{cm}, <v_r>)^{\gamma}_{p\to s} \right] \tag{B9}$$

REFERENCES

1 D.B.M.Klaassen, J.M.H.Reijnders, J.J.ter Meulen and A.Dymanus, J.Chem.Phys. 76, 3019 (1982)

2 T.Oka, "Collision-induced transitions between rotational levels", Advances in Atomic and Molecular Physics 9, 127 (1973)

3 F.Matsuhima, N.Morita, S.Kano and T.Shimizu, J.Chem.Phys. 70, 4225 (1979); T.Shimizu, F.Matsuhima and Y.Honguh, page 212, Laser Spectroscopy V, Ed. A.R.W.McKellar, T.Oka and B.P.Stoicheff, Springer, New York (1981)

4 T.Oka, J.Chem.Phys. 48, 4919 (1968)

5 N.v.Hulst, Internal Report, Katholieke Universiteit, Nijmegen, The Netherlands (1981)

6 D.B.M.Klaassen, Quarterly Report 55 of the Atomic and Molecular Research Group, Fysisch Laboratorium, Katholieke Universiteit, Nijmegen, The Netherlands (1977)

7 P.W.Anderson, Phys.Rev. 76, 647 (1949)

8 C.J.Tsao and B.Curnutte, J.Quant.Spectrosc.Radiat.Transfer 2, 41 (1962)

9 J.S.Murphy and J.E.Boggs, J.Chem.Phys. 47, 691 (1967); J.Chem.Phys. 50, 3220 (1969)

10 H.A.Rabitz and R.G.Gordon, J.Chem.Phys. 53, 1831 (1970)

11 E.A.Gislason and D.R.Herschbach, J.Chem.Phys. 64, 2133 (1976)

12 J.A.Th.Verhoeven, Thesis, Katholieke Universiteit, Nijmegen, The Netherlands (1969)

13 K.L.Peterson, J.Chem.Phys. 75, 5655 (1981)

BEAM MASER INVESTIGATION OF INELASTIC SCATTERING OF NH_3

III. CROSS SECTIONS FOR ROTATIONAL TRANSITIONS INDUCED BY CO_2, N_2 and H_2

D.B.M. Klaassen, J.J. ter Meulen and A. Dymanus

Fysisch Laboratorium, Katholieke Universiteit

Toernooiveld, 6525 ED Nijmegen, The Netherlands

ABSTRACT

Cross sections for rotational transitions between various low-lying inversion doublets of NH_3 in collisions with CO_2, N_2 and H_2 are measured in a double-resonance beam maser set-up[2]. A modification of Anderson's theory presented in Ref. 2 yields values for the cross sections that are in good agreement with the experimental results for CO_2 and N_2. For the system NH_3-H_2 transition probabilities are evaluated in Anderson's theory using "bent" trajectories. Induction and dispersion terms up to R^{-7} are considered in the long-range intermolecular potential. For the short-range repulsive part two empirical potentials are proposed with parameters that are fitted to the experimental results. Integral cross sections for rotational transitions calculated with these potentials are also presented.

1. INTRODUCTION

In the first paper[1] (hereafter referred to as I) of a series on collision-induced population transfer in ammonia, the special importance of NH_3-H_2 collisions for the interstellar ammonia problem was indicated. A brief summary of known techniques used to obtain state-to-state collision cross sections showed that they either cannot be applied to ammonia or give only indirect information about the cross sections. In a consecutive paper[2] (hereafter referred to as II) a double-resonance beam maser experiment was described. Measurements for ammonia-polar gas systems demonstrated that direct information on the rotational cross sections could be obtained. The differential equations governing the population transfer in ammonia induced by collisions were solved and a method for comparison of experiment with theory was presented.

In this investigation the same experimental method is applied to ammonia-nonpolar gas systems. <u>Before</u> the ammonia beam collides with the secondary beam a sharp change in the population of the upper and lower levels of a specific inversion doublet is produced by strong radiation of a microwave cavity tuned to that inversion transition. Transitions induced by collisions with the secondary beam can transfer this change in population to a different doublet, to which a cavity <u>behind</u> the scattering region is tuned. For the system NH_3-CO_2 collision-induced rotational transitions are measured between a number of inversion doublets at a secondary beam temperature of 300 K. For nitrogen as scattering partner one rotational transition is investigated at three secondary beam temperatures: 77 K, 300 K and 350 K. With molecular hydrogen as scattering gas, cross sections are determined for collision-induced transitions between the $(J,K)=(1,1)$ and $(2,1)$ inversion levels and between the $(2,2)$ and $(3,2)$ levels.

In II a modification of Anderson's theory was described that yields a proper description of transition probabilities at small impact parameters. This modification is used for CO_2 and N_2 taking only dipole-quadrupole and quadrupole-quadrupole interactions into account. For the system NH_3-H_2 these interactions are not sufficient to explain the observed cross sections. Induction and dispersion potential terms, containing the quadrupole polarizability, are found to be competitive with the low-order permanent-multipole interaction. Moreover, the main contribution to the rotational cross sections turns out to originate from the small impact parameter region. Therefore, instead of the straight-line approximation, "bent" paths are used in Anderson's theory. As the short-range repulsive potential for the system NH_3-H_2 is not known from ab initio calculations, a model function is introduced for this short-range part of the potential with parameters adapted to the experimental results. With this empirical potential integral state-to-state cross sections are calculated and used for the interpretation of line broadening experiments[3] and the steady-state double-resonance experiments of Oka[4]. Also for these investigations a reasonable agreement between theoretical and experimental results is found, which supports the potential and cross sections obtained.

2. EXPERIMENT

The experimental set-up and method are described in I and II. In the present investigation the secondary beam is not always at room temperature. When molecular hydrogen is used as scattering gas, the cryopump is kept at a temperature of about 3.5 K. At this temperature the vapour pressure of the hydrogen frozen on the cryopump is well below the background pressure of 6×10^{-5} Pa in the molecular beam apparatus[5]. In order to keep the cryopump at such a low temperature, the shield by which it is surrounded is cooled with liquid nitrogen. The multi-channel array, mounted on this shield, and the secondary beam are then also at liquid nitrogen temperature.

With nitrogen as scattering gas, measurements were performed for three temperatures of the secondary beam. In addition to room and liquid nitrogen temperature, a temperature of 350 K was achieved by circulation of warm water through the reservoir to which the shield is attached, which carries the secondary beam source. The water is kept at constant temperature by a thermostat (Tamson).

3. THEORY

In II a modified form of Anderson's theory was presented to explain the observed rotational cross sections. The modifications were required for the calculation of the transition probabilities in the small impact parameter region and for the proper treatment of so-called "off-resonance" transitions. In this investigation essentially the same theory is used for NH_3-CO_2 and NH_3-N_2 scattering. For the system NH_3-H_2 the resonance function[6] is calculated using "bent" trajectories instead of straight paths.

When both primary and secondary beam molecules have large dipole or quadrupole moments, the transition probabilities derived in the permanent-multipole interaction scheme (Eq. (18) of II) are sufficient to describe the scattering process. For molecules with small permanent multipoles other terms in the intermolecular potential may become important. The long-range part of the intermolecular potential can be split into an electro static, an induction and a dispersion part[7]. Within the framework of Anderson's theory the contribution of a large number of individual terms in the potential to the transition probability is well-known[8,9,10]. For the systems NH_3-CO_2 and NH_3-N_2 calculations of pressure broadened line widths show, that the contribution of induction and dispersion terms in the intermolecular potential is negligible relative to the dipole-quadrupole interaction[11]. Similar (pressure broadening) calculations, however, indicate that for the ammonia-hydrogen system besides the electrostatic terms also the induction and dispersion terms up to R^{-7} play an important role in the intermolecular potential[11]. These conclusions are confirmed by our computations of rotational transition probabilities, which included all these potential terms. Moreover, these computations show that for the NH_3-H_2 system besides the dipole-quadrupole and quadrupole-quadrupole interaction only the induction and dispersion terms proportional to R^{-7} are important. The contributions of these terms to the transition probability are summarized in Appendix A. Two (parity changing) contributions (Eqs. (A1) and (A2)) originate from the quadrupole-induced dipole interaction and the dispersion interaction caused by the anisotropy in the quadrupole polarizability of the ammonia molecule. A third (parity conserving) contribution (Eq. (A3)) comes from the dispersion interaction proportional to the isotropic quadrupole polarizability of the ammonia molecule. This last contribution, given by Eq. (A3), is non-zero only for $\Delta K=\pm 3$ transitions, whereas the contributions given by Eqs. (A1-A2) are non-zero for $\Delta K=0$ transitions.

The probabilities for rotational transitions for the systems NH_3-CO_2 and NH_3-N_2 are so large, that for small impact parameters the normalization procedure (Eq. (19) of II) is working properly. This means that small impact parameters do not contribute significantly to the integral cross section for an individual rotational transition. For the system NH_3-H_2 the transition probabilities are much smaller. Consequently the normalization procedure becomes effective only for very small impact parameters. For the $(1,1)\rightarrow(2,1)$ transition this results in a contribution of about 75% to the integral cross section from impact parameters smaller than the zero-crossing of the isotropic Lennard-Jones (12,6) potential, $\sigma=0.345$ nm[12]. Since in the straight-path approximation, used to evaluate the resonance functions, the distance of nearest approach is equal to the impact parameter b, a different method has to be followed for the system NH_3-H_2. A simple, but also rather artificial, approach is introducing, in the ordinary straight-path approximation, a somewhat arbitrary parameter d and setting the transition probability $P(b)=P(d)$ for $b\leq d$[13]. Physically more satisfactory is the "bent"-trajectory approximation adapted for the present calculations. In this approximation each trajectory is replaced by two straight-line segments; the angle between these segments is equal to the deflection angle of the isotropic L-J (12,6) potential[14] (see Appendix B).

The anisotropic potential for the NH_3-H_2 system is not well-known to date. For similar systems ab initio calculations have been performed for H_2CO-He by Green et al.[15] and Garrison et al.[16] and for NH_3-He by Green[17,18]. The calculations of Bonamy and Robert[19] were limited to the long-range part of the NH_3-He potential. Therefore some model has to be used for the anisotropic NH_3-H_2 potential. Most potential models[20] commonly used in the interpretation of molecular beam scattering data, contain several adjustable parameters. For the system NH_3-H_2 reasonable estimates for the long-range anisotropic potentials are available[11]. However, the present experiments yield only a limited number of data that can be used for the determination of the adjustable parameters (see Sect. 4). Instead of using an anisotropic potential model with a few adjustable parameters we have chosen two different models each with only one adjustable parameter that does not affect the long-range behaviour. In the first model (e-type) each long-range potential term proportional to R^{-n} is multiplied by

$$h_c(R)=1-e^{-c(R/\sigma-1)} \tag{1}$$

and in the second model (LJ-type) by

$$h_d(R)=1-d(\sigma/R)^{12-n} \tag{2}$$

Both models have a minimum in the potential. With the e-type model the zero-crossing is fixed at $R=\sigma$. The second potential model has the form of an isotropic L-J (12,n) potential. The factors c and d in Eqs. (1) and (2) are determined from the experiment. For the two types of potentials the expression for the resonance functions with bent trajectories is given in Appendix B.

Resonance functions for straight and bent trajectories are compared in Fig. 1, where $\omega=|\delta E|/\hbar$ (Eq. (15) of II) and v_r is the relative velocity.

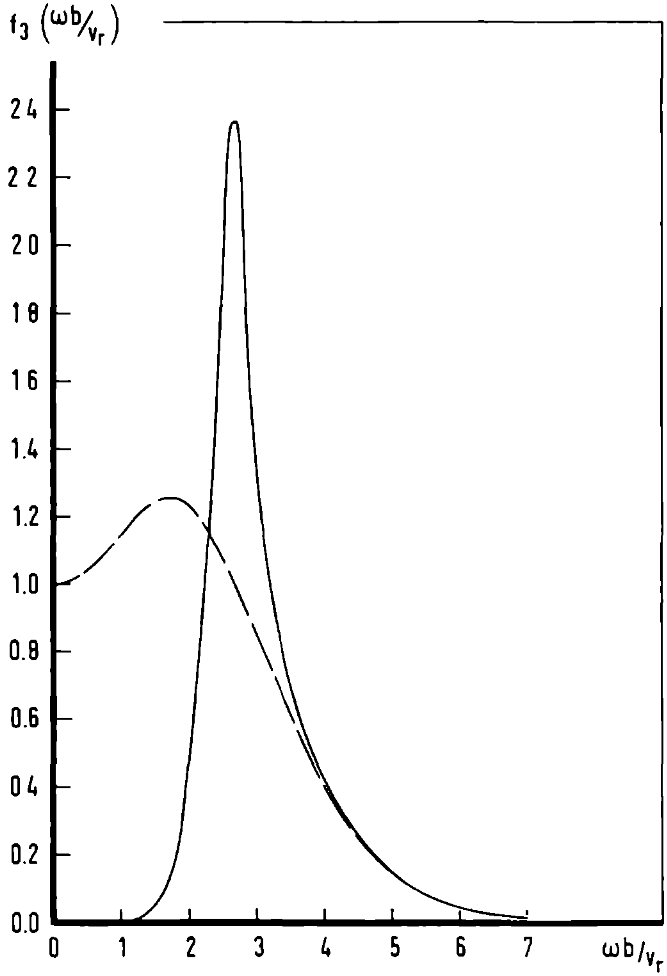

Figure 1: Comparison between resonance functions for dipole-quadrupole interaction with bent (solid line) and straight (dashed line) trajectories.

For large values of $\omega b/v_r$ the functions are identical. The resonance function calculated with bent trajectories shows a sharp maximum at the impact parameter that corresponds to the rainbow angle. This is caused by the fact that with bent trajectories negative deflection angles (attraction) result in longer and positive deflection angles (repulsion) result in shorter interaction times than with the corresponding straight paths. For small values of $\omega b/v_r$ the resonance function for bent trajectories is several orders of magnitude smaller than the one for straight paths. This can be explained by the fact that with bent trajectories the distance of closest approach has a non-zero lower limit (see Fig. 6), whereas for straight paths this distance becomes equal to zero. Consequently the transition probabilities for backward scattering, obtained from the resonance functions by dividing by the appropriate power of the impact parameter (Eqs. (A1)-(A3)), are finite.

For the interpretation of the experimental results also a deflection function for the systems NH_3-CO_2 and NH_3-N_2 is needed. In II it was pointed out that for two polar symmetric top molecules it is quite difficult to construct such a function that takes into account the relative rotation of the molecules. This is even more difficult for the system of a polar symmetric top molecule and a linear molecule possessing a quadrupole moment, because of the complicated expression for the interaction. Therefore for NH_3-CO_2 and NH_3-N_2 the classical deflection function for a potential $V(R)=C_4/R^4$ is adopted[21]

$$\theta_{cm}(b) = \frac{3}{4}\,\frac{C_4}{(\frac{1}{2}\mu v_r^2)}\,b^{-4} \quad ; \tag{3}$$

μ is the reduced mass and C_4 is proportional to the product of primary dipole (μ_1) and secondary quadrupole (Q_2) moment. As in II an adjustable parameter κ_g, which is fitted to the experimental results, is introduced by setting $\frac{3}{4}C_4=\kappa_g\mu_1 Q_2$.

		$\sigma^{\alpha,app}_{p\to s} - \sigma^{\gamma,app}_{p\to s}$			
	transition	type A		type B	
	$p\to s$	theory	experiment	theory	experiment
	$(1,1)\to(2,1)$	11.2(11)	13.2(12)	11.4(10)	12.8(11)
	$(2,1)\to(1,1)$	7.9(8)	9.3(13)	8.1(7)	9.6(13)
CO_2	$(2,2)\to(3,2)$	2.9(3)	2.6(3)	3.2(3)	2.9(3)
1050 m/s	$(3,2)\to(2,2)$	2.7(3)		2.9(3)	
$0.481\times10^{17}m^{-2}$	$(2,1)\to(3,1)$	5.6(7)	3.8(10)	6.1(6)	4.2(11)
	$(3,1)\to(2,1)$	5.1(6)		5.5(5)	
	$(1,1)\to(3,1)$	-0.07(2)		-0.05(1)	

TABLE 1 : Summary of theoretical and experimental apparatus cross sections (in 10^{-20} m^2) for NH_3-CO_2 scattering, for both types of apparatus functions (A and B). In the first column also $\langle v_r \rangle$ and $(nl)_{eff}$ for a secondary beam flow of 1 sccm are given.

4. EXPERIMENTAL RESULTS AND INTERPRETATION

a. The system NH_3-CO_2

Measurements were performed for a number of rotational transitions $p=(J_p,K_p) \rightarrow s=(J_s,K_s)$ given in Table 1. Calculated cross sections were fitted to the experimental results following the procedure described in II. Both non-resonant (type A) and resonant (type B) apparatus functions were used (Sect. 3 of II). The resulting values of κ_g (Eq. (3)) are given in Table 2. As the primary beam conditions were kept the same as in previous experiments (II) the ratios of population differences R_s^p were taken as determined in II. Transition probabilities were calculated for dipole-quadrupole and quadrupole-quadrupole interaction. The molecular constants used for NH_3 are given in Table 4. The quadrupole moment and rotational constant used for CO_2 are 14.33×10^{-40} Cm^2 and 11.67 GHz, respectively[22]. The experimental apparatus cross sections shown in Table 1 are determined from the measurements in the same way as in II (Sect. 5 of II).

b. The system NH_3-N_2

With nitrogen as a scattering gas, measurements were performed on the $(2,2) \rightarrow (3,2)$ rotational transition of ammonia for three temperatures of the secondary beam (see Table 3). For each temperature new apparatus functions were calculated, but the same factor κ_g was used for all temperatures. The factor κ_g obtained and ratios of population differences R_s^p used are given in Table 2. As with CO_2 only low-order multipole interactions are considered in the theoretical calculations. The quadrupole moment and rotational constant used for N_2 are 5.0×10^{-40} Cm^2 and 59.96 GHz, respectively[22]. The fit with the apparatus functions of type A yielded a χ^2 value (the sum of least squares)

	type A	type B
κ_{CO_2}	2.55(25)	2.64(13)
κ_{N_2}		3.62(54)
R_{21}^{11}	3.96(26)	4.09(25)
R_{32}^{22}	4.07(35)	3.57(28)
R_{31}^{21}	17.2(24)	15.5(19)

TABLE 2 : Population ratios R_s^p adopted from II and values for κ_g obtained in the fits.

secondary beam temperature (K)	$\langle v_r \rangle$ (m/s)	$(n\mathcal{l})_{eff}$ (m^{-2})	$\sigma_{p\to s}^{\alpha,app} - \sigma_{p\to s}^{\gamma,app}$ theory	experiment
77	992	0.719×10^{17}	0.71(11)	0.60(8)
300	1103	0.395×10^{17}	1.12(17)	1.13(14)
350	1128	0.372×10^{17}	1.08(16)	1.55(19)

TABLE 3 : Summary of the theoretical and experimental apparatus cross sections (in 10^{-20} m^2) for NH_3-N_2 scattering on the (2,2)→(3,2) transition. The $(n\mathcal{l})_{eff}$ value is given for a secondary beam flow of 1 sccm.

that was twice as large as the value obtained with the apparatus functions of type B. So only the results obtained with the type B functions are summarized in Table 3.

c. The system NH_3-H_2

With normal hydrogen as scattering gas, only effects for the $(1,1) \rightarrow (2,1)$ and $(2,2) \rightarrow (3,2)$ transitions were found. No effects could be measured on the $\Delta k \neq 0$ transitions between the inversion doublets with low (J,K) values (k is the signed K value). Since the cross sections for NH_3-H_2 are very small their measurements required rather lengthy time averaging procedures. As an example, the results shown in Fig. 2 are obtained by combining measurements of several days at the same flow setting. Each point in Fig. 2 is the average of about 150 measuring cycles. The Gaussian distribution of the results from the individual cycles confirmed that all settings of the apparatus could be reproduced within the experimental error. The values for ζ are an order of magnitude smaller than for NH_3-NH_3 scattering (Fig. 3 of II).

Calculations of transition probabilities showed that $\Delta J_2 \neq 0$ transitions of the hydrogen molecules are negligible. This means that for NH_3-H_2 scattering the apparatus functions of type A, with the energy defect set equal to that of the primary beam molecule (see Eq. (15) of II and further), should be used. For the $(1,1) \rightarrow (2,1)$ and $(2,2) \rightarrow (3,2)$ transitions the apparatus functions have values of about 0.95 and 0.70, respectively, at $\theta_{cm}=0$ (Fig. 3). This is due to a rather large loss of kinetic energy in the centre of mass system for these transitions (26% and 39%, respectively). Computations of transition probabilities established that the inversion splitting of the ammonia molecule can be disregarded for the calculation of the energy defect $\hbar\omega$, except of course for the inversion transitions. Moreover they showed that over the entire range of impact parameters the values of transition probabilities are

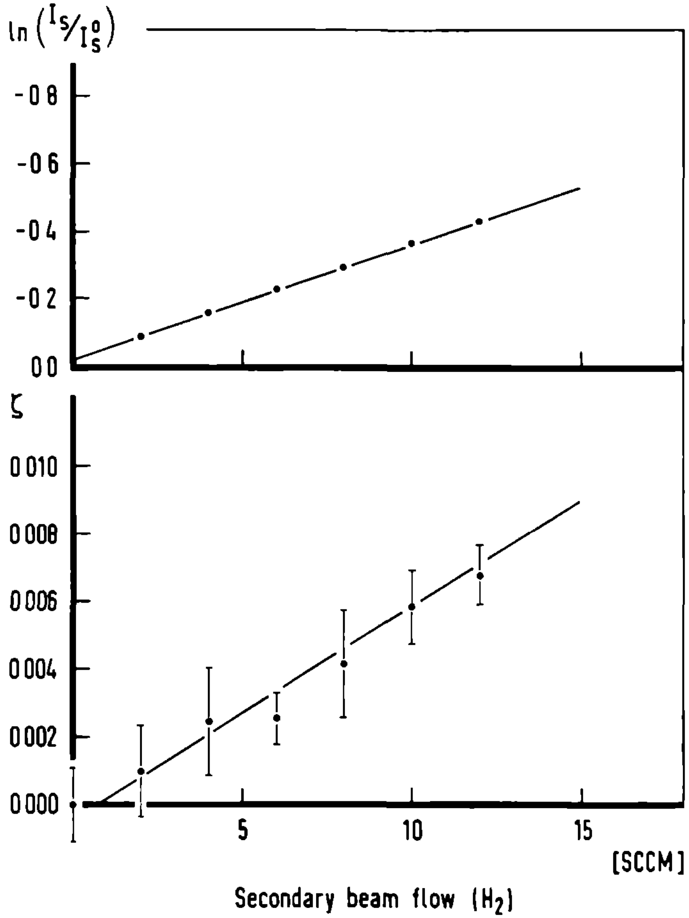

Figure 2: ζ as function of the secondary beam flow (H_2) for the transition $p=(1,1) \rightarrow s=(2,1)$. In the upper part the attenuation of the (2,1) microwave line intensity is shown.

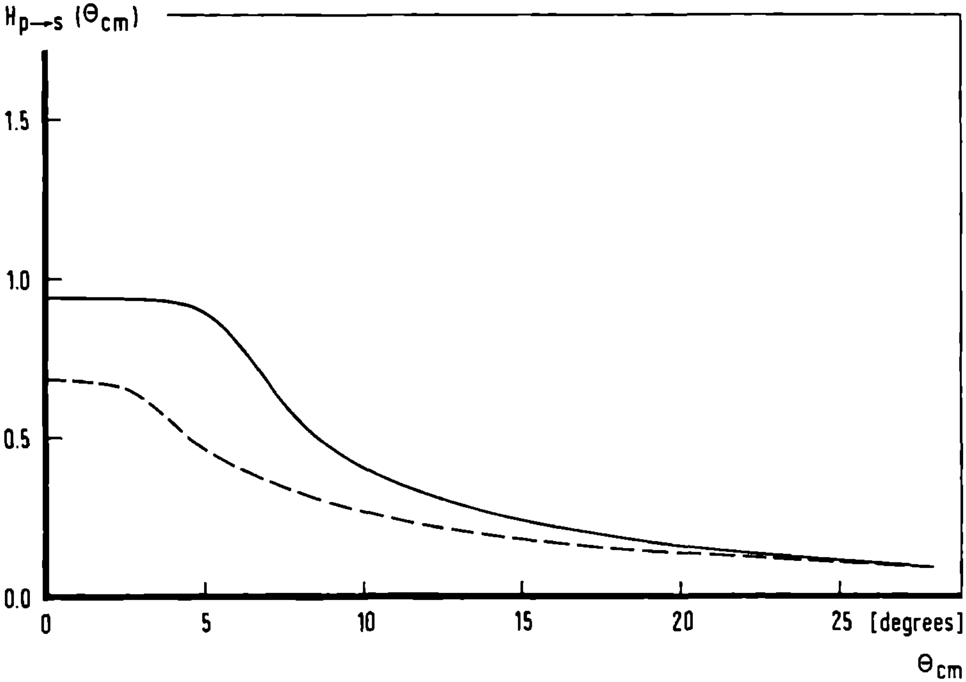

Figure 3: Apparatus functions for NH_3-H_2 for the transitions $p=(1,1) \to (2,1)$ (solid line) and $p=(2,2) \to (3,2)$ (dashed line).

		NH_3	Ref.	H_2	Ref.
B	(GHz)	298.12	*23*	1777.3	*22*
C	(GHz)	186.71	*23*		
μ	(Cm)	4.92×10^{-30}	*24*		
Q	(Cm^2)	9.74×10^{-40}	*25*	2.17×10^{-40}	*22*
α	(m^3)	2.22×10^{-30}	*26*	0.819×10^{-30}	*26*
$A_{//}$	(m^4)	-0.0633×10^{-40}	*10*		
$A_{\perp}$	(m^4)	0.793×10^{-40}	*10*		
A'	(m^4)	-0.81×10^{-40}	*10*		
ε	(J)		0.1573×10^{-20}		*12*
σ	(m)		3.45×10^{-10}		*12*
C_6	(Jm^6)		1061×10^{-80}		

TABLE 4 : Molecular constants and potential parameters.

		$\sigma^{\alpha,app}_{p\to s} - \sigma^{\gamma,app}_{p\to s}$		
	transition $p\to s$	theory (e-type)	theory (LJ-type)	experiment
H_2 1426 m/s	$(1,1)\to(2,1)$	0.74(16)	0.70(14)	0.570(75)
0.257×10^{17} m^{-2}	$(2,2)\to(3,2)$	0.089(34)	0.084(36)	0.122(22)

TABLE 5 : Summary of theoretical and experimental apparatus cross sections (in 10^{-20} m^2) for NH_3-H_2 scattering, for both types of potential models. In the first column also $\langle v_r \rangle$ and $(nl)_{eff}$ for a secondary beam flow of 1 sccm are given.

well below the values at which the normalization procedure (see II) becomes effective. The actual computation of probabilities for a rotational transition is considerably simplified by these observations, because the normalization procedure can be left out and for each impact parameter the resonance functions have to be evaluated only once.

For each rotational transition calculations were performed, using the molecular constants given in Table 4. As discussed in Sect. 3, for NH_3-H_2 the low-order permanent-multipole interactions are taken into account together with the induction and dispersion interactions proportional to R^{-7}. The population ratios used were those obtained with the type B apparatus functions in II (Table 2). For both types of potentials (Eqs. (1) and (2)) the parameters c and d were varied to get the best agreement between theoretical predictions and experimental results. The parameters c and d, the theoretical values for the cross sections, given in Table 5, and their uncertainties were determined graphically from the experimental results. For c the average of the values that yielded optimum agreement for the individual transitions is 6.6(24) and for d this average is 1.0(4).

5. DISCUSSION

For the system NH_3-CO_2 both fits yield a good agreement between theory and experiment. As with the polar secondary beam gases in II, a somewhat higher value for κ_g is obtained in the fit with the "resonant" apparatus functions (type B). For the system NH_3-N_2 the agreement between theory and experiment is reasonable, except for some discrepancy at 350 K. This deviation might be caused by the fact that the measurements at 350 K were less extensive than those at the other two temperatures. The factor κ_{N_2} is larger than the factor κ_{CO_2}. This leads to the conclusion that NH_3-N_2 collisions are more resonant than NH_3-CO_2 collisions, due to the larger rotational constant of N_2. This conclusion is supported by the fact that for the $(2,2) \rightarrow (3,2)$ transition the energy defect (Eq. (15) of II) is zero for the initial states of CO_2 and N_2 with J=38 and 8, respectively, whereas the largest contributions to the integral parity changing cross section come from initial states with J values around 26 and 8, respectively.

The integral cross sections and the parity changing (α) and conserving (γ) contributions to the rotational apparatus cross sections are given in Table 6 for both types of apparatus functions. It is seen from this table that for NH_3-CO_2 scattering (as with the polar scattering gases) $\sigma^{\gamma,app}_{p\rightarrow s} \leqq 0.1\ \sigma^{\alpha,app}_{p\rightarrow s}$, except for the transitions between the (J,K)=(2,2) and (3,2) levels. For these transitions $\sigma^{\gamma,app}_{p\rightarrow s} \approx 0.2\ \sigma^{\alpha,app}_{p\rightarrow s}$, whereas for NH_3-N_2 scattering the parity conserving contribution is about 25% of the parity changing contribution.

The apparatus function of type B has the value of 0.5 at $\theta_{cm}=2.05^{\circ}$ for NH_3-CO_2 scattering. With N_2 as scattering gas, these angles are 2.46°, 2.33° and 2.28° for 77 K, 300 K and 350 K, respectively. With this angular resolution for NH_3-N_2 scattering only about 4.5% of the integral cross sections for parity changing transitions is probed in the present experiment. For CO_2

	transition $p \to s$	integral $\sigma^{\alpha}_{p\to s}$	integral $\sigma^{\gamma}_{p\to s}$	type A $\sigma^{\alpha,app}_{p\to s}$	type A $\sigma^{\gamma,app}_{p\to s}$	type B $\sigma^{\alpha,app}_{p\to s}$	type B $\sigma^{\gamma,app}_{p\to s}$
	(1,1)→(2,1)	91.1	77.3	12.8	1.6	12.8	1.5
	(2,1)→(1,1)	68.8	56.5	9.0	1.0	9.1	1.0
	(2,2)→(3,2)	43.9	56.4	3.7	0.8	4.0	0.8
CO_2	(3,2)→(2,2)	38.9	60.3	3.3	0.7	3.6	0.7
	(2,1)→(3,1)	67.3	29.9	6.0	0.3	6.4	0.3
	(3,1)→(2,1)	73.7	27.7	5.4	0.3	5.8	0.3
	(1,1)→(3,1)	0	20.6	0	0.07	0	0.05
N_2							
77 K	(2,2)→(3,2)	25.16	33.90			0.96	0.25
300 K	(2,2)→(3,2)	31.00	35.59			1.53	0.40
350 K	(2,2)→(3,2)	30.88	35.48			1.49	0.41

TABLE 6 : The theoretical integral cross sections and the parity changing and conserving parts of the apparatus cross section (in 10^{-20} m^2) for NH_3-CO_2 and NH_3-N_2 scattering, for both types of apparatus functions (A and B).

	transition $p \to s$	$\sigma^{\alpha}_{p \to s}$	$\sigma^{\gamma}_{p \to s}$	$\sigma^{\alpha,app}_{p \to s}$	$\sigma^{\gamma,app}_{p \to s}$
e-type	(1,1)→(2,1)	5.9(12)	1.48(33)	0.97(20)	0.23(5)
	(2,2)→(3,2)	1.8(6)	1.07(24)	0.23(7)	0.14(3)
LJ-type	(1,1)→(2,1)	6.3(21)	1.62(35)	0.94(17)	0.24(3)
	(2,2)→(3,2)	2.1(11)	1.27(21)	0.24(6)	0.15(3)

TABLE 7 : The theoretical integral cross sections and the parity changing and conserving parts of the apparatus cross section (in 10^{-20} m^2) for NH_3-H_2 scattering, for both types of potential models.

as scattering gas this fraction is 13.5% for transitions between the (J,K)= (1,1) and (2,1) levels and 8% for the other transitions. Only 1-2% of the cross sections for parity conserving transitions is probed. As expected a smaller fraction of the integral cross sections is measured with non-polar scattering gases than with polar gases (see II). This is caused by the fact that the dipole-quadrupole interaction, which is mainly responsible for parity changing transitions (see Sect. 3), is only effective for small impact parameters, which result in large deflection angles.

Due to the short-range character of the dipole-quadrupole interaction the impact parameter below which the normalization procedure (Eq. (19) of II) reduces the transition probability is rather small. This results in quite large contributions from the small impact parameter region (cf. the cross sections for parity conserving transitions in II, originating mainly from quadrupole-dipole interaction). For example for NH_3-CO_2 scattering on the (1,1) $\rightarrow$ (2,1) and (2,2) $\rightarrow$ (3,2) parity changing transitions, 17% and 30%, respectively, of the integral cross sections stems from impact parameters smaller than 0.3 nm. For NH_3-N_2 scattering (300 K) on the (2,2) $\rightarrow$ (3,2) parity changing transition this number is 40%. Consequently the integral cross sections for NH_3-CO_2 and NH_3-N_2 may be somewhat too large.

With hydrogen as scattering gas, the parameters c and d in the potential models (Eqs. (1) and (2)) were varied to find the best agreement between theoretical and experimental apparatus cross sections for the (1,1) $\rightarrow$ (2,1) and (2,2) $\rightarrow$ (3,2) transitions. Also the integral cross sections (α and γ) and the parity changing and conserving parts of the apparatus cross sections were calculated as function of these parameters. From these results the values given in Table 7 and their uncertainties were determined graphically (Sect. 4). From Table 8 it is seen that the relative contribution of a specific interaction to $\sigma^{\alpha,app}_{p\rightarrow s} - \sigma^{\gamma,app}_{p\rightarrow s}$ is not the same for the (1,1) $\rightarrow$ (2,1) and (2,2) $\rightarrow$ (3,2) transitions. Therefore a better matching between theory and experiment, which

transition $p \to s$	contribution k	$\sigma^{\alpha}_{p\to s}$	$\sigma^{\gamma}_{p\to s}$	$\sigma^{\alpha,app}_{p\to s}$	$\sigma^{\gamma,app}_{p\to s}$
	1	3.86	0	0.641	0
	2	0	1.63	0	0.255
(1,1)→(2,1)	3	0.20	0	0.028	0
	4	2.89	0	0.404	0
	total	6.96	1.63	1.073	0.255
	1	0.98	0	0.144	0
	2	0	1.17	0	0.158
(2,2)→(3,2)	3	0.24	0	0.034	0
	4	0.63	0	0.080	0
	total	1.85	1.17	0.259	0.158

TABLE 8 : Contributions of different interactions to the cross sections (in 10^{-20} m^2) for NH_3-H_2 scattering with c=6.9.

k=1 dipole-quadrupole

k=2 quadrupole-quadrupole

k=3 induction and dispersion (l_1=3; Eq. (A2))

k=4 induction and dispersion (l_1=1; Eq. (A1)) results in smaller uncertainties in the calculated integral cross sections, would be obtained by introducing separate parameters c (and d) for each term in the potential. But only additional experimental data on other rotational transitions would make such a procedure possible. Although both potential models can certainly be improved it is satisfying that they give essentially the same integral cross sections.

In Fig. 4 the leading induction and dispersion term in the potential (resulting in the transition probability given by Eq. (A1)) is compared with the corresponding term in the ab initio potential for NH_3-He obtained by Green[17]. The parameters σ and ε (the well depth of the isotropic L-J potential), used to construct Fig. 4, are those for the NH_3-H_2 system. For the long-range part the NH_3-He potential is scaled with the appropriate $C_6=4\,\varepsilon\sigma^6$ constant[27]. The differences between the potentials for both models and the quite large uncertainties in the parameters c and d indicate, that the anisotropic potential is not well-determined from the present experiment. However, the shape of the NH_3-He potential of Green is similar to that of the present potential models, but its minimum is shifted to smaller intermolecular distances. In order to investigate which impact parameters are probed, a cut-off impact parameter b_{co} is introduced that replaces the lower integration limit in the expressions for the apparatus (Eq. (16) of II) and integral cross sections,

$$\sigma_{p\to s}(b_{co}) = 2\pi \int_{b_{co}}^{\infty} (2J_s+1)\ P_{p\to s}(b)\ b\,db \qquad (4)$$

The results of these calculations are given as a function of b_{co} in Fig. 5. From this figure it is seen that the main contributions to the apparatus cross sections originate from impact parameters around 0.4 nm.

In Fig. 6a the deflection angle θ (Sect. 3) and the distance of closest

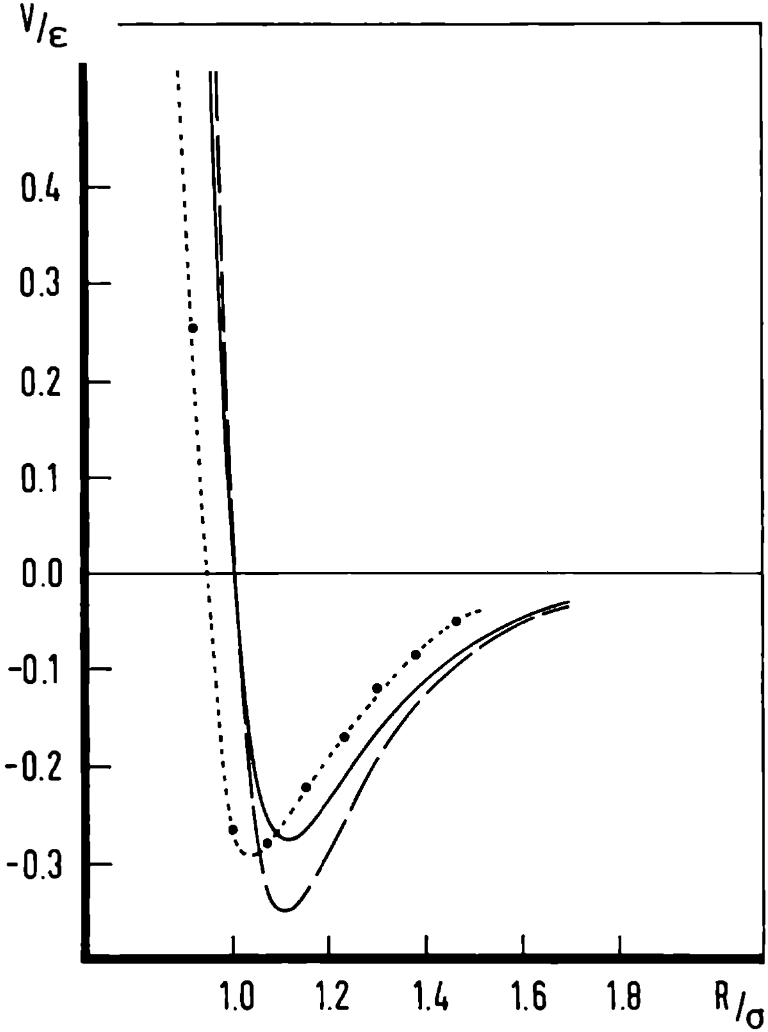

Figure 4: Comparison between obtained potentials for NH_3-H_2 (e-type: dashed line; LJ-type: solid line) and the corresponding NH_3-He potential term (short dashes with dots, representing the points calculated by Green[17]; see text).

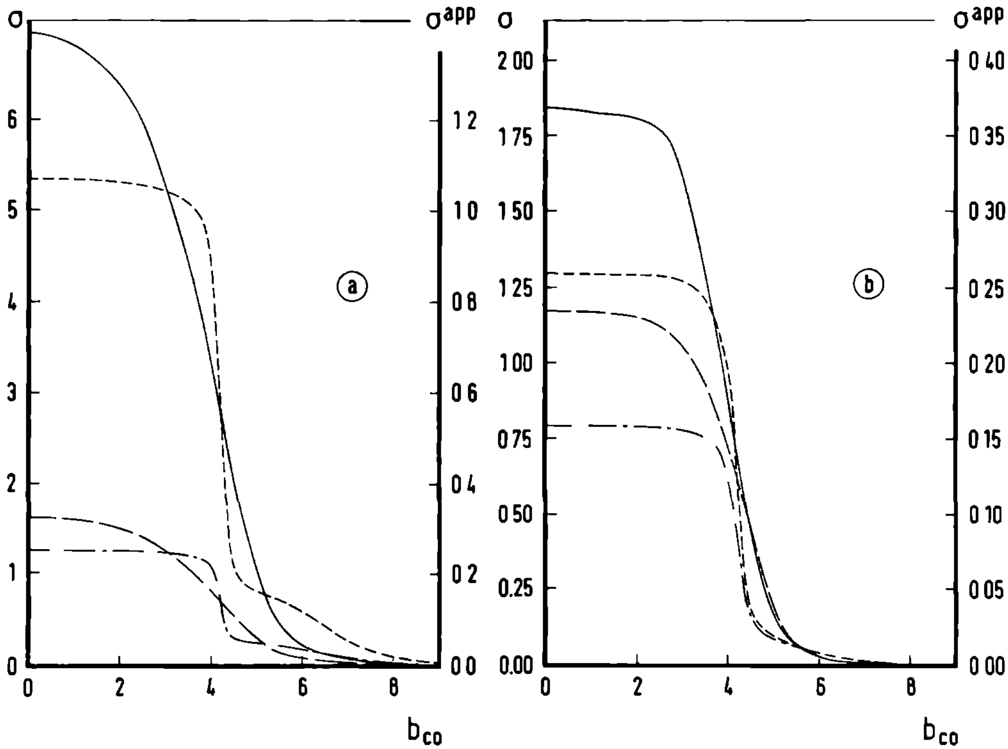

Figure 5: Cross sections for the system NH_3-H_2 (in 10^{-20} m^2) as function of the cut-off impact parameter b_{co} (in 10^{-10} m ; Eq. (4)) for the (a) (1,1) → (2,1) and (b) (2,2) → (3,2) transition.

Integral, parity changing: solid lines.

Integral, parity conserving: long dashes.

Apparatus, parity changing: short dashes.

Apparatus, parity conserving: dashed-dotted lines.

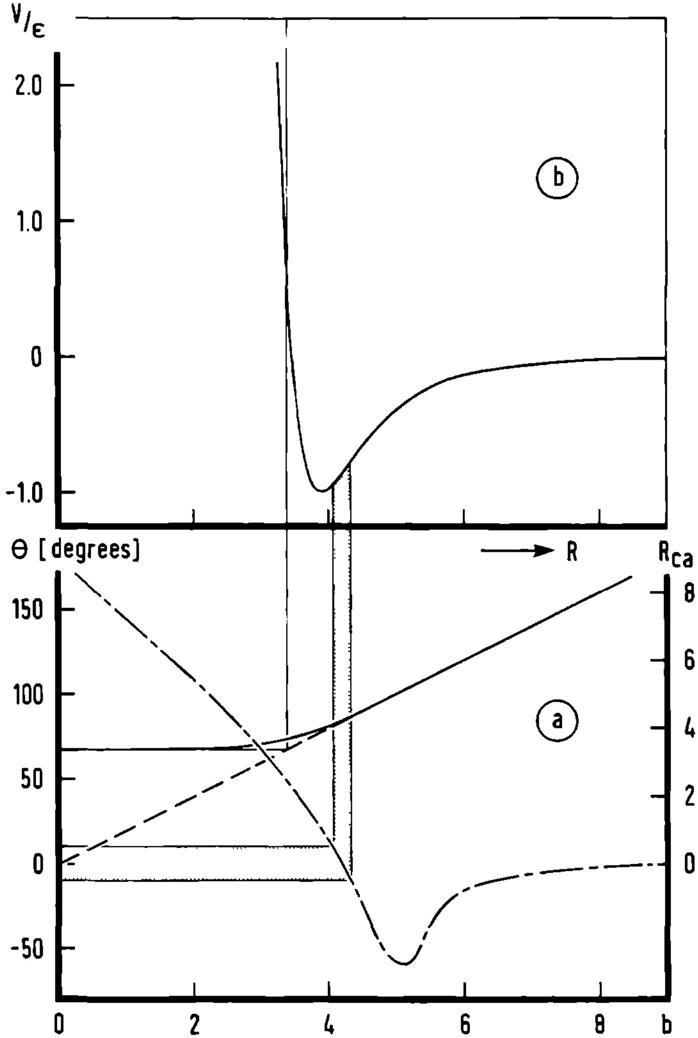

Figure 6: (a) Deflection angle θ and distance of closest approach R_{ca} (in 10^{-10} m) as function of the impact parameter b (in 10^{-10} m) and (b) the isotropic potential shown as function of the intermolecular distance R (in 10^{-10} m) for the system NH_3-H_2.

approach R_{ca} are given as function of the impact parameter b. For negative deflection angles R_{ca} equals b and for positive deflection angles $R_{ca}=R_0=b/\cos(\frac{1}{2}\theta)$ (see Appendix B). In Fig. 6b the isotropic L-J (12,6) potential is displayed. The shapes of isotropic and anisotropic potentials are almost identical for the system NH_3-H_2 (d=1.0(4); Eq. (2)). The shaded area in Fig. 6 corresponds to the range of deflection angles for which the apparatus function for the $(1,1)\rightarrow(2,1)$ transition is larger than half its maximum value (Fig. 3). From Fig. 5 it is seen that about half of the apparatus cross sections for this transition originates from that region. For the corresponding distances of closest approach the (an)isotropic potential reaches almost its minimum value. The lower limit (0.33 nm) of the distance of closest approach is also indicated in Fig. 6. The integral cross sections are not sensitive to the anisotropic potential at smaller intermolecular distances. It turns out that the deflection angles for the probed impact parameters correspond to the inner branch of the deflection function. As the inner branch is quite steep, the range of probed impact parameters is rather small. This explains that in spite of the large acceptance angles compared to the polar scattering gases in II, only about 15% of the integral cross sections is measured via the apparatus cross sections.

About 50% of the integral cross sections for parity changing transitions originates from the dispersion and induction terms in the potential (Table 8). The ratio of these two contributions to the potential is 7 : 1. From state-to-state small-angle scattering of CsCl and KCl with rare gas atoms Meyer and Toennies[28] found an averaged ratio for these terms of 0.63 : 1 and 13.3 : 1 for CsCl and KCl, respectively. For these systems they take only the long-range part of the potential into account in their deflection function and interpretation.

In order to perform a further test of the potentials and of the method of calculating cross sections, for the NH_3-H_2 system all cross sections necessary

$(J_i,K_i)=(1,1)$			$(J_i,K_i)=(2,2)$		
(J_f,K_f)	$\sigma^{\alpha}_{i\to f}$	$\sigma^{\gamma}_{i\to f}$	(J_f,K_f)	$\sigma^{\alpha}_{i\to f}$	$\sigma^{\gamma}_{i\to f}$
(1,1)	2.060	0.053	(2,2)	1.660	0.090
(2,1)	0.983	0.173	(3,2)	0.330	0.127
(3,1)	0.052	0.067	(4,2)	0.017	0.010
(4,1)	0.010	0	(5,2)	0.003	0
(4,4)	0	2.427	(5,5)	0	1.768

TABLE 9 : Degeneracy-averaged cross sections (in 10^{-20} m^2) for NH_3-H_2 scattering; c=6.9, v_r=1887 m/s.

to interpret line broadening (see I) and double-resonance experiments[4] involving the $(J,K)=(1,1)$ and $(2,2)$ inversion levels, were calculated for a relative velocity of 1887 m/s (cell at 300 K). The resulting degeneracy-averaged cross sections are summarized in Table 9 for c=6.9. For the transitions $(1,1)\rightarrow(4,4)$ and $(2,2)\rightarrow(5,5)$ the cross sections originate solely from the interaction leading to the probability given by Eq. (A3). A numerical evaluation of the resonance functions $g_3(\omega\tau)$ and $g_7(\omega\tau)$[9,10] showed that they are almost identical for the straight-path approximation. Therefore for the bent trajectories the g_3 function is used instead of the g_7 function. For impact parameters smaller than 0.23 nm the resulting probability (Eq. (A3)) is set equal to unity, since the theory predicts a larger value. Because the contributions to the other cross sections from this region are only a few percent (Fig. 5), the errors introduced by not using the normalization procedure for the transition probabilities are very small.

With the values of Table 9 cross sections for line broadening or T_2 experiments on the (1,1) and (2,2) inversion transitions are found to be[29] 34.9×10^{-20} m^2 and 31.7×10^{-20} m^2, respectively. The cross sections for T_1 experiments on the same transitions are 40.9×10^{-20} m^2 and 39.5×10^{-20} m^2, respectively. The theoretical values are in good agreement with the experimental results[3] (see Table 1 of I). In steady-state double-resonance experiments Daly and Oka[30] found for NH_3-H_2 $\Delta I/I$ values of 5.2% and 2.3% for the combination $(J_p,K_p) \Leftrightarrow (J_s,K_s) = (2,1) \Leftrightarrow (1,1)$ and $(3,2) \Leftrightarrow (2,2)$, respectively. The values obtained with the results in Table 9 are 10% and 3.5%, respectively (Eq. (23) of II). The agreement with the experimental values is reasonable if compared to that found for NH_3-He on the same transitions by Davis and Boggs[31] and by Green[18]. With the same technique as used for NH_3-H_2 Fabris and Oka[32] observed negative relative intensity changes for NH_3-He on these transitions, while theoretical predictions are positive[18,31]. In the same paper Fabris and Oka[32] reported also negative effects for NH_3-H_2 on a number of combinations of pump and signal doublets with $\Delta k=\pm 3$. The largest effects were found for the combinations (2,2)-(1,1), (4,4)-(1,1) and (5,5)-(2,2). In the present investigation only effects for $\Delta k=0$ transitions have been observed. No effects were found for the (2,2)-(1,1) transition, which might be due to the fact that the differential cross section is less peaked in forward direction for this transition than for the $\Delta k=0$ transitions. For $\Delta k=\pm 3$ transitions the potential model and collision theory used in the present investigation yield non-zero cross sections only for the (1,1)-(4,4) and (2,2)-(5,5) transitions (Table 9). In Anderson's theory some new term in the potential would be needed to produce other $\Delta k=\pm 3$ transitions. But within the framework of the same theory such a potential term would not contribute to the cross sections for $\Delta k=0$ transitions. Therefore the values presented for the cross sections for the transitions between the (1,1) and (2,1) and between the (2,2) and (3,2) doublet levels are not influenced by the presence or absence of such a potential term.

Experiment and interpretation, presented in this paper, show that for the systems NH_3-CO_2 and NH_3-N_2 the long-range permanent-multipole interactions are sufficient to explain the measured apparatus cross sections. For the system NH_3-H_2, however, the short-range interactions are dominating. The influence of induction and dispersion terms is clearly demonstrated. With an empirical potential, which includes a repulsive part, a satisfying agreement between theory and experiment has been obtained. Using this potential cross sections for $\Delta J=\pm 1$, $\Delta k=0$ rotational transitions are predicted with an estimated accuracy of 30%. A reasonable overall agreement with other experiments has been obtained. The integral state-to-state cross sections for the system NH_3-H_2 are important for the interstellar ammonia problem[33] (see also I). For the relevant transitions and relative velocities these cross sections can be calculated from the NH_3-H_2 potential obtained in the present investigation. For NH_3-H_2 this paper presents the first cross sections for transitions between well-defined initial and final states, supported by experimental observations.

ACKNOWLEDGEMENTS

The authors thank Professor J. Reuss for his critical reading of the manuscript and Mr. N. van Hulst for his unfailing enthusiasm and assistance during the measurements. The technical assistance of Messrs. J. Holtkamp and E. van Leeuwen is greatly appreciated.

APPENDIX A : TRANSITION PROBABILITIES RESULTING FROM THE R^{-7} TERMS IN THE INTERMOLECULAR POTENTIAL

A summary of transition probabilities obtained within the framework of Anderson's theory is given by Robert et al.[9] for a large number of terms in the long-range intermolecular potential. The induction and dispersion terms that are proportional to R^{-7} and relevant for the NH_3-H_2 are in their notation $U_{\mu_1\alpha_2 Q_1}$, $U_{\alpha_2 A_{1//}}$ and $U_{\alpha_2 A_{1\perp}}$ (with Q_1 instead of θ_1). The resulting transition probability is obtained by adding all corresponding contributions and cross-term contributions as given in Ref. 9. When this probability is written as given by Eq. (18) of II, there are two contributions to the probability from the R^{-7} terms in the intermolecular potential that can only cause $\Delta k=0$ transitions.

1) with l_1-1, $l_2=0$ and

$$C_1 = \frac{3\pi}{8}\sqrt{\frac{3}{2}}\left\{\mu_1 Q_1 \alpha_2 + \left(\frac{A_{1//}+2A_{1\perp}}{3\alpha_1}\right) C_6\right\}\Big/\hbar v_r b^6 , \qquad \text{(A1)}$$

the resonance function appropriate for this term is the g_3 function[9].

2) with $l_1=3$, $l_2=0$ and

$$C_3 = \frac{\pi}{32}\sqrt{\frac{17}{7}}\left\{3\mu_1 Q_1 \alpha_2 - \left(\frac{4A_{1\perp}-3A_{1//}}{3\alpha_1}\right) C_6\right\}\Big/\hbar v_r b^6 ; \qquad \text{(A2)}$$

the resonance function appropriate for this term is the g_4 function[9]. Furthermore there is also a contribution with $l_1=3$ and $l_2=0$, arising from the R^{-7} term $U_{\alpha_2 A'_1}$[10,19] that can only cause $\Delta K=\pm 3$ transitions:

$$P_{p\to s}^{2\to 2'} = 2C^2 \left[\begin{pmatrix} J_p & 3 & J_s \\ -K_p & 3 & K_s \end{pmatrix}^2 + \begin{pmatrix} J_p & 3 & J_s \\ -K_p & -3 & K_s \end{pmatrix}^2 \right] \times \begin{pmatrix} J_2 & 0 & J_2' \\ -K_2 & 0 & K_2' \end{pmatrix}^2 g_7(\omega\tau) \tag{A3}$$

where

$$C = \frac{\pi}{48} \sqrt{\frac{4285}{7}} \; \frac{A_1' \, C_6}{\alpha_2 \hbar v_r b^6} \tag{A4}$$

and $g_7(\omega\tau)$ is the resonance function as given by Bonamy and Robert[10]. In the formulas given above, the following notation is used: μ_1 is the dipole moment of the primary molecule, Q_1 is the quadrupole moment of the primary molecule, α_i is the polarizability of the i-th molecule, C_6 is the Lennard-Jones 12-6 potential constant; A_1', $A_{1//}$ and $A_{1\perp}$ are the quadrupole polarizability and its anisotropies of the primary molecule[10,19]. The transition probabilities given by Eqs. (A1) and (A2) are parity changing, that of Eq. (A3) is parity conserving.

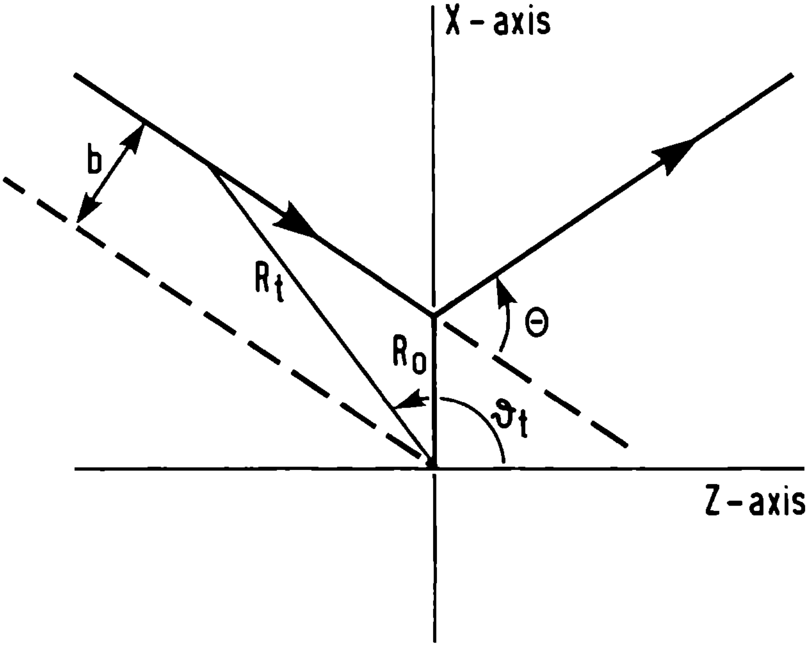

Figure A1: Geometry of the bent paths.

The contributions of $P_{l_1 l_2}$ to the transition probability $P^{2\to2'}_{1\to1'}$, as given by Eq. (18) of II are deduced from the expression

$$P_{l_1 l_2} = \begin{pmatrix} J_1 & l_1 & J_1' \\ -K_1 & 0 & K_1' \end{pmatrix}^2 \begin{pmatrix} J_2 & l_2 & J_2' \\ -K_2 & 0 & K_2' \end{pmatrix}^2 \sum_m |I_{lm}|^2 \tag{B1}$$

where the subscript 1 (2) stands for the primary (secondary) beam molecule and primes indicate the final states; I_{lm}, with $l=l_1+l_2$, is the time integral factor as defined by Eq. (9) of Gray and Van Kranendonk[13]. The time integrals I_{lm} are usually calculated using straight trajectories. In the present investigation bent trajectories instead of straight paths are used for the system NH_3-H_2 in combination with potentials that include a repulsive part.

In the notation of Gray and Van Kranendonk[13] the bent trajectories are defined for positive deflection angles θ by (see Fig. A1)

$$R_t = R_0 \{1+z^2+2|z|\sin(\theta/2)\}^{\frac{1}{2}} \tag{B2}$$

where

$$R_0 = b/\cos(\theta/2) \tag{B3}$$

$$z = v_r t/R_0 \tag{B4}$$

$$\sin \vartheta_t = \frac{R_0}{R_t} \{ |1+|z|\sin(\theta/2)| \} \tag{B5}$$

$$\cos \vartheta_t = \frac{R_0}{R_t} \{ z \cos(\theta/2) \} \tag{B6}$$

$$\phi_t = 0 \tag{B7}$$

The time t runs from $-\infty$ to $+\infty$ and the trajectory is symmetrical around t=0. The dimensionless variable corresponding to z is

$$x = \omega R_0/v_r \tag{B8}$$

For a potential term $\varepsilon_l(R)$ with a long-range radial dependence given by

$$\varepsilon_l(R) = \frac{S_l}{R^n} \tag{B9}$$

the expression for the time integral I_{lm}, using bent trajectories and the potential models h(R) given by Eqs. (1) and (2), is

$$|I_{lm}|^2 = \left(\frac{R_0\varepsilon_l(R_0)}{\hbar v_r}\right)^2 \left[\left\{\int_{-\infty}^{\infty} h(R_t)\left(\frac{R_0}{R_t}\right)^n \cos(xz) Y_{l-m}(\vartheta_t,0)\,dz\right\}^2 + \left\{\int_{-\infty}^{\infty} h(R_t)\left(\frac{R_0}{R_t}\right)^n \sin(xz) Y_{l-m}(\vartheta_t,0)\,dz\right\}^2\right] \tag{B10}$$

If the deflection angle θ is negative (attraction) ϕ_t changes from $0(\pi)$ to $\pi(0)$ when ϑ_t becomes $\pi(0)$, but the resulting expression (Eq. (B10)) is the same. The resonance functions are expressed in terms of $|I_{lm}|^2$ as follows

$$f_l(x) = D_l \times b^{2(n-1)} \sum_m |I_{lm}|^2 \tag{B11}$$

The normalization constant D_l is defined by

$$D_l = \left[b^{2(n-1)} \sum_m |I_{lm}|^2 \right]^{-1} \tag{B12}$$

with $\theta=0$ and d (c) set equal to 0 (∞) in Eq. (B10). The advantage of this definition for the normalization constants is, that the same constants C_l in Eq. (18) of II can be used as with straight trajectories. It should be noticed that for the induction and dispersion term with $l=1$ (3) the notation g_3 (g_4) is commonly used for the resonance function[9]. From Eqs. (B11) and (B12) it is seen that the constant S_l in Eq. (B9) is not needed for the calculation of the resonance function.

REFERENCES

1 D.B.M.Klaassen, J.M.H.Reijnders, J.J.ter Meulen and A.Dymanus, J.Chem.Phys. 76, 3019 (1982)

2 D.B.M.Klaassen, J.J.ter Meulen and A.Dymanus, to be published.

3 P.Varasani, J.Quant.Spectrosc.Radiat.Transfer, 12, 1283 (1972); J.S.Margolis, J.Quant.Spectrosc.Radiat.Transfer, 15, 637 (1975); J.S.Margolis and S.Sarangi, J.Quant.Spectrosc.Radiat.Transfer, 16, 405 (1976); T.Amano, T.Amano and R.H.Schwendeman, J.Chem.Phys. 73, 1238 (1980)

4 T.Oka, "Collision-induced transitions between rotational levels", Advances in Atomic and Molecular Physics, Vol.9, Academic Press (1973)

5 J.M.H.Reijnders, Thesis, Katholieke Universiteit, Nijmegen, The Netherlands (1978)

6 C.J.Tsao and B.Curnutte, J.Quant.Spectrosc.Radiat.Transfer, 2, 41 (1962)

7 A.D.Buckingham, "Permanent and induced molecular moments and long-range intermolecular forces", Advances in Chemical Physics, J.O.Hirschfelder, editor, Vol.12, Chap.2, John Wiley & Sons, New York (1967); H.Margenau and N.R.Kestner, Theory of Intermolecular Forces, Pergamon Press, Oxford (1969); S.Stolte and J.Reuss, "Elastic Scattering Cross Sections II: Noncentral Potentials", Atom-molecule collision theory, Ed. R.B.Bernstein, Plenum Press, New York (1979)

8 G.Birnbaum, "Microwave Pressure Broadening and its Application to Intermolecular Forces", Advances in Chemical Physics, J.O.Hirschfelder, editor, Vol.12, Chap.9, John Wiley & Sons, New York (1967)

9 D.Robert, M.Giraud and L.Galatry, J.Chem.Phys. 51, 2192 (1969)

10 J.Bonamy and D.Robert, J.Quant.Spectrosc.Radiat.Transfer, 15, 855 (1975)

11 J.Bonamy, J.Quant.Spectrosc.Radiat.Transfer, 16, 213 (1976)

12 A.Kupperman, R.J.Gordon and M.J.Coggiola, Disc.Faraday Soc. 55, 145 (1973)

13 C.G.Gray and J.Van Kranendonk, Can.J.Phys. 44, 2411 (1966)

14 J.O.Hirschfelder, C.F.Curtiss and R.B.Bird, "Molecular Theory of Gases and Liquids", Chap.1 and Appendix, J.Wiley & Sons, New York (1965)

15 S.Green, B.J.Garrison and W.A.Lester Jr., J.Chem.Phys. 63, 1154 (1975)

16 B.J.Garrison, W.A.Lester Jr. and H.F.Schaefer III, J.Chem.Phys. 63, 1449 (1975); B.J.Garrison, W.A.Lester Jr., P.Siegbahn and H.F.Schaefer III, J. Chem.Phys. 63, 4167 (1975)

17 S.Green, J.Chem.Phys. 64, 3463 (1976)

18 S.Green, J.Chem.Phys. 73, 2740 (1980)

19 J.Bonamy and D.Robert, Chem.Phys.Letters, 6, 591 (1970)

20 H.Pauly, "Elastic Scattering Cross Sections I: Spherical Potentials", Atom-molecule collision theory, Ed.R.B.Bernstein, Plenum Press, New York (1979)

21 M.S.Child, "Molecular collision theory", page 23, Academic Press, London (1974)

22 P.B.Foreman, K.R.Chien and S.G.Kukolich, J.Chem.Phys. 62, 4710 (1975)

23 D.Laughton, S.M.Freund and T.Oka, J.Mol.Spectrosc. 62, 263 (1976)

24 E.A.Cohen and R.L.Poynter, J.Mol.Spectrosc. 53, 131 (1974)

25 J.A.Th.Verhoeven and J.M.H.Reijnders, Quarterly Report 27 of the Atomic and Molecular Research Group, Fysisch Laboratorium, Katholieke Universiteit, Nijmegen, The Netherlands (1970)

26 N.J.Bridge and A.D.Buckingham, Proc.Roy.Soc.A, 295, 334 (1966)

27 R.W.Bickes Jr., G.Duquette, C.J.N.van den Meijdenberg, A.M.Rulis, G.Scoles and K.M.Smith, J.Phys.B. 8, 3034 (1975)

28 G.Meyer and J.P.Toennies, J.Chem.Phys. 75, 2753 (1981)

29 R.H.Schwendeman, "Transient effects in microwave spectroscopy", Annual Review of Physical Chemistry, Vol.29 (1978)

30 P.W.Daly and T.Oka, J.Chem.Phys. 53, 3272 (1970)

31 S.L.Davis and J.E.Boggs, J.Chem.Phys. 69, 2355 (1978)

32 A.R.Fabris and T.Oka, J.Chem.Phys. 56, 3168 (1972)

33 J.S.Sweitzer, Astrophys.J. 225, 116 (1978); M.Morris, P.Palmer and B.Zuckerman, Astrophys.J. 237, 1 (1980); T.Pauls and T.L.Wilson, Astron. Astrophys. 91, L11 (1980)

BOTSINGSDOORSNEDEN VOOR ROTATIEOVERGANGEN VAN NH_3

Het proefschrift beschrijft een experimenteel onderzoek van rotatie-overgangen in ammoniak (NH_3) geinduceerd door botsingen met moleculaire waterstof (H_2) en andere moleculen. Inelastische overgangen van NH_3 ten gevolge van botsingen met H_2 vormen een belangrijk onderdeel van de modellen waarmee fysische processen in interstellaire wolken beschreven worden. De intensiteit van inversieovergangen van NH_3, waargenomen in de interstellaire ruimte, wordt door astrofysici gebruikt als een test voor deze modellen.

Het onderzoek werd verricht met behulp van een moleculaire-bundel-maser, waarin de primaire NH_3 bundel gekruist wordt met een dwarsbundel. Met behulp van een microgolftrilholte werd toestandsgevoelig een bepaalde inversieovergang gedetecteerd. Een soortgelijke trilholte werd gebruikt om de bezetting van een ander inversiedoublet te beinvloeden voor het strooigebied. Met behulp van deze dubbelresonantietechniek werd de rotatietoestand van het ammoniakmolecuul voor en na de botsing bepaald.

De experimentele resultaten werden geinterpreteerd in termen van botsingsdoorsneden voor rotatieovergangen van NH_3. Met behulp van een semi-klassieke botsingstheorie werden voorspellingen gedaan van de te meten effecten. Metingen met als strooigassen ammoniak, methylfluoride (CH_3F), fluoroform (CF_3H), kooldioxide (CO_2) en stikstof (N_2) konden worden verklaard met bekende intermoleculaire potentialen. Voor het systeem NH_3-H_2 werd een empirische potentiaal bepaald. Met behulp van

deze potentiaal zijn integrale botsingsdoorsneden berekend voor een aantal rotatieovergangen van NH_3. Met deze berekende doorsneden kunnen experimenten elders aan het systeem NH_3-H_2 gedaan verklaard worden.

D.B.M.Klaassen werd op 17 december 1952 geboren te Geleen. Na het eind-examen gymnasium β aan de Scholengemeenschap St.Michiel te Geleen in 1971, volgde de natuurkundestudie aan de Katholieke Universiteit te Nijmegen. Het candidaatsexamen werd in maart 1974 behaald. Na het afstudeerwerk op de afdeling Atoom- en Molecuulfysica onder leiding van prof.dr.J.Reuss volgde het doctoraalexamen (cum laude) in maart 1977. In april 1977 werd het onderzoek dat in dit proefschrift wordt beschreven, begonnen op de afdeling Atoom- en Molecuulfysica onder leiding van prof.dr.A.Dymanus.

STELLINGEN

1. Bij de interpretatie van hun dubbelresonantie-experimenten aan NH_3 dienen Matsuhima et al. en Shimizu et al. het door hen veronderstelde tweetrapsproces expliciet in rekening te brengen.

   F.Matsuhima, N.Morita, S.Kano and T.Shimizu,
   J.Chem.Phys. 70, 4225 (1979)
   T.Shimizu, F.Matsuhima and Y.Honguh,
   Laser Spectroscopy V, p.212,
   Ed. A.R.W.McKellar, T.Oka and B.P.Stoicheff,
   Springer-Verlag, New York (1981).

2. De verhouding waterstofdichtheid/ammoniakdichtheid is in de experimenten van Oka niet groot genoeg om de aan ammoniak gemeten effecten alleen aan botsingen tussen ammoniak- en waterstofmoleculen toe te kunnen schrijven.

   P.W.Daly and T.Oka, J.Chem.Phys. 53, 3272 (1970)
   A.R.Fabris and T.Oka, J.Chem.Phys. 56, 3168 (1972)

3. Voor het systeem KCl-He kan het gedeelte van de intermoleculaire potentiaal rond het minimum niet zonder meer verwaarloosd worden.

   G.Meyer and J.P.Toennies, J.Chem.Phys. 75, 2753 (1981)

4. Het gebruik van reciproque centimeters als frequentie-eenheid is slechts dan niet verwarrend wanneer uitgegaan wordt van de golflengte in vacuüm.

   F.M.Behlen, D.B.McDonald, V.Sethuraman and
   S.A.Rice, J.Chem.Phys. 75, 5685 (1981)

5. Bij de interpretatie van de absorptiepiek van CO-paren in edelgasmatrices, die tot nu toe nog niet volledig in overeenstemming met de experimenten is, moet Dubost ook de resonante dipool-dipool interactie van de aangeslagen toestand beschouwen.

H.Dubost, Chem.Phys. 12, 139 (1976)

6. De ontsiering door druk- en andere fouten in het boek van W.Demtröder over laserspectroscopie bereikt op pagina 512 een hoogtepunt.

W.Demtröder, Laser Spectroscopy,
Springer-Verlag, New York (1981)

7. Wie bij het ontwerpen van computerprogramma's uitsluitend geimplementeerde talen gebruikt legt zich beperkingen op die niet alleen van notationele aard zijn.

8. Voor een chemicus of bioloog is het voldoende de chemie respectievelijk biologie te bestuderen, een fysicus of mathematicus echter dient de fysica respectievelijk mathematica te beoefenen.

van Dale's Groot Woordenboek der Nederlandse
Taal, Martinus Nijhoff, 's Gravenhage (1976)

Nijmegen, 23 juni 1982

D.B.M. Klaassen